Methodology for testing subcomponents; background and motivation for subcomponent testing of wind turbine rotor blades

Antoniou, Alexandros ; Branner, Kim; Lekou, D.J.; Nuin, Iñaki; Nijssen, Rogier

Publication date:
2016

Document Version
Publisher's PDF, also known as Version of record

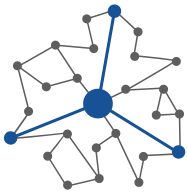

IRPWind

Integrated Research Programme on Wind Energy

Project acronym: **IRPWIND**

Grant agreement nº 609795

Collaborative project

Start date: 01st December 2013

Duration: 4 years

"Methodology for testing subcomponents; background and motivation for subcomponent testing of wind turbine rotor blades"

WP7.1: Improved and validated wind turbine structural reliability - Efficient blade structure
Deliverable Number D7.1

Lead Beneficiary: Centre for Renewable Energy Sources and Saving (CRES)

Delivery date: 23/01/2015

Dissemination level: PU

The research leading to these results has received funding from the European Union Seventh Framework Programme under the agreement 609795.

Author(s) information (alphabetical):		
Name	Organisation	Email
Alexandros Antoniou	IWES	alexandros.antoniou@iwes.fraunhofer.de
Kim Branner	DTU	kibr@dtu.dk
D. J. Lekou	CRES	dlekou@cres.gr
Iñaki Nuin	CENER	inuin@cener.com
Rogier Nijssen	WMC	rogier@mail.wmc.eu

Aknowledgements/Contributions:		
Name	**Organisation**	**Email**
Konstantinos Bacharoudis	CRES	kbach@cres.gr

Document Information

Version	Date	Description			
1	17/08/2015	Revised version; Extended Executive summary, explaining the Annex			
			Prepared by	**Reviewed by**	**Approved by**
		Name	D. J. Lekou		

Definitions

Table of Contents

Executive Summary

This report aims to provide an overview of the design methodology followed by wind turbine blade structural designers, along with the testing procedure on full scale blades which are followed by testing laboratories for blade manufacturers as required by the relevant standards and certification bodies' recommendations for design and manufacturing verification. The objective of the report is not to criticize the design methodology or testing procedure and the standards thereof followed in the wind energy community, but to identify those items offered by state of the art structural design tools that cannot be verified through the currently followed testing procedures and recommend ways to overcome these limitations.

The work is performed within Work-Package WP7.1 entitled "Improved and validated wind turbine structural reliability - Efficient blade structure" of the IRPWIND programme. The numerical investigations performed are based on the INNWIND.EU reference 10MW horizontal axis wind turbine [1]. The structural properties and material and layout definition used within IRPWIND are defined in the INNWIND.EU report [2].

The layout of the report includes a review of the structural analysis models used for blade design, highlighting the current state of the art. The review of the full-scale blade testing procedure is performed under Section 3, followed by the discussion on the issues of verification of design and manufacture performed through testing. Finally, methodologies for testing blade subcomponents and/or blade parts are described in 5. The present report is complemented by all details of the comparison of blade test loads against design loads on the reference blade, as provided in Annex 1. These data will facilitate direct comparisons in fine points of interest along the reference blade for the load cases considered.

The recommendations of this report are relevant for the design and testing of wind turbine subcomponents, in order to verify the numerical analysis tools used in the structural design of wind turbine blades.

Introduction

This report includes the results of the review of the design methodology and the verification through testing of blades, as well as the numerical investigations of blades and blade subcomponents and the findings thereof. These results are combined with specifications for the design of blade subcomponents and recommendations on the performance of testing in order to be used for the verification of the blade design within the frame of Work-Package 7.1 “Improved and validated wind turbine structural reliability - Efficient blade structure” of the IRPWIND project. The report is a literature study complemented by numerical investigations performed with reference data and relevant analysis tools available. The report shall form the basis for the definition of the experimental campaign by the testing laboratories within the next step of the activities of WP7.1. The report is also to the interest of standardization committees and certification bodies, since it includes findings applicable to very large wind turbines blades.

1. Structural design review

For the structural design of wind turbine blades, the international standard IEC 61400-1:2005 [3] is followed[1]. This standard provides a minimum set of specifications regarding wind turbine blade design. More detailed recommendations for the blade design are provided by certification bodies design guidelines, such as GL [4] and DNV-DS-J102 [5] and these are usually followed during structural blade design to cover items too generally described in IEC 61400-1.

The structural design of blades involves the compliance to a number of design constraints, some stemming from safety requirements, e.g. strength and deflections, while others originate from the operation of the wind turbine as a system, e.g. the geometry of the blade. For the smooth operation of the wind turbine as a system, operational characteristics of the blade form constraints for the blade structure. These include the natural frequencies of the blade. Especially the first flap and edge bending natural frequencies have a direct effect on the dynamic response of the wind turbine system. Additional constraints on the structural design are posed through the limits on the blade’s deflection, the strength under extreme loading and of course the strength under alternating wind loading conditions during the operational lifetime of the blade (fatigue). Obviously the tip deflection limits are controlled through constraints on the stiffness, while the load carrying capacity of the blade is controlled through constraints on the strength (ultimate and fatigue). Combined constraints occur: strength constraints include buckling limitations, which are in turn affected by the (local) stiffness of the blade, see also GL [4] and DNV [5].

In addition, constraints on the structural design are imposed by manufacturing. These might include limitations set as a precaution for reducing manufacturing uncertainties, e.g. oversizing of gluing areas between adherent parts of the blade, or restrictions set as

[1] The standard for the design of offshore wind turbines IEC 61400-3:2009 covers load cases and component requirements that are specific to offshore wind turbines, referring to IEC 61400-1 for component requirements that are common to both on-shore and off-shore wind turbines, such as rotor blades.

limits on the manufacturing procedure, e.g. minimum thickness of composite material layers.

Therefore, to comply with the operational constraints following is considered during the structural analysis of the wind turbine blade ([4], [5]):

- Deflection
- Natural frequencies (modal analysis)
- Buckling
- Extreme Load carrying capacity (static analysis)
- Variable load carrying capacity (fatigue analysis)

Following the above, the structural design of the blade is integrated in the loop of the whole wind turbine design, since the mass and response of the blade (stiffness, etc.) affects the loading on the blade during the wind turbine operation. This integrated design loop is performed through aeroelastic simulations, where the blade is modelled in a simplified way (usually as a beam structure) with information on the mass and stiffness properties obtained through the detailed structural design, reaching up to the strains and stresses exhibited on the layer level of the composite structure.

According to GL and DNV-OS-J102, the material properties to be used in the design of a blade should be determined (through experiments) at the layer (lamina, ply) level. For ultimate load cases the multiaxial failure criterion recommended by GL [4] is the Puck criterion [9], while DNV [5] recommends the maximum strain criterion or modifications to the Tsai-Wu criterion [10]. For fatigue analysis requirements for both GL and DNV guidelines refer to the laminate, although DNV mentions that fatigue analysis may be conducted on the ply level of the laminate.

GL [4] requires that verification data should be provided for a sufficient number of sections along the blade length. Data should be provided at a number of sections (usually 10) between the root of the blade and the largest (local) chord section of the blade and at least at 10 sections between the largest chord section of the blade and the blade tip. The maximum distance between two sections is 2.5m.

The design of bolted and bonded joints in the blade is addressed in the design standard and the design guidelines only in general terms. Only directions are given for the design of the joint and/or test data are required to support assumptions.

An inherent requirement for the structural design of blade is to achieve a target reliability level. The design philosophy followed presently [11] requires that, the variability of loading and material properties, uncertainties in the measurement or estimation of these, as well as manufacturing tolerances is taken into account through application of appropriate safety factors. In this way safety factors are applied to increase the design loads (considering adverse conditions in load estimation) and decrease the material strength or elasticity properties (considering adverse effects on material properties, due to external conditions or degradation).

To ensure the level of safety requested for the certification of the wind turbine blade, given the state of the art in modelling methods available to the industry, all certification schemes necessitate verification of the design assumptions through testing of a full-scale blade. This full-scale blade test actually involves a series of testing usually on a single blade from the production series and is performed following IEC 61400-23 [12].

2. Structural analysis models

Current wind turbine blades are massive composite structures. As such their internal structure comprises a large number of different composite material layers, each resulting in different effective properties, depending on the constituents (fibre and matrix) as well as their positioning (orientation of fibres, stacking sequence of different layers, etc.).

The analysis models described in this section are derived from a literature review on structural wind turbine blade models, extended through input from the IRPWIND partners on their tools. Focus is given, therefore, on analysis models that are developed and/or used by the partners of IRPWIND and the EERA JP-Wind SP "Structures and materials".

In the present report, the loading is assumed to be independent of the structural blade design and is regarded only as an input parameter. In other words, it is assumed that the tools and methodologies used in the structural design are detached from the full wind turbine design loop, in order to allow assessment of these tools.

Current state of the art aero-elastic tools, such as Bladed and Focus [6] used for the prediction of loading on the rotor blades but also for the assessment of the whole wind turbine, model the blades encompassing finite elements with beam formulation, specially adapted for more accurate predictions of the wind turbine response (e.g. [7] and [8]). Therefore, information regarding the loading and the response is given in terms of the beam model, and then this information has to be interpreted to enable feeding in the structural model of the blade for further analysis.

To perform a detailed structural design of the blade, examining the internal stress distribution within the blade a 3-D finite element model of the blade is necessary [13]. Such a model comprises thousands of composite shell elements, typically using commercial finite element analysis codes (e.g. [14], [15]). Elements suitable for modelling thick layered, anisotropic shells are usually used. Such a blade model is shown for example in Figure 1. The tip of the blade is cut off to enable view of the modelling of the internal structure. In some cases, solid (or brick) elements in combination with shell elements are employed to refine the analysis of the blade (e.g. [16]).

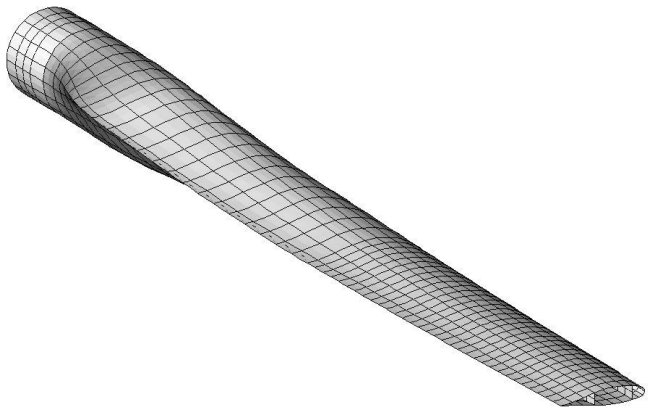

Figure 1 Example blade model

The modelling level required for accurately and effectively predicting the response of the wind turbine blade is still a matter of investigations, especially regarding the local stresses, which play a significant role in damage initiation (e.g. [17]).

Within the EC co-funded research project INNWIND.EU (www.innwind.eu) a benchmark study on the structural analysis tools of wind turbine blades has been carried out [18] with the participation of six organizations, where estimations on strains, stresses and critical buckling loads were compared among others. It suffices to note that all partners employed multi-layered shell or solid finite element models to provide all or part of the requested data for comparison.

Due to the high computational cost of three-dimensional finite element models, they are not suitable for direct use in a system of aero-elastic analysis [13], [19]. The aero-elastic simulations result in a distribution of sectional stress resultants along the blade length. To use this to assess the structural efficiency of the blade, the loads resulting from aero-elastic simulations have to be converted to allow application as external loading on the 3D finite element model of the blade. This will be discussed in more detail in a following section.

On the other hand, the size of multi-MW-sized blades requires blade and wind turbine designers to consider the structure of the blade and its response earlier in the design process [13]. To accurately represent the mechanical properties of the full 3-dimensional blade in the 1-dimensional beam element, for the load estimation using aero-elastic codes, approaches for estimation of the sectional properties along the blade length have been developed. There are several tools available for extracting the three-dimensional information of composite rotor blades into one-dimensional beam elements, e.g. [20] and [21]. Chen et al. in [22] assess the output of these tools. It suffices to note that all partners participating in the INNWIND.EU benchmark of structural analysis tools presented the sectional properties estimated through in-house codes [18].

Going one step further, to take advantage of modern aero-elastic codes and be able to perform the necessary detailed strength, stiffness and/or stability assessment directly after stress resultants at each section have been calculated, approaches for sectional analysis have been developed. This way a closer and more effective interaction between codes performing aero-elastic analysis for the wind turbine system and tools used for the blade structural design is achieved. Yet, despite the multitude of numerical tools for extracting the properties along the blade length, there is less work dealing with transforming the one-dimensional results of aero-elastic codes to detailed internal strain/stress analysis of the three-dimensional structure. This is, nevertheless, an essential step in the loop during the structural design of the wind turbine blade, if detailed finite element analysis is to be kept to a minimum, while keeping up to date information on the necessary structural modifications of the blade during the complete aero-elastic analysis of the wind turbine.

In the INNWIND.EU benchmark [18] several partners provided results for comparing strains, stresses, failure indices under both ultimate and cyclic loading based on estimations from in-house developed tools. Details of the underlying theory and the capabilities of each of these tools can be found in references in [23] and [24] for THIN (CRES), [25] for PROBUST (University of Patras), [26] for BASSF (CENER) and [6] for FOCUS (WMC).

Of course, the accuracy of these models is inferior to that of three-dimensional finite element models in terms of stresses and strains developed on the composite material level. Yet, their capability of directly using results of aero-elastic codes, as well as the tailor-made output to allow an adequate description of the blade structure for performing aero-elastic simulations raises their value, especially if proven to be of acceptable accuracy. The latter will be discussed in a subsequent section of the present report.

2.1 Boundary conditions

Should the analysis be performed by use of a finite element model consideration of boundary conditions is necessary. Excluding transport and installation load cases, the blade is constrained only on the root section of the structure. Modelling usually assumes a rigid connection to the hub by restraining the nodes on the root of the blade, neglecting elasticity of the pitch bearing or the hub, or (in the case of the full-scale testing) of the reaction wall of the laboratory. Within the INNWIND.EU benchmark the majority of the partners preferred restraining all degrees of freedom (i.e. translational and rotational) for the nodes forming the root of the blade. One partner restrained only the translational degrees of freedom for these nodes, assuming a more flexible connection between the root and the "hub". This selection resulted in differences in strains and stresses predictions, limited, nevertheless in the root area. The differences in strain could reach twice the average strain value of other partners. Another option is to use rigid links to constraint the centre of the root section and connect with the actual nodes on the root, as in the case of the simulations performed within the IRPWIND by CENER relevant to the loading of the full-scale blade in experimental validations (see also Annex 1).

As mentioned earlier, for the application of the load results from aero-elastic simulation on the structural finite element model of the blade, the loads have to be suitably converted. The definition of an equivalent system is required to this end, which can be performed by modifying the methodology used for the evaluation of the blade strength on the basis of load component distribution during blade testing [12], as e.g. presented in [27]. An image of the distributed load in the flap and lead lag direction for the blade finite element model is shown in Figure 2. Even so, without proper treatment, application of the concentrated forces on the 3D shell elements could result in fictitious stress concentrations near the application points [28] or introduction of torsion not predicted by the aero-elastic simulation if the concentrated forces are applied on nodes on each section without adjustment for the torsion value produced [29].

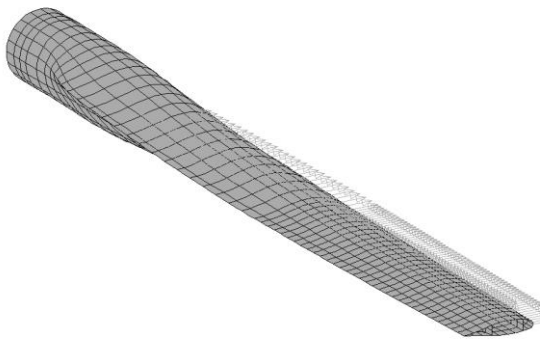

Figure 2 Example of point load distribution along the blade length

Alternative to the use of concentrated forces directly on the 3D shell element model links may be employed, by which the forces are applied at a point in the centre of the section and then, distributed through these links on the slave nodes on the blade structure [28].

Both methods, i.e. direct application of concentrated forces and use of rigid links were used by partners within the INNWIND.EU benchmark [18]. The results show that the most affected response is that of the torsion, especially on the outboard sections of the blade. Differences in the response prediction of up to 2 degrees were observed between those two groups [18].

Further to that, CENER performed a comparison of the damage under fatigue loading estimated by use of sectional analysis tool and 3D shell finite element model (see specific results in Annex 1). It was found that the loading of the sections through links (RBE3 equations in the specific case) strongly affects the results leading them to conservative estimations. This indicates that further study on the modelling of the loading on the blade is necessary.

2.2 Joints

As already mentioned of special importance are the joints of the blade, whether bolted (e.g. for the connection of the blade on the hub) or bonded (e.g. between the shear web and the caps).

Analysis for both joint types is usually performed as a sub-modelling case during the blade structural design. For bolted joints the VDI 2230 [30] is used, as for example presented in [31] for the blade root connection or in [32] and [33] for the case of a 30m split wind turbine blade.

The adhesive joints (with the exception of one manufacturer) run through the entire length of the blade in the trailing and leading and between the spar caps and the shear webs, strongly depending on the manufacturing solution. Due to the complex stress state at the location of the joints, to properly address the joint strength during the design, solid finite elements are needed. As discussed earlier, these models are too computationally costly. In addition to that, the joints are sensitive to the small alterations of the joint geometry (adhesive thickness, width, etc.), which are in turn sensitive to manufacturing methods used. These, are hard to accurately capture during the design phase, thereby leading to assumptions relevant to the manufacturing tolerances in order to accurately model the joint and capture the joint behaviour.

Two paths are followed: the first uses engineering judgment and simplifications to provide solutions for the joint specifications. The second employs detailed sub-modelling on key locations. Yet, in this case, the research community is still investigating the best way to achieve the required accuracy of estimating the strength of composite material adhesive joints (see also discussion under section 2.3). Recommendations for analysis and failure predictions have been suggested in [34] for the aeronautics sector mainly addressing metallic adherents. Specifically for the wind turbine blades a discussion on the modelling of the bonded joint can be found for example in [35] and [36].

Bottom line, especially for the bonded joints of wind turbine blades the collection of design data, as well as the verification of design and manufacturing is performed through extensive testing. This experimental research path will be discussed in section 5.

2.3 Failure criteria

When discussing strength, irrespective of whether this is under semi-static or cyclic loading conditions the subject of failure function should be addressed. For composite materials the designer has available a large number of failure criteria, which lead to different results. The differences in failure predictions using these criteria increase with the complexity of the exhibited loading and the material layout.

This issue is supressed in the design of wind turbine rotor blades, due to the fact that the certification bodies ([4], [5]) specify the failure criterion that should be used. Therefore, in the structural design of the blade the modeller/designer follows specifications, at least for the cases under ultimate loading. Under cyclic loading, fatigue, the specifications of the design guidelines and standards are contradicting the requirement of performing calculations on the layer level of the material and require calculations on the laminate level.

Still relevant, the results of the world wide exercise on failure criteria for composite materials (WWFE-I) [37] under monotonic loading, exhibit large differences in the performance of the various theories studied including test cases relevant to wind turbine blade design. The predictions for failure initiation (first ply failure) for multiaxial laminates and predictions of laminate deformations are the most relevant for use in the design of blades. Yet, should these be verified through experiments, then the prediction of the final failure becomes of relevance. Important to note is that most of the theories applied and reviewed through this exercise include features of modelling non-linear stress strain behaviour under shear stress and degradation effects, the latter to improve predictions for the deformation of the laminates and final failure. In [37] authors provide recommendation to designers based on the findings of the exercise. Selecting the 5 best ranking theories under the 19 theories in the benchmark, recommendations are provided for application on the different test cases. The selected theories of [37] are:

- Zinoviev [38] using the Maximum Stress failure criterion with a post failure analysis. Theory applied assumes linear elastic stress–strain behaviour up to initial failure but includes a continuous correction for the effects fibre orientation change throughout loading.
- Bogetti [39] using a three-dimensional form of the Maximum Strain failure criterion, with allowance for non-linear lamina shear stress–strain behaviour and a simple progressive failure analysis.
- The well-known Tsai-Wu [40], [10] interactive failure criterion that does not explicitly identify failure mechanisms, assuming linear elastic material properties and reduced matrix stiffness after initial failure.
- Puck's theory [41], [9] considers three-dimensional failure and includes non-linear analysis to predict progressive failure.
- Cuntze's approach [42] is similar to Puck's in some respects but assumes interaction between failure modes due to probabilistic effects.

It is important to note that the WWFE-I failed to provide recommendations on initial failure prediction case of multi-directional laminates, which is quite important for the wind turbine blade design, mainly due to uncertainties regarding the available test data. In [37] it is recommended to increase the experimental data base in order to allow assessment of the theories' performance.

Supported by:

The long term response of the composite materials was not addressed within WWFE-I, nor has it been addressed in the second world wide failure exercise (WWFE-II) considering three-dimensional load cases of composite materials [43]. Yet, the performance of theories in predicting multiaxial laminate's response under 3-dimensional state of stress discussed in [43] becomes more relevant for state of the art wind turbine blades. This is so for two reasons: a) the laminate thickness is increasing significantly as the length of the blades is increasing which might give rise to stresses through the thickness, that cannot be further neglected, and b) 3-dimensional state of stress is exhibited in details of the blade, such as bonded joint locations (discussed above) and ply-drop locations, which are of importance for optimizing the structural blade design.

Capabilities of cracking and damage models to predict progressive damage are assessed within the third world wide failure exercise (WWFE-III) [44]. This benchmark involves comparison of predictions relevant to matrix cracks evolution, effects of ply constraints and stacking sequence, loading-unloading phenomena and failure due to stress gradients of multi-axial laminates, under in-plane stresses caused by in-plane loading, bending and thermal loading. Large differences in predictions have been observed between the various contributors in this exercise, while comparison against experimental data is pending [44].

Acknowledging that the current practice of the industry is depicted by certification bodies requirements for the wind turbine blades, under cycling loading there are available state of the art fatigue formulations, which consider multiaxial cyclic loading on multidirectional laminates, starting from the layer (lamina) level. Within INNWIND.EU benchmark most of the contributing partners took into account only the axial stress to estimate fatigue damage for the wind turbine blade. Consideration of multiaxial state of stress in fatigue formulation following [45] has been implemented by one of the participants in the benchmark [18]. Results show that in cases the damage estimated when taking into account multiaxial stresses is larger than that neglecting shear and in other cases the opposite holds, making conservative estimations when neglecting shear. More recent efforts in considering multiaxial stress state for multidirectional laminates are presented for example in [46], where the multiaxial fatigue model is based on Puck's failure criterion and in [47] and [48] where progressive damage is considered to estimate the fatigue life of multidirectional laminates.

CENER performed simulations relevant to strength prediction under extreme loading on the reference 86m blade using different failure criteria (for details see Annex 1). Tsai-Wu, Hill, Hoffman and Maximum strain criteria were among the applied ones. As expected, strength ratio estimations had large differences depending on the failure criterion. The following figure presents results along the blade length corresponding to the minimum strength ratio on each section. Depending on the stress condition on the various elements of each section the differences between the failure criteria increase or decrease.

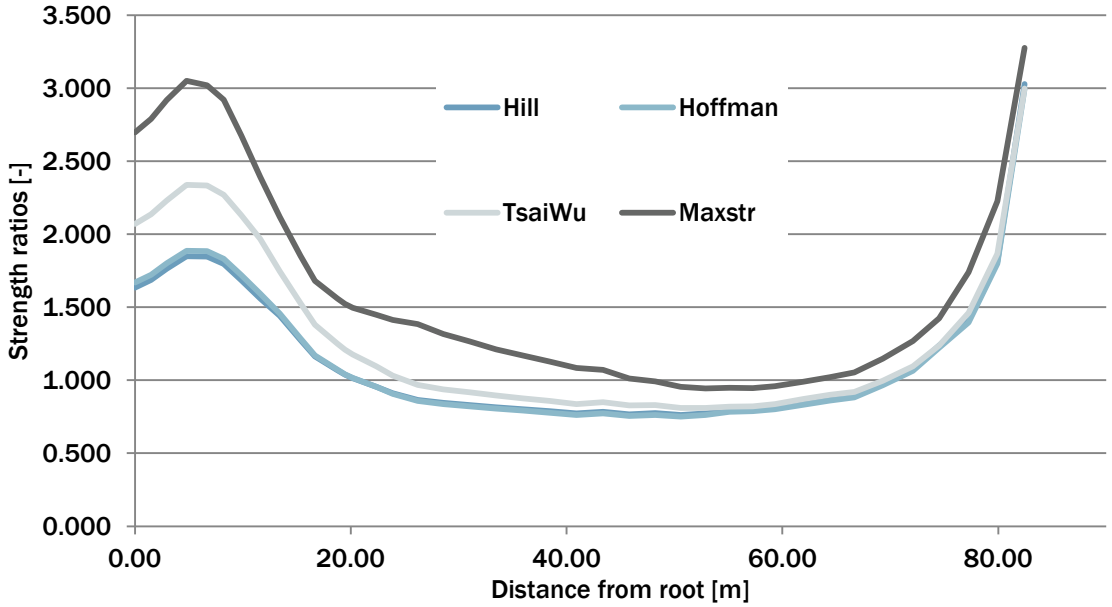

Figure 3 Minimum strength ratios along the blade span with different failure criteria

The above discussion supports the need for verification through testing for the wind turbine blades. The design community is still wary of the various formulations for the estimation of failure, partly due to the large differences between these formulations.

2.4 Model uncertainty

The work performed within the INNWIND.EU project [18] sets the baseline for the estimation of model uncertainty. As all partners were provided with the same information regarding the blade external structure, the internal material lay-out and configuration, as well as the loading that should be imposed on the blade it is possible to compare the output and assess the variability of the results. At this stage neither the accuracy nor the correctness of the numerical simulation results can be assessed, since for that purpose comparison against experimental data should be available. Yet, given the capacity of the participants in the benchmark study and their experience in comparing numerical simulation results of wind turbine blades against test data the relevance of the results is evident. Further to that the number of independent results increases the statistical significance of the data.

Since the benchmark covered both stiffness, as well as strength aspects, model uncertainty estimated through these covers most of the measurable parameters through an experiment. This issue was addressed in [11], where it was suggested that this model uncertainty could be estimated through experimental data. But, as discussed in a subsequent section of the present document, in this case there are additional uncertainties intervening and potentially blurring the statistical interpretation of results.

The results of the INNWIND.EU benchmark indicated that the gross properties of the blade (mass and centre of gravity) are estimated with a very low variation between the partners. Coefficient of variation is 1% for the blade mass and the position of centre of gravity along the length of the blade, while a standard deviation of 2mm in the flap direction and 30mm in the edge direction was noted for a section having a chord of about 6m. A little higher was the coefficient of variation for the sectional mass properties

(linear mass and mass moment of inertia). Disregarding the inconsistencies observed probably due to misinterpretation of reference coordinate systems between the partners, the coefficient of variation for mass properties of inertia is about 5%, while the standard deviation of the mass centre on the section is below 90mm in the edge and 20mm in the flap direction (on section with 6000mm chord). Similar results are obtained for the sectional elastic properties (axial, bending and torsional stiffness, elastic and shear centre). The coefficient of variation for the natural frequencies of the blade was found to be below 3% up to the 5th mode of vibration, i.e. mainly flap and edge modes. A larger coefficient of variation of about 5% was noticed for the torsional eigen-frequency of blade. Regarding the tip deflection of the blade under load, in two different load cases the coefficient of variation was found below 7% for the flap direction and up to 15% for the edge direction. These results include different modelling methods for the load, as discussed for the boundary conditions, as well as the non-linear analysis performed by DTU. The variation noted for the deflections is considerably reduced if the results of two partners are excluded. Specifically, disregarding the results of PoliMi, which did not include the third shear web of the reference blade in the model, as well as that of CRES, which modelled the mid-plane of the shell elements on the external surface of the blade, the coefficient of variation for the displacement drops to below 3%. The results by non-linear geometric analysis performed by DTU are close to the average of the other partners, possibly indicating that a linear analysis suffices for this case. The results of the INNWIND.EU benchmark on the torsion of the blade revealed larger differences. In this case, all differences in modelling affect the results. That is, even when excluding partners with modelling differences in the internal structure of the blade, as per the deflections, the standard deviation of the torsion is 1 degree. The difference in the torsion at the tip of the blade for the linear and the non-linear case is above 1 degree, indicating that the analysis type has an effect on the results for this case. Further to that, the different modelling of the imposed loads, as discussed in the previous section, also affects the results, leading to a difference of about 2 degrees.

Coefficients of variation of strain data reported within the benchmark were below 5% for longitudinal strains (along the blade direction) for positions on the spar caps, but, they were above 15% for positions on the leading edge and close to the trailing edge of blade. Even larger differences were obtained for the shear and transverse strains, irrespective of the position on the blade.

The same large differences were obtained for predictions of strength. Whether buckling, strength under extreme loads or fatigue, the estimations where in some cases double. Even for buckling predictions, which depend on the (local) stiffness and the loading the differences were above 50%. The modelling of loads was found as playing a significant role in these. Probably the differences in local stiffness, as indicated by strain/stress results also play a significant role. Similar for strength predictions, both under extreme loading, where multiaxial stress was taken into consideration by the participants, as well as for fatigue, where only longitudinal stress was considered, there were large differences, as discussed in the previous section.

3. Full-scale blade testing

Full-scale blade testing is performed following IEC 61400-23 [12]. The standard focuses on aspects of testing related to an evaluation of the integrity of the blade. The

fundamental purpose of a wind turbine blade test following IEC 61400-23 is "to demonstrate to a reasonable level of certainty that a blade type, when manufactured according to a certain set of specifications, has the prescribed reliability with reference to specific limit states, or, more precisely, to verify that the specified limit states are not reached and the blades therefore possess the load carrying capability and service life provided for in the design."

To achieve its objective IEC 61400-23 considers following tests:

- static load tests;
- fatigue tests;
- static load tests after fatigue tests;
- tests determining other blade properties (among them mass, centre of gravity and natural frequencies)

From the above tests the majority is used to assure the load carrying capability (strength) of the blade. Yet, some are used to determine blade properties in order to validate some vital design assumptions used as inputs for the design load calculations.

Following the standard a blade passes the test if the limit state is not reached when the blade is exposed to the test load, which in turn is representative of the design load. Under limit state the ultimate limit state and the fatigue are considered in the standard, whereby the limit state is the state of the structure and the loads acting upon it, beyond which the structure no longer satisfies the design requirements.

Inherent in the testing standard is that the design loads form the basis of the test loading and that according to the design calculation the blade is able to survive the design loading, i.e. no failure is predicted under the design loads.

The practical constraints within the blade testing are also recognized. Included in these are that the distributed load on the blade can be simulated only approximately, the time available for testing is generally one year or less (especially concerning fatigue tests) and that certain failures are difficult to detect.

For the determination of test loads to be applied on the blade, the IEC 61400-23 [12] requires the application of a blade-to-blade variation factor of 1.1 applicable to both static and fatigue test, as well as a load factor accounting for possible errors in fatigue formulation ranging from 1.065 to 1.015, depending on the number of fatigue cycles to be applied ($5x10^5$ to $1x10^7$ cycles). A factor accounting for possible more benign environmental conditions in the laboratory is also suggested in the standard.

For the static load test in general all locations are regarded as sufficiently tested if the loading during the test is equal to or higher than the target test load. For a fatigue test the test loading is generated such that it produces a fatigue damage equivalent to the fatigue damage caused by the target (design) loads.

It is recognized that the test will not exactly match the design situation. Purpose during the test design is to assure that the critical regions of the blade (as identified during the design) will be properly loaded during the test in order to confirm that the areas can sustain the load. Neither overloading nor benign loading is wanted, but, due to the load distribution achievable in the laboratory, it is certain that some of the regions will have lower loads (than in the design) and other will be overloaded. Compromises are foreseen.

With use of the reference blade used in the INNWIND.EU project, a test case for the flap direction using 5 pullers along the blade length was considered. The distributions of target and test load are shown in Figure 4. Clearly in some parts the test load exceeds the target and in other parts the opposite is experienced, showing at first glance a not so good approximation of the target load.

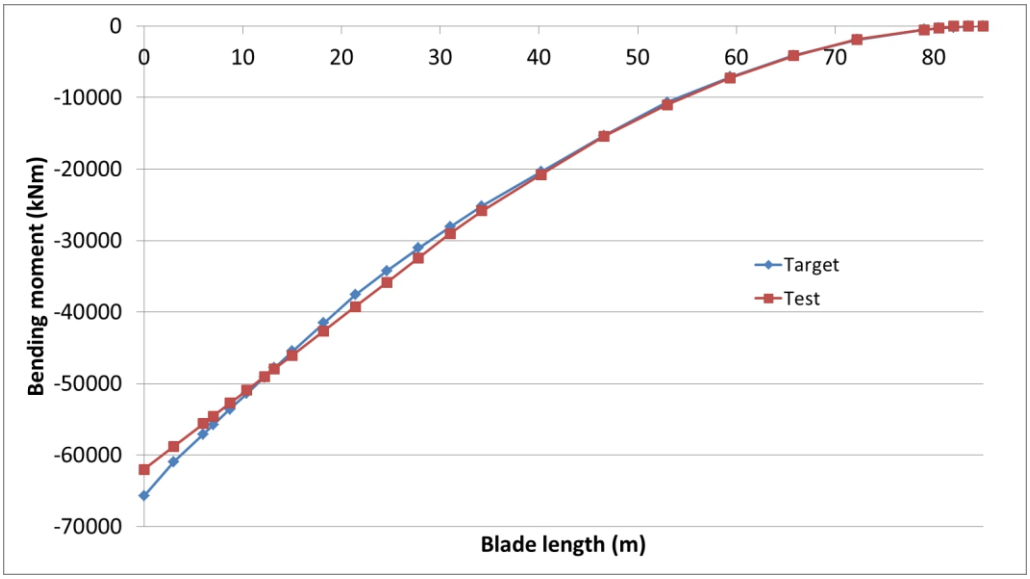

Figure 4 Example of comparison target versus test load for the reference blade

A closer examination of the differences between target and test values is shown in Figure 5, where the actuator position is also shown (with red lines). The inboard part of the blade is underloaded, while the part between about 10% and 75% of the blade length is overloaded with a peak of 5% at about the maximum chord section of the blade, which is considered as the critical section.

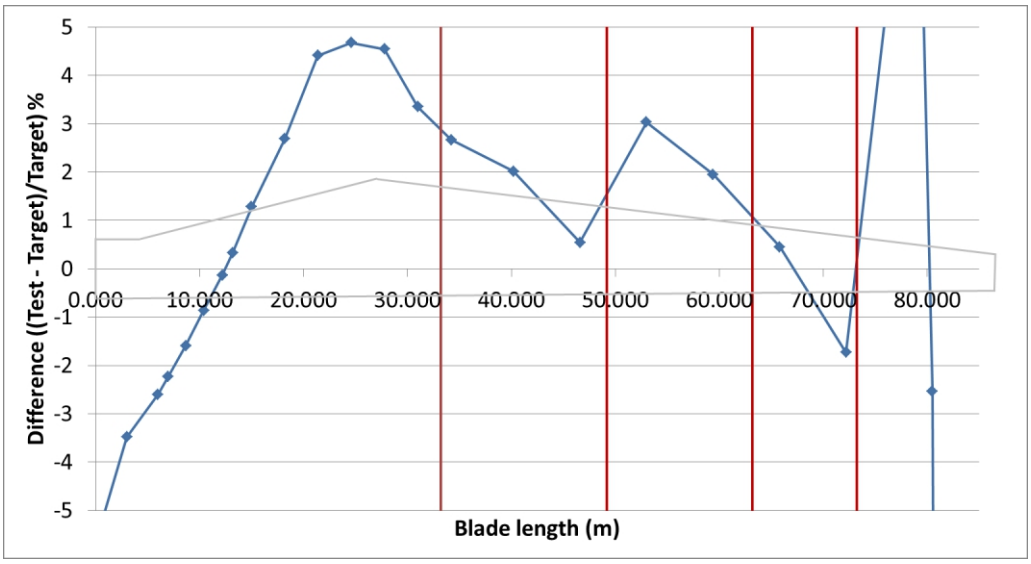

Figure 5 Example of difference between test and target load along the blade (actuator positions marked in red)

Looking at IEC 61400-23 directions the sections at the load introduction points should be disregarded at an area (along the blade) extending 75% of the relevant chord both

Supported by:

inboard and outboard of the load application position. This is due to the influence of the load introduction and the reinforcement provided by the saddles to ameliorate the action of concentrated forces on the blade shells. For the example case, the areas that should be neglected due to the above load introduction influence are marked in the following figure. This in turn means that increasing the number of saddles to closer approximate the loading along the blade length, necessitates neglecting larger parts of the blade (along the length) because of the influence at the load introduction points.

Going one step further the areas that should be disregarded since the blade at these locations is underloaded is shown in Figure 7, along with the previous mentioned ones. It is clearly seen that the areas can be actually tested against strength is quite limited.

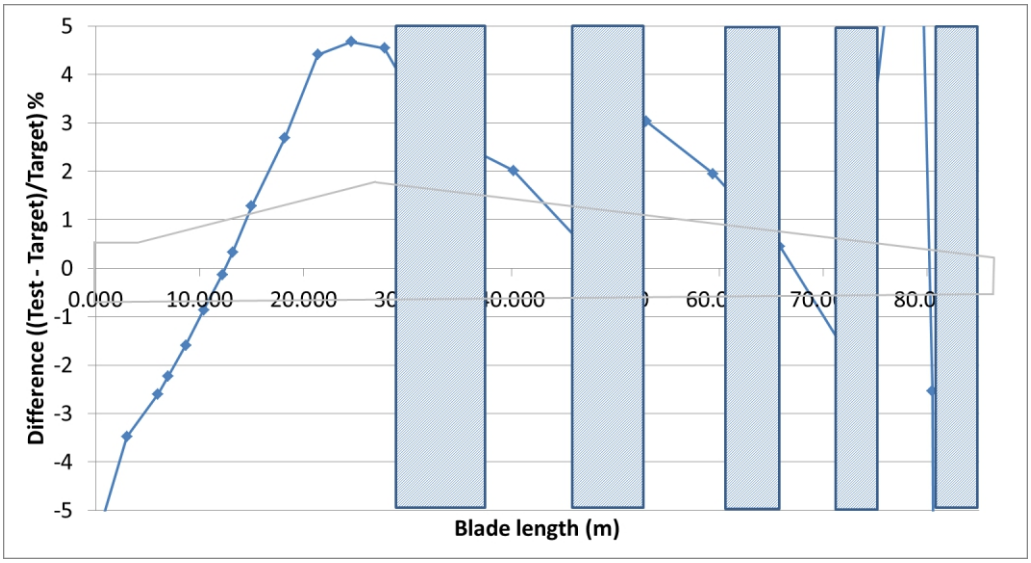

Figure 6 Areas to be disregarded during testing because of load introduction points along the blade.

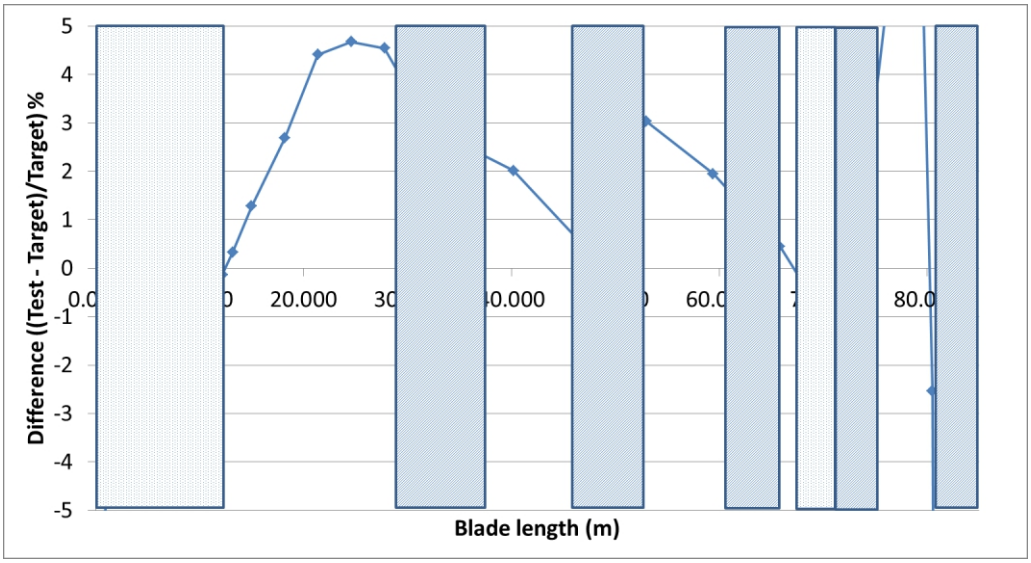

Figure 7 Areas to be disregarded during testing because of load introduction points along the blade and locations where test load introduced is lower than the target load case.

Supported by:

Working similar for the shear stress resultants along the blade the difference between test and target load is seen in Figure 8. In this figure it is also seen that the test shear stress resultants are for the largest part of the blade less than the target loads.

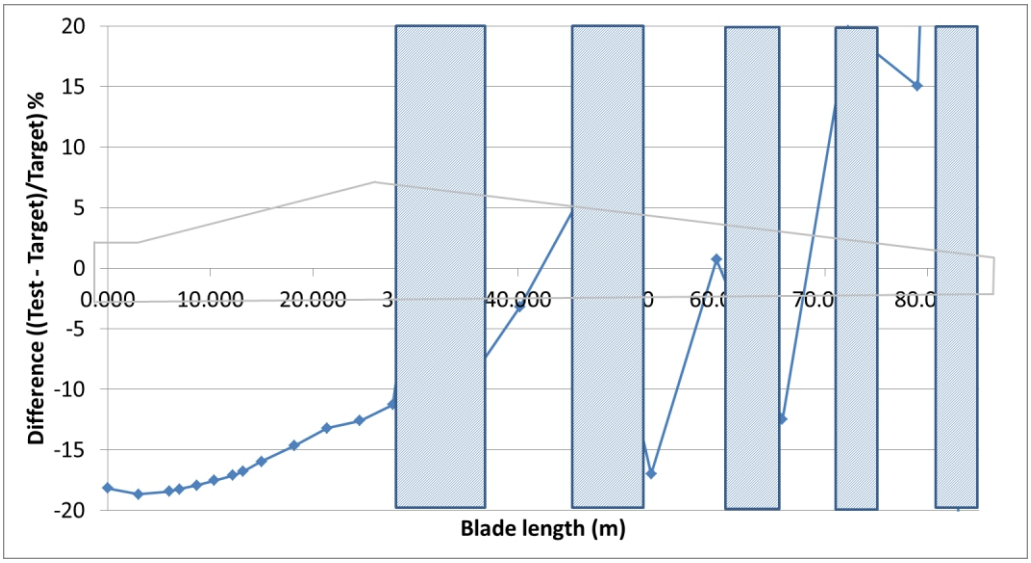

Figure 8 Example of difference between test and target shear load along the blade (areas to be disregarded due to actuator marked through boxes)

Increase of the applied load at the most inboard load application point to lift the test load in the root area (between 0% and 10% of the blade length), would result in an overshoot of the test bending moment at the critical area of the maximum chord section to about 7%. Still, the test shear stress resultants would be less than the target ones. The bending moment distribution for the test and target case are shown in Figure 9, while the differences between target and test for the bending moments and shear stress resultants of this case are shown in Figure 10 and Figure 11, respectively.

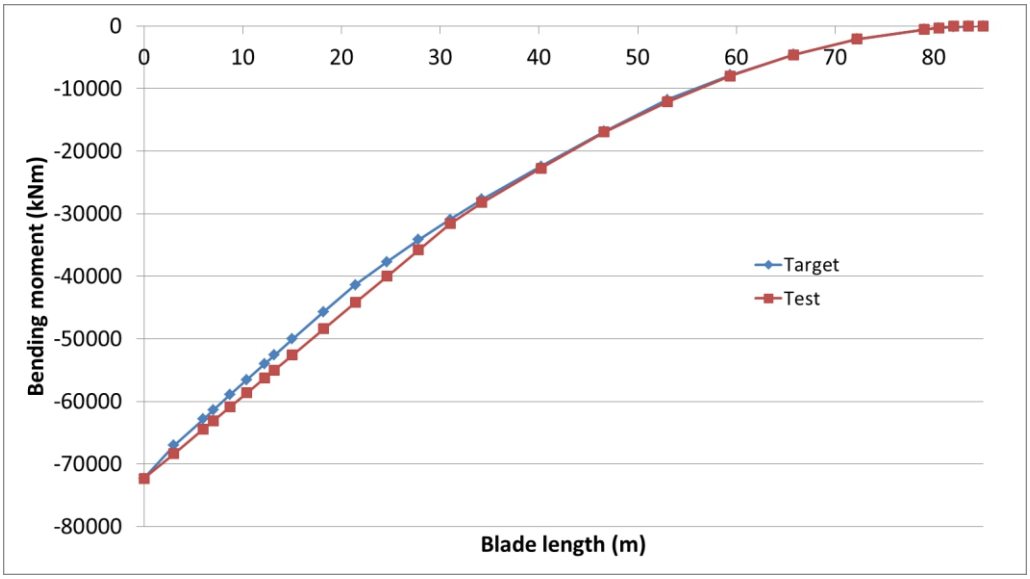

Figure 9 Example of comparison target versus test load for the reference blade (test load at root equal to target)

Supported by:

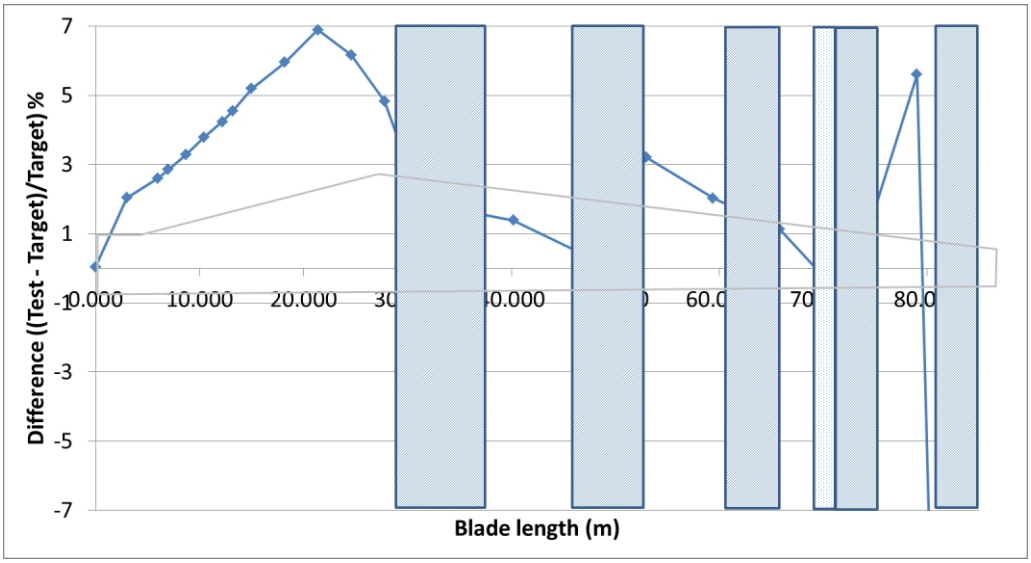

Figure 10 Areas to be disregarded during testing because of load introduction points along the blade and locations where test load introduced is lower than the target load case for load shown in Figure 9.

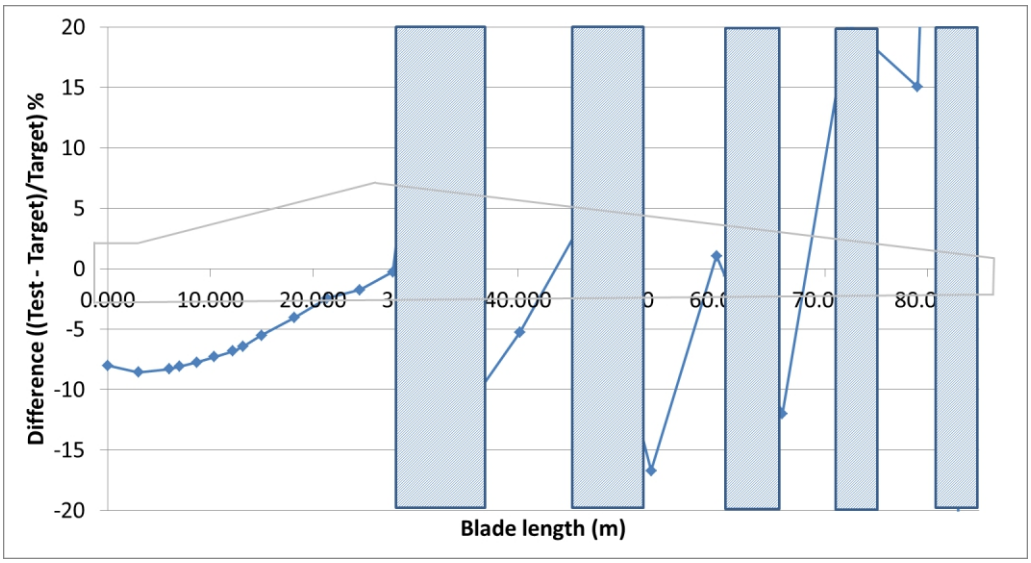

Figure 11 Example of difference between test and target shear load along the blade (areas to be disregarded due to actuator marked through boxes) for load shown in Figure 9

Despite the differences between the two test cases, especially regarding the higher overload value of about 7% in the second case, simulations with both test load cases in comparison to target load case performed by CRES, did not show alteration or increase of critical area on the blade, nor expectation of failure due to buckling in the overloaded area.

At this point it should be mentioned that the design load case of the reference blade used in INNWIND.EU was based in aeroelastic simulation results performed by DTU and reported in [2], but was adapted to the needs of the benchmark as explained in [18]. Thus, the proposed load case does not describe simultaneous applied loads across all sections and it does not cover all load cases that the blade should sustain (as in a

complete structural design of a blade). The performed adaptation to the sectional stress resultants might be also the reason for the different behavior of the bending moments and shear loads. It is also recognized that the selected "design" case might lead to non-conservative or conservative results regarding the blade strength output. Nevertheless, the "design" load case is considered to be effective for the purposes of this report.

CENER has applied the methodology described in the IEC 61400-23 standard for the simulation of the test for the 86m reference blade, considering single axis multiple location configuration (for details see Annex 1). In this application the number of pullers selected is 7 and the difference between target and test load is below 2% for all sections at least up to 75% of the blade length. Critical areas of the blade in this simulation are those that have a strength ratio below 1, with a focus on the section providing the minimum strength ration at 50.6m. The areas of the blade that should be neglected following the previous discussion are marked in the following figure. Maximum chord section at 24.5m as well as the section with the minimum strength ratio at 50.5m can be tested.

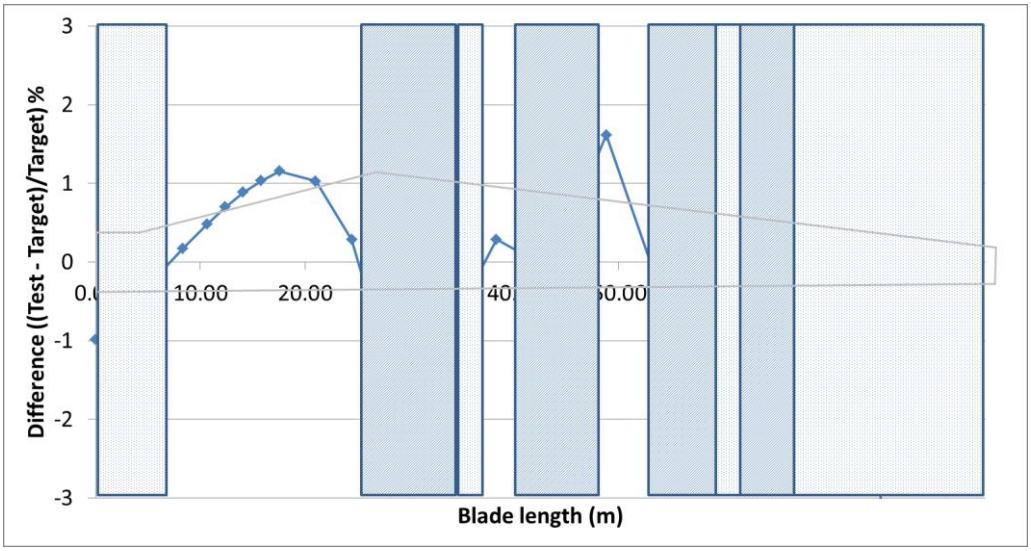

Figure 12 Areas to be disregarded during testing because of load introduction points along the blade and locations were test load introduced is lower than the target load case.

In Figure 13, the areas have a strength ratio below 1 are coloured light blue to red. On the left of Figure 13 the simulation results applying the design loads are shown (i.e. multiaxial loading along the blade length). On the right the simulation results of the single-axis test are presented (loading only on the flap direction). It is seen that the critical area is reduced towards the centre of the spar. In other words, areas of the trailing and leading side of the blade are loaded more benign under this testing configuration.

Supported by:

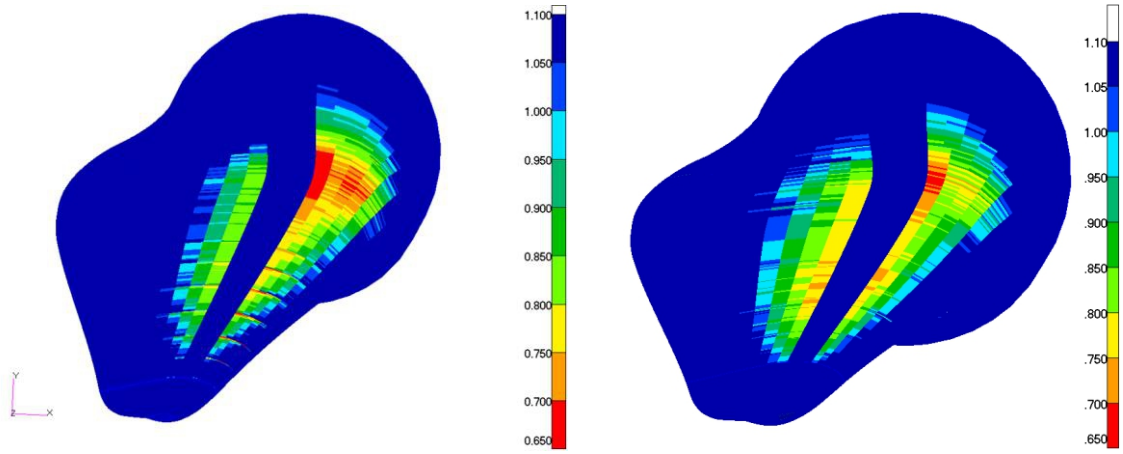

Figure 13 Example comparison between design (left) and single axis multiple location test loading (right)

The fact that parts of the blade are conservatively tested, while others are not loaded to the design/target load is extensively discussed within the IEC 61400-23 standard, both for the static tests as well as for the fatigue tests. For the fatigue case the reserve against fatigue failure can be expressed by the fatigue strain factor (FSF), the factor by which the load has to be multiplied to obtain damage equal to unity [49]. As explained in [49] in order to properly test a given area, the damage estimated by the test load must be equal or higher than the damage estimated through the target load. In turn, the FSF for the fatigue test load must be equal to or lower than the FSF for the fatigue target load. To enable comparison the relative fatigue strain factor (rFSF), i.e. the ratio of the FSF for the target load over the FSF for the test load [49]. Figure 14 presents results for the fatigue case, comparing the relative fatigue strain factor (rFSF) for a single axis, sequential flapwise and edgewise test case (on the left) and a dual axis, combined flap and edge test (on the right) [49]. Clearly introduction of dual axis testing achieves a larger area on the blade that is properly tested, than the single axis (sequential) case.

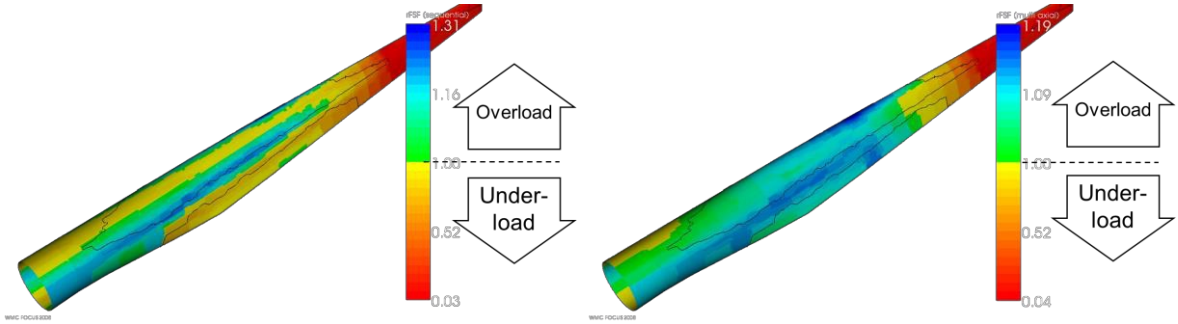

Figure 14 Sequential flapwise and edgewise test (left), combined flap and edge testing (right)

From CENER's work it is also seen that one of the reasons leading to increased stress ratios (i.e. benign loading) is that the multiaxial ratio is changing from design to test case. Taking for example the loading of section at 50.574m the stress ratio under the design load for Puck's Fibre Failure (FF) is 2.845, while for Inter-Fibre Failure (IFF) 0.672. For the test load the Puck's FF is 2.611, indicating that the stresses along the fibre direction have increased, but the IFF is 1.090, indicating that shear and transverse

stresses dropped. For failure criteria ignoring the failure mode (as for example the quadratic failure criterion and its expressions) the change in stress direction leads to increase of strength ratio.

To achieve the objectives of the standard it is the test designer's responsibility to assure that the critical areas of the blade are sufficiently loaded, even if this means that some parts will be overloaded. The stress direction ratios are ignored if a failure criterion identifying the failure mode is not used.

Failure during the experiment is classified in catastrophic failure, permanent deformation or loss of stiffness and superficial damage. To identify failure visual observation is required, while in the IEC 61400-23 standard it is suggested that visual inspection may be supplemented by infrared or ultrasonic inspection and recording of sound emission.

Catastrophic failure, including breaking or collapse of the structure, separation of parts, complete failure of structural parts such as bondlines, etc., is assumed to be readily observed during the experiment. According to the standard superficial damages, such as small cracks in laminate or bond lines, gelcoat cracking, paint flaking and surface bubbles, etc., if identified they should be evaluated to determine their effect on safety against catastrophic or functional failure. Possible stiffness loss or permanent deformation is identified by evaluation of the strain distribution and deflection of the blade during the first static test and both after the static test and after the post fatigue static test.

According to IEC 61400-23 apart from measurements relevant for the determination of the blade mass and the centre of gravity of the blade, the standard requires that imposed load and load direction is measured along with blade deflections and strains during strength tests. Deflection should be measured along the length of the blade with emphasis on measurements at high loads for the flap direction to validate tip deflections. Typically for strains on the skin of the blade, strain in the longitudinal direction is to be measured along the spar cap and at two positions (maximum chord and mid-span section) on the leading and trailing edge. For the webs, measurement by strain gauge rosettes for the shear strain near the root and at a section with high strain values is required.

Finally, according to the standard, uncertainty in measurement should be estimated reported for the magnitude, direction and location of any applied load, measured displacement and strain.

3.1 Blade to blade variation

Usually a complete series of test (modal, static, fatigue) is performed on a single blade. Therefore, information on the blade to blade variation due to manufacturing tolerances is quite limited.

In the early stages of wind energy development, within a research project PROFAR [53] a large number (37) of small blades of 3.4m length were tested to failure through static and fatigue tests by three laboratories (TUD, Risø and CRES) in order to determine among other issues the blade to blade variation. During this experimental campaign information regarding the mass and stiffness properties of the blades was also collected and statistically analysed in Jørgensen and Fahmüller [54]. The blades were manufactured by a single manufacturer using procedures that reflected the technology

used for manufacturing large blades at that time, i.e. hand lay-up. Det Norske Veritas (DNV) supervised the manufacturing procedure to attain the required high quality manufacturing process.

The coefficient of variation for the total mass of the blades was 2.1%. The coefficient of variation for the centre of gravity of the blade was 0.9%, i.e. even lower than that of the blade mass. Laboratory to laboratory variation in these measurements was judged negligible [54], but it has to be noted that at that time no laboratory estimated measurement uncertainty for their results.

The first and second flapwise, as well as the first edgewise natural frequencies were measured along with the damping ratio for 32 of the blades. The experiments revealed a coefficient of variation for the blades' natural frequency from 1.1% to 2.3% [54]. Some laboratory to laboratory variation should also be taken into account, since the testing procedure and equipment was not the same for all laboratories. The damping properties were measured for some of the blades (23) and showed a coefficient of variation of 13.7% for the first mode in the flap direction and 6.7% for the respective mode in the edge direction [54]. Since this variation is the result not only of blade to blade variation, but also laboratory to laboratory as well as testing conditions and analysis within each laboratory, the variation of the damping properties is not thought as inherent to the blades.

The bending stiffness of the blades was estimated during the PROFAR experimental campaign through measurements of exhibited strain and load during initial static tests (not strength test) performed on each blade by the three laboratories. At this point it should be noted that the location for the strain measurement was marked on the mould of the blade, leaving a permanent hairline mark on the blade, so as to eliminate strain gauge position differences between the laboratories. In Jørgensen and Fahmüller [54] it is reported that coefficient of variation of stiffness (EI) in the tensile and compressive side of the blade along the length of the blade (in the range 0.06R to 0.8R) varies from 6.8% to 15.7% depending on the strain gauge position. Yet, in the report it is also noted that laboratory to laboratory variation is present in these figures, since if the results of each laboratory were treated independently a coefficient of variation below 10% would be seen for all measurement positions.

Results regarding fatigue tests from the large experimental campaign in the PROFAR project are presented in [55] and [56], see Figure 15. The blades were designed to fail either in a section near the root or in the aerodynamic part of the blade. The results include comparisons of blade fatigue tests in both flapwise and edgewise loading, with fatigue tests on specimens having the same laminate as that of blades. Variation in results includes material uncertainty, laboratory to laboratory variation as well as blade to blade variation. A rigourous analysis has been performed in order to arrive at this rational experimental data comparison. Although most of the parameters were specified for these fatigue experiments, differences between testing procedures at each laboratory affected the results. The main differences were the strategy for updating the stroke in these displacement driven tests, as well as the non-linear relation between the actuator force and the blade bending moment at the position of interest, due to the large deflections exhibited. Adding laboratory to laboratory variation, on top of the blade to blade inherent variation, increases the scatter of the test results, as discussed in the next section.

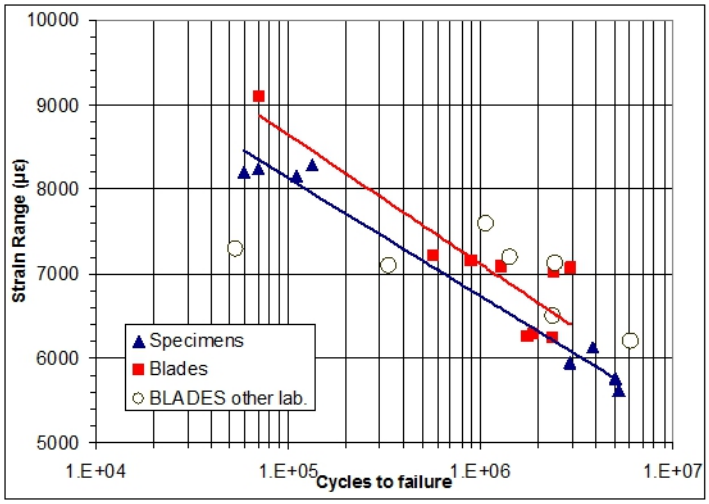

Figure 15 Example of PROFAR results. (Blue triangles: coupon tests conducted by CRES, Red squares: blade tests conducted by CRES, Open circles: blade tests conducted by other laboratories)

It should be noted that the above blade to blade variation analysis has been performed using small blades manufactured by hand lay-up. Therefore, these results presents only an indication for the current blades, which are of uncomparable size and are manufactured with more controlled methods, such as resin injection and prepreg technology. This technological improvement in combination with the higher quality monitoring methods applied today during manufacturing is expected to lead to reduction of blade to blade variation in the same production line.

The difference between the results by coupon tests and those by blade tests shown in Figure 15 is by large attributed to the different loading control used in the two sets of experiments; coupon tests were performed by load control, while blade tests have been performed as indicated above by stroke control. For the tests in the edgewise direction the blade data were below the coupon results in relevant S-N graphs. This difference was due to initialization of crack along the bond line of the trailing edge at largest chord. Crack initiation period was exhibited mainly at less than 10% of the fatigue life. Further crack development took place in the laminate starting from the trailing edge in transverse direction. For tests in edgewise direction blades were regarded as collapsed if loss of stiffness exceeded 20%.

In [55] blade results have been treated to account both for the different stroke updating strategy and the non-linear behavior between actuator force and stress/strain on the section. Rainflow counting method was applied and an equivalent stress load at the area of interest, actually at the blade failure location, was determined. Using the processed results the comparison between blades and coupons strongly improved, even for the tests in the edge direction, leading to the conclusion in [55] that coupon test data can serve as a reasonable accurate first impression of the blade fatigue behaviour. Figure 16 presents the raw coupon and blade results of the PROFAR project from [55] with respect to the strain range on the left, while on the right the results of the analysis performed using equivalent stress load for the blades tested for failure in the root area is presented in the right [55].

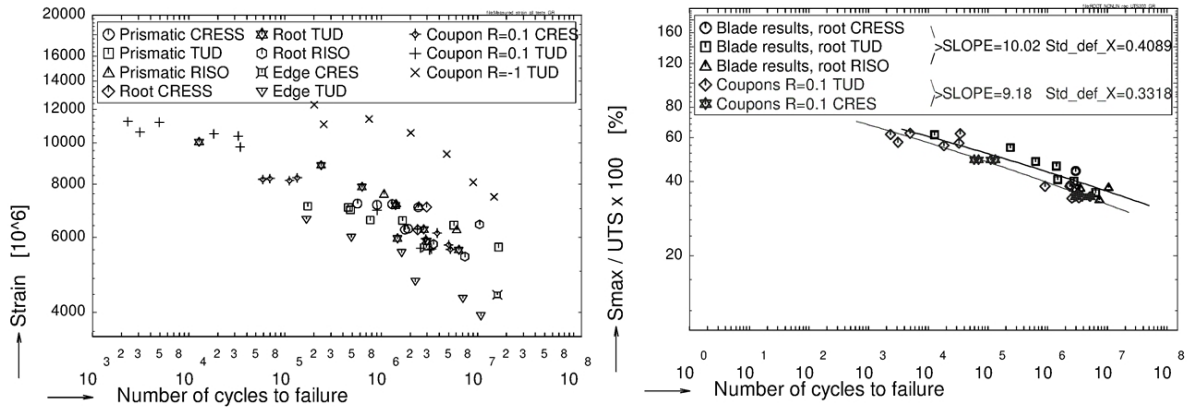

Figure 16 Raw results with respect to strain range of PROFAR blade and coupon tests (left). Comparison of blades vs coupon results with respect to stress range after reanalysis (right) [55]

3.2 Laboratory to laboratory variation

Laboratory to laboratory variation is expected in the tests performed for blades. The effect of the different testing methods was the concern of a past SMT research project [57]. In this case 7 commercial blades were tested by 5 different laboratories. The test plan resembling a blade certification test plan, yet, not reaching the target test loads to avoid failure was common to all laboratories. However, the specific methodology for performing the test, taking measurements and analysing the experimental data was free to each participant. To facilitate comparison some common locations for application of strain gauges were marked on each blade by a single participant. The results obtained were similar to the ones discussed earlier (see section 3.1) relevant to the mass and centre of gravity of the blade with a coefficient of variation of about 1%. Yet, in this case the results for the natural frequencies were higher, ranging from 2% to 4% and up to 6% for the torsional mode, which was not part of the measurements in PROFAR. As noted earlier the differences in damping ratio estimations are large and these are mainly the result of significant differences in testing procedures. Using the information from the strain and load measurements from each participant in [57] also the sensitivity to the strain gauges on the flap and edge load is compared. Longitudinal, transverse and strain at 45º (for shear) were measured. Result show that the coefficient of variation is quite large. For the longitudinal strain under flap loading the coefficient of variation is on average 10%. Under edge loading the coefficient of variation for the longitudinal strain is 15%. Similar is the outcome for the shear strain under flapwise loading. But the results under edgewise loading and those for transverse strain show that there are huge underlying differences.

Reporting of measurement uncertainty was introduced later than the discussed projects above, as the result of adopting laboratory accreditation criteria and the relevant IEC 17025 standard [58], with its initial edition appearing in 1999. The standard requires the expression of measurement uncertainty, which should follow the procedures described in relevant guidelines, such as the latest ISO/IEC Guide 98-3 [59], first appearing in 1993. However, the testing procedures for wind turbine blades, involve simultaneous measurement of many parameters, with commonly agreed procedures for reporting uncertainty not yet available.

The measurement uncertainty from tests on blades is not reported publicly. Recently the discussion opened within the IEC Certification Advisory Committee (IEC CAC). As a preliminary step the results of an Interlaboratory Comparison (ILC) for Participants Conducting Structural Blade Tests to IEC 61400-23 performed within the frame of IEC CAC Test Laboratory subgroup, might shed light on this [60].

4. Verification through testing

The certification standard IEC 61400-22 [61] and the certification bodies require the verification of the blade structural design and the assessment of the suitability of manufacturing processes is done through full scale testing performed following IEC 61400-23. As described in the previous section, the aim of the test is that the blade sustains the loading imposed during testing without damage, and in parallel to confirm the values that were used as input in the design phase for the blade properties. In the latter case, the input values mainly refer to stiffness and mass properties, which drive the response of the blade and in turn the loading computations performed through aeroelastic calculations.

GL [4] prescribes allowed deviations between design values and experimental data: Deviations of at most ±7 % for the bending deflection, ±5 % for the natural frequencies and ±10 % for the strains are permissible as a rule.

Usually the comparison between test results and design values is performed by the blade designer. Testing laboratories that perform experiments on full scale blades might have such information, but they are in most of the cases bound by confidentiality agreements. Therefore, comparisons between test and simulation data with adequate information provided on the details of the simulation model or scarce in the literature. In those cases that comparisons are published, the results are presented in graphical form, rarely providing detail results on differences between simulation and experiment (especially blind simulation results) and never presenting uncertainty in measurements. Usually these comparisons are provided to support investigations for failure estimations.

Such an example is the recent reference [50], where a series of static tests leading to failure for a 2.5MW wind turbine blade is presented. Simulation results for deflections and strains in the longitudinal direction are compared against experimental data in graphical form. While the deflections and the strains in most locations seem to be in good agreement, there are no explanations provided as to the large differences observed in strain data on one of the measurement locations.

On the other hand it should be noted that in comparing simulation with experimental results mostly through a single blade test, the inherent variability of the blade properties and (in turn) response, as well as the measurement uncertainty should be taken into account, preferably separately.

During the recent symposium (2014) on the future of rotor blades it was discussed to pay additional attention to blade design detail verification through subcomponents In future editions of the DNV-GL guidelines.

4.1 Validation of failure prediction

Numerical models of wind turbine blades used for the structural design of the blade, as discussed in section 2 address the issue of failure initiation (onset). In other words, the

simulation results, in cases of static and fatigue strength refer to first ply failure. However, this is quite difficult to visually observe during the experiment. It is only at the time that the failure has progressed significantly to enable visual observation that the damage is noted. There are cases where large cracks go undetected, due to limitations in inspecting the blade's internal structure, or because these open (and become visible) during loading, while are closed (and therefore not visible) while unloaded.

During a static test (verification of strength under extreme loading) the blade is inspected after the unloading of the structure. Therefore, even if damages are detected without a monitoring method during the loading of the blade, there is no way to determine the exact load step of damage initiation. This is the reason also that monitoring of acoustic emission is suggested by IEC 61400-23 and other researchers (e.g. [51], [52], [62]) to enhance experimental findings.

The missing information on failure modes when using experiments to validate theories was also discussed in [43]. Information on initial failure, as well as failure mode observed during experiments is important to assess the response predicted through numerical simulation. Yet, this is also connected with the maturity of the methods applied for the "measurement" of the failure onset during the experiment. Visual observation alone does not suffice.

5. Methodology for testing subcomponents

To achieve experimental validation of the numerical tools used for the design of wind turbine blades, the component, as well as the loading conditions should be as close as possible to the model. Areas of the component, which deviate significantly from the model, cannot be taken into account during comparisons.

Testing of subcomponents is not a new introduction. There are several publications reporting on testing of subcomponents and blade parts. Yet, these present large differences as to the objectives of the testing performed. A review of such tests is attempted in this section.

5.1 Beam subcomponent tests

In the European Project UPWIND (2006-2011), beam subcomponents were numerically and experimentally investigated, aiming at development of a subcomponent for bondline testing of the shear web-flange joint in a rotor blade. The findings from all partners in this effort are summarised in [63]. Two sets of composite material beams were manufactured and distributed to several partners for 3- or 4-point bending tests. Recommendations resulting from the subcomponent experiments and several relevant references can be found in [64].

The work conducted within UPWIND on the beam subcomponents covers a number of issues discussed of significance to the work for the validation of numerical methods within IRPWIND. For example, on Figure 17 results on the deflection from numerical simulation are compared against experimental data. Numerical simulation denoted "FEM" in the figure was performed by CRES using information for the material as provided by the manufacturer of the beams and test results for the materials performed within the UPWIND project by WMC. Experimental data from tests performed by WMC are shown in the figure by continuous line denoted "exp.".

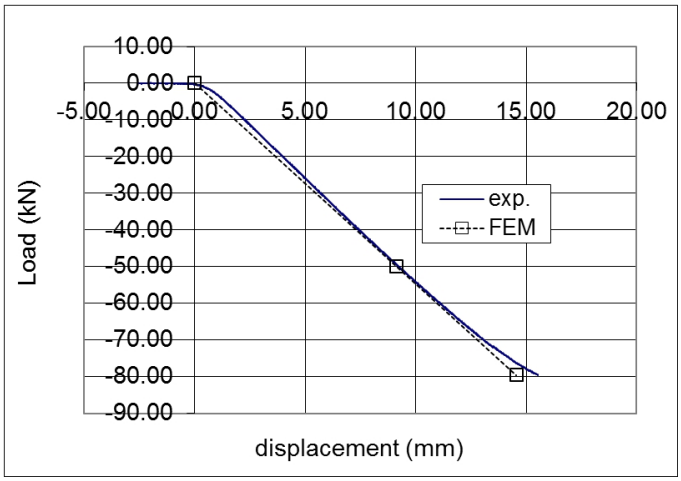

Figure 17 Comparison of estimation of deflection (numerical simulation) versus experiment

Similarly in Figure 18 the longitudinal and shear strain values are compared. In addition the experiment performed by WMC an experiment on the beam performed by CRES is also shown (marked on the figure with a red line). For the longitudinal strain (shown on the left) a good agreement between experimental data and numerical simulations is obtained. However for the shear strain (shown on the right) some deviation in the results is observed. It should be noted that the beam had a constant cross section along the length and for the above numerical simulation tuning on the material thickness was performed (i.e. the nominal thickness was used for the reinforced material). The measurement uncertainty in the strain measurements are in general in the order of 2%.

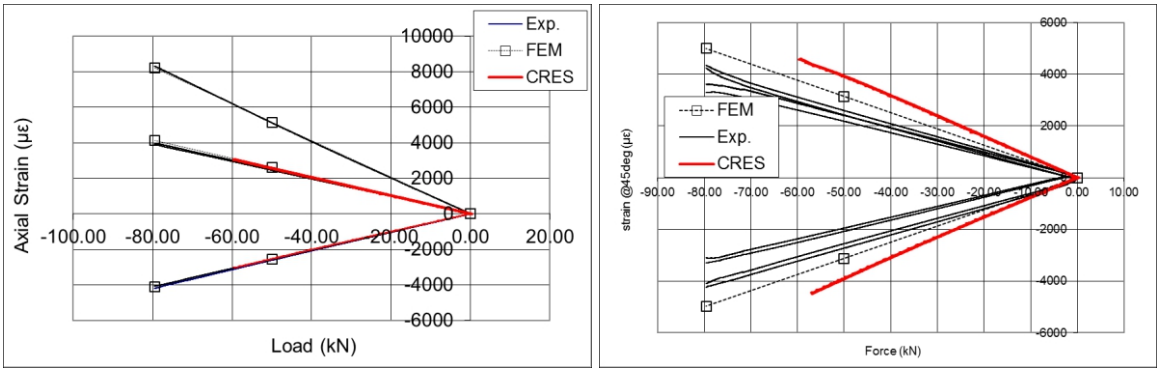

Figure 18 Comparison of estimation of strains (numerical simulation) versus experiment (left axial strain, right shear strain)

From a parallel study in [72] the deviation of the longitudinal strain on the top and bottom flange when compared to numerical simulation reaches 20%. However, this could be very well attributed to small variation in stiffness of the beam tested. In Figure 19 the bending stiffness of the beams tested within the UPWIND project is shown, as estimated numerically and observed during testing. Underscore H ("_H") refers to the symmetrically manufactured batch of the beams. Stochastic simulation using characteristic stiffness values for the material properties is denoted char. (95%), while the simulation using experimentally obtained mean values of the properties is denoted "exp." and "exp._H". Experimental data are taken from tests conducted by CRES and IWES. The lines on each bar indicate standard deviation. For both beam configurations

(unsymmetric and symmetric) the numerical estimation was more conservative. In all cases the range of the bending stiffness within one standard deviation is 5%.

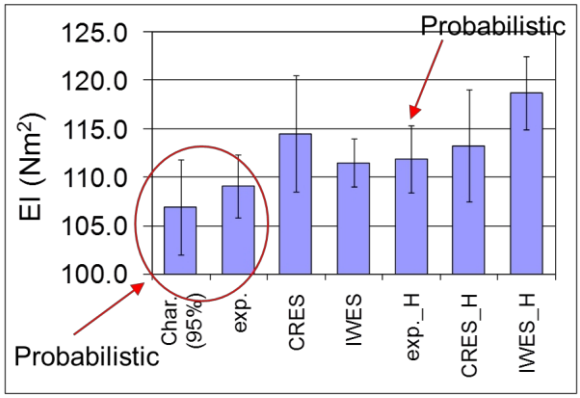

Figure 19 Bending stiffness probabilistically estimated and observed during testing (left side: unsymmetrical beams, right side: symmetric beams)

This variation in stiffness could very well lead to differences in estimation of strain of 20%.

5.2 Blade section tests

In a study done at DTU six specimens were cut from the load carrying box girder of a 25m Vestas wind turbine blade and tested to failure under a type of 3-point bending (see Figure 20) [65], [66]. The purpose was to study a very simple way to simulate the flattening of the cross-section. Such flattening may occur in wind turbine blades due to the so called Brazier effect.

The Brazier effect [67] is a geometrically non-linear effect resulting from high curvature when bending a slender, thin-walled structure. Because of the high curvature, the longitudinal compressive and tensile stresses result in transverse stresses towards the neutral plane of the beam. This causes flattening of the cross-section, which results in a reduction of the bending stiffness. The transverse stresses also introduce compressive stresses into the shear webs. These transverse stresses vary with the square of the applied load when the bending moment is proportional to the curvature as found by Brazier [67].

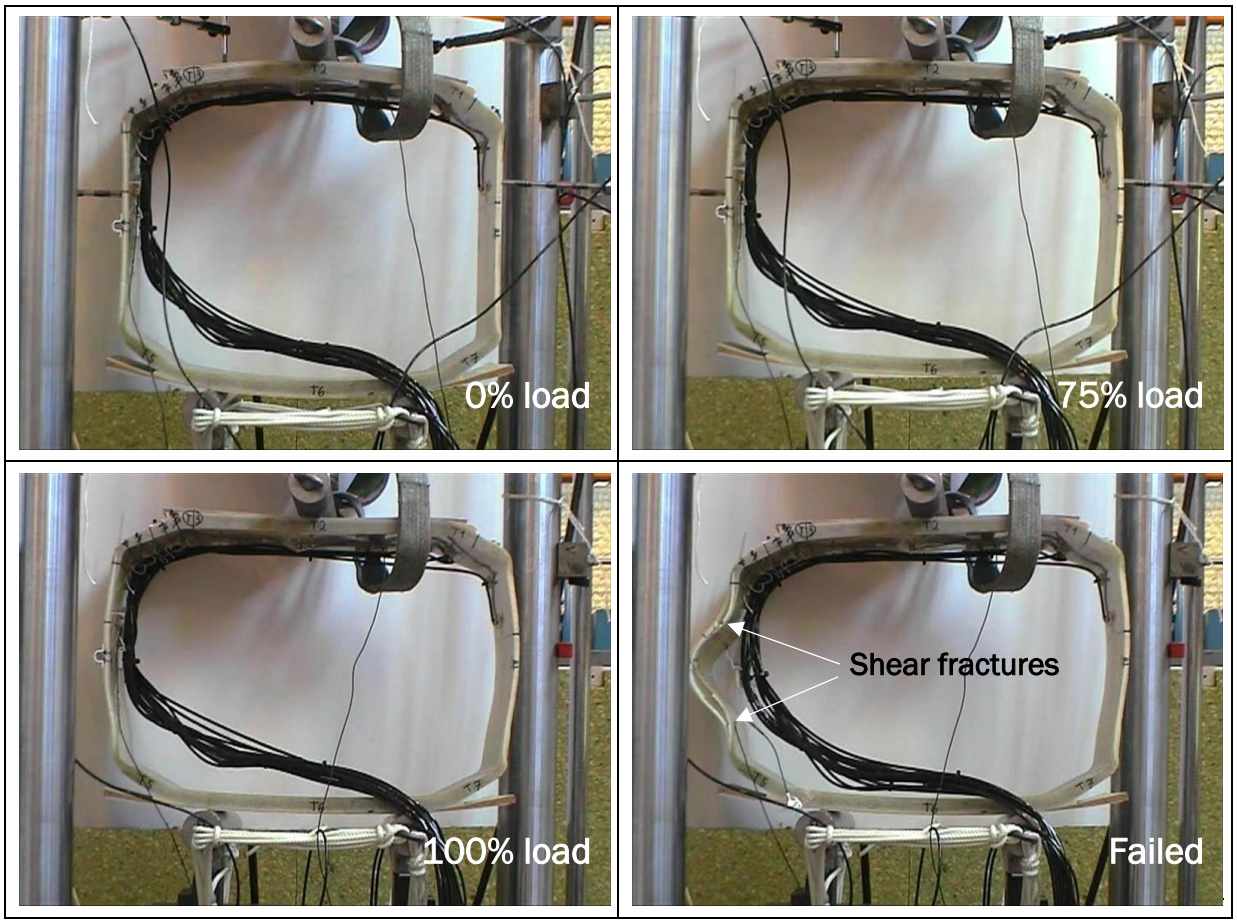

Figure 20 Picture sequence showing specimen deformation from unloaded to failure. First test series from inner part of box girder (30% length position)

In the study at DTU two series of tests were performed. For the first series three specimens of different depth were cut from a position corresponding to approximately 30% of the blade length from the root. For the second series three specimens of equal depth were cut from a position corresponding to approximately 60% of the blade length from the root. The specimens are found to be able to withstand a remarkable high forced displacement of approximately 10% of the specimen height.

The core in one of the webs is failing for all six specimens and the inner skin of the web is also failing in some cases. The probably reason for ultimate failure was found to be shear fracture in the core leading to delamination and ultimate failure [65].

These subcomponent tests lead to a greater understanding of the importance of transverse strength on the ultimate failure of wind turbine blades. And that the strength of the quite weak webs may govern the ultimate strength of the blades. Full-scale tests of wind turbine blades and load-carrying girders have shown substantial damage in the webs after ultimate failure [68]. It is normally difficult to draw solid conclusions on the failure sequence. However, there are indications from the full-scale tests that the ultimate failure, at least in some cases, is initiated by collapse of the sandwich webs due to the Brazier effect [68], [69].

Similar subcomponent tests were performed using sections from the load carrying box girder of a 34m SSP Technology wind turbine blade [70]. These tests were performed using a similar three-point loading arrangement. The DIC technique was used for strain

mapping on the sandwich webs to fully capture the evolution of strain with applied load. The high levels of shear also here led to shear fracture of the core, which resulted in collapse of the structure.

Even though the loading of these subcomponents is very different from what they experience in the full wind turbine blade, the tests have shown to be of value in order to observe the transverse strength of the load carrying box girders when they are exposed to flattening from the Brazier effect.

5.3 Trailing edge subcomponent tests

In a national Danish project headed by DTU, three 34m SSP Technology blades were tested to failure by loading the blades in a 30° angle to the flapwise direction. For all three blades pronounced buckling waves in the trailing edge region occurred before failure as shown in Figure 21

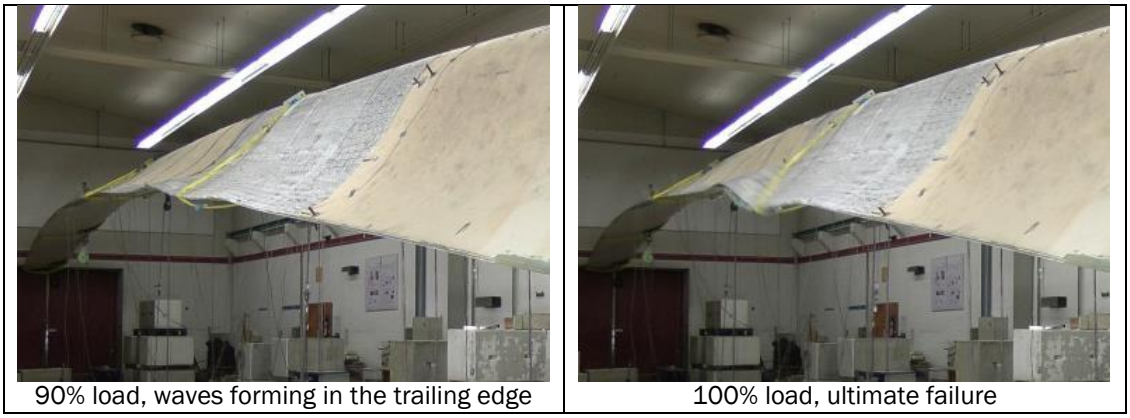

Figure 21 34m SSP Technology blade tested to failure by loading 30° to the flapwise direction

A test rig for subcomponent testing of trailing edge panels and adhesive bonds has been developed and constructed at DTU and a test series is under preparation. The test setup (see Figure 22) is designed for testing cut-outs of the same blades tested in full-scale. The cut-outs consist of the trailing edge panels, the shear web closest to the trailing edge and part of the caps.

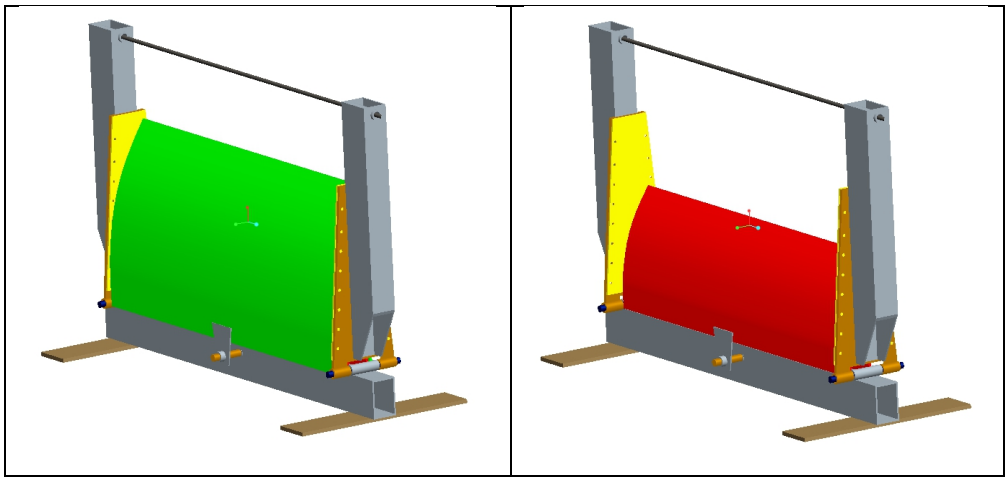

Figure 22 Test rig for subcomponent testing of trailing edge panels and adhesive bonds. Two subcomponent specimens from different lengthwise position are shown

Supported by:

The idea with the subcomponent tests is to mimic the compressive loading of the trailing edge panels and bondline, which this region is subjected to under predominantly edgewise loading in full-scale tests. Furthermore a minor bending moment generated by asymmetric loading is assumed to trigger the buckling waves in the trailing edge region as observed in numerical analyses and full-scale tests.

The focus will be on the buckling induced failure mode in the trailing edge. If failure does not occur in the middle part of the subcomponent specimen, then further specimens can be modified to force failure in the middle part of the specimen. This can be done by introducing crack in the adhesive bond and/or strengthening the boundary region. The load will be introduced in the test setup via a spindle and the load history is monitored via load cell designed for this setup.

The purpose of this subcomponent test setup is to check the compressive strength of the trailing edge region under a simplified loading. Another method is to test larger subcomponents with much more complicated and realistic loading along their boundaries. This can in principle be done by applying intelligent boundary conditions to the subcomponents. With the use of a detailed numerical model of the full blade the behavior of the subcomponent boundaries can be calculated and then applied during testing so that the subcomponent behaves as it was part of the full blade. Methods for obtaining and applying intelligent boundary conditions on larger subcomponent specimens are currently studied by different research groups, but we do not believe the technology is matured enough to be used for practical testing.

The method to test subcomponents under a somewhat simplified loading with a specific failure mechanism in mind is more realistic for practical testing at the present state.

5.4 Lessons learned

From the benchmark study conducted within INNWIND.EU, the strain state at various locations of interest was reported. Figure 23 shows the result under the reference load at the trailing edge, leading edge, on the pressure cap side joint with the shear web and at the middle of the suction cap. At the joint location between the shear web and the pressure side skin the ratio of the longitudinal strains over shear strains ranges between 7 and 17 along the blade length. On the trailing edge nose this ratio ranges from about 1 to 22. At the section of the largest chord (section at 26m) the ratio is around 15 for the locations on the trailing edge, the leading edge and the pressure cap joint with the shear web. However, caution is advised to the reader, since strains and stresses reported by the participants in the benchmark exhibited large variation.

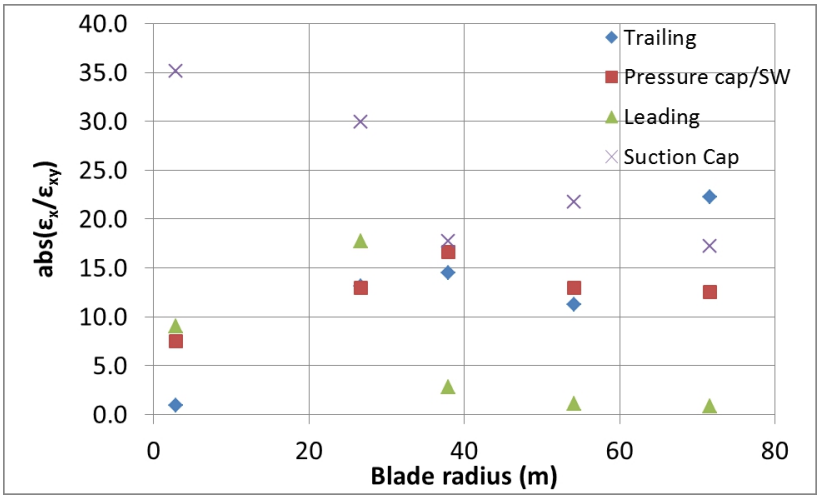

Figure 23 Longitudinal over in-plane shear strain at various locations along the reference blade.

The above range covers also the strain state investigated within [71]. Having such a broad range of strain/stresses it is expected that not a single test will match the multiaxiality anticipated for the full-scale blade. It is therefore, important to validate the numerical tools keeping a broader view of the multiaxial cases.

From the review conducted in the previous sections it is seen that if verification of failure and failure onset is sought for, it should be assured already from the design phase that the specimen will fail by the required failure mode at the location of interest. To achieve that and due to the uncertainties discussed for the estimation of failure prediction, other parts of the specimen should be significantly overdesigned. The latter is required to preclude failure outside the region of interest, because of the support or load introduction of the specimen. Support with structural health monitoring methods should be incorporated within the experimental design in order to allow “measurement” of failure onset in combination with loading condition during the test.

Measurement uncertainty should be reported from the testing laboratory. The researcher performing the experiment has a full understanding on the deviations from the design of experiment and what was achieved during the testing. Compromises made due to test limitations, as for example the force applied as a load follower in full-scale blade tests instead of having a specific direction during the whole loading procedure, as required during design, should be reported, in order to adjust the corresponding numerical prediction.

For a successful validation of simulation through testing it is important to know the structural details of the specimen. This includes information on material used as well as lamination sequence in the various locations of the test component. Thus, information on the manufacturing of the specimen should be shared with the simulation performing organization. On the other side, details of the support and loading environment are also important to be provided for the simulation. This information should be shared between the testing laboratory and the simulation organization.

Manufacturing tolerances, as well as testing tolerances should be taken into account when simulation estimates are compared against testing data. Information on manufacturing tolerances are quite difficult to estimate and account for, but locations on the testing component that differences between design and final product are more

pronounced can be identified. These provide also locations where it is expected that simplifications are introduced in the simulation/design environment. Therefore, differences are expected between test and simulation at these locations. It is more appropriate to avoid measuring directly on these locations. Tolerances in testing configuration may be approximated through measurement uncertainty analysis. In this case, the testing tolerances can be directly taken into account in comparisons between test and simulation results.

6. Conclusions

Clearly the full-scale validation tests set as a prerequisite during wind turbine blade certification as performed ascertain that the blade will sustain the design loading with a prescribed level of confidence. They do not, however, provide insight on the accuracy of the design methodology employed especially considering strength estimations. These full-scale tests were easy to perform at the early stages of wind energy applications, some 20 years ago. The size of the blades was limited to maybe 20m and the mass of a single blade was below 2 tonnes. Yet, at the current state of wind energy development, the popular size of the wind turbines is about 4MW operating with blades of 50m in length and weighing 12 tonnes, with designs for 100m long blades, weighing 40 tonnes appearing. It becomes obvious that relying only on the design verification through testing in full-scale is not an option.

According to the results of the various analysis presented in this document it is recommended to perform experiments for the validation of numerical analysis tools on subcomponents of the blade through which the subject areas with large uncertainties in modelling will be reduced. These include multiaxial strain predictions, predictions of buckling bifurcation, as well as strength estimations both under extreme and cyclic loading. Locations of major interest are the shear webs, as well as the trailing and leading edge of the blade. This was seen not only by the analysis in the frame of the testing standard review (section 3), but also by the variation of the results on numerical simulation predictions discussed in section 2.4.

7. References

[1] INNWIND.EU project, Grant Agreement No. 308974, www.innwind.eu
[2] Bak C, Zahle F, Bitsche R, Kim T, Yde A, Henriksen LC, Andersen PB, Natarajan A, Hansen MH, 2013, “Design and performance of a 10 MW wind turbine”, submitted to J. Wind Energy.
[3] IEC 61400-1:2005, Wind Turbines - Part 1: Design Requirements, 3rd Edition
[4] Germanischer Lloyd Industrial Services GmbH, Rules and Guidelines, IV Industrial Services, Part 2 Guideline for the Certification of offshore Wind Turbines, 2012
[5] DNV-DS-J102, Design and Manufacture of Wind Turbine Blades, Offshore and Onshore Wind Turbines, Det Norsk Veritas, 2010
[6] Brood RRH, Numan R, De Ruiter MJ, De Winkel GD. Focus 6 – Integrated modular wind turbine design tool, presented in Sandia Blade Workshop 2010, 2010 http://windpower.sandia.gov/2010BladeWorkshop/PDFs/2-2-E-2-Numan.pdf

[7] Riziotis VA, Voutsinas SG, Manolas DI, Politis ES, Chaviaropoulos PK. Aeroelastic analysis of pre-curved rotor blades, European wind energy conference EWEC2010, Scientific Track, 2010
[8] Jonkman JM, Buhl MLJr, Fast User's Guide, NREL Technical Report NREL/EL-500-38230, Golden, Colorado, USA, National Renewable Energy Laboratory (NREL), 2005
[9] Puck A. Festigkeitsanalyse von Faser-Matrix-Laminaten; Modelle für die Praxis, Carl Hanser Verlag, 1996
[10] Tsai SW, Wu EM, A general theory of strength for anisotropic materials, Journal of Composite Materials, Vol. 5, pp. 58-80, 1971
[11] Toft HS, Sørensen JD, Branner K, Nijssen R, Lekou D, Amezqueta Pueyo C. Probabilistic methods for wind turbine blades, EERA JPWind Report, SP-Structural Design & Materials, RT2, 2013
[12] IEC 61400-23:2014, Wind turbines – Part 23: Full-scale structural testing of rotor blades
[13] Veers PS, Ashwill TD, Sutherland HJ, Laird DL, Lobitz DW, Griffin DA, Mandell JF, Musial WD, Jackson K, Zuteck M, Miravete A, Tsai SW, Richmond JL. Trends in the design, manufacture and evaluation of wind turbine blades, *Wind Energy*, 6, 245-259, 2003
[14] Philippidis TP, Roupakias GS, Vionis P. Assessment of composite rotor blade structural modelling efficiency through comparison of FEM numerical results and experimental data, Tsipouridis JL, Proceedings of European Wind Energy Conference EWEC 94, 155-160, 1994
[15] Kong C, Bang J, Sugiyama Y. Structural investigation of composite wind turbine blade considering various load cases and fatigue life, Energy, 30, 2101-2114, 2005
[16] Jensen FM. Ultimate strength of a large wind turbine blade, PhD Thesis, Risoe, Risoe-Phd-34, Roskilde, Denmark, 2008
[17] Pardo DR, Branner K. Finite element analysis of the cross-section of wind turbine blades; A comparison between shell and 2D-solid models, *Wind Engineering*, 29(1), 25-32, 2005
[18] Lekou DJ, Bacharoudis KC, Chortis D, Fariñas AB, Amézqueta C, Nuin I, Pavese C, Berring P, Branner K, Bottasso CL, Croce A, Gualdoni F, Philippidis TP, Masmanidis IT, Roukis GA, de Winkel GD, Dekker H. Benchmark on structural design methods for composite wind turbine rotor blades, in Deliverable D2.21 Benchmarked aerodynamic-structural design methods, INNWIND.EU project, Grant Agreement No. 308974, 2015
[19] Malcolm DJ, Laird DL. Modeling of blades as equivalent beams for aeroelastic analysis, 41st Aerospace Sciences Meeting and Exhibit, AIAA-2003-870, Reno, Nevada, 2003
[20] Malcolm DJ, Laird DL. Extraction of Equivalent Beam properties from blade models, Wind Energy, 10, 135-157, 2007
[21] Hodges DH, Yu W. A rigorous, engineer-friendly approach for modelling realistic, composite rotor blades, Wind Energy, 10, 179-193, 2007
[22] Chen H, Yu W, Capellaro M. A critical assessment of computer tools for calculating composite wind turbine blade properties, Wind Energy, 13(6), 497-516, 2010

[23] Lekou DJ, Philippidis TP. PRE-and POST_THIN: A Tool for the Probabilistic Design and Analysis of Composite Rotor Blade Strength, Wind Energy, 12(7), 676-691, 2009
[24] Philippidis TP, Vassilopoulos AP, Katopis KG, Voutsinas SG. THIN/PROBEAM: A software for fatigue design and analysis of composite rotor blades, Wind Engineering, 20(5), 349-362, 1996
[25] Bacharoudis KC, Philippidis TP. Estimating design reliability of composite rotor blades under ultimate loading, Wind Energy, 2014; DOI: 10.1002/we.1728
[26] BASSF: Blade Analysis Strain Stress Failure. CENER, http://www.cener.com/en/wind-energy/en_signup.asp
[27] Bacharoudis KC, Philippidis TP. Structural reliability analysis of a composite rotor blade in ultimate loading, in Voutsinas S, Chaviaropoulos T, Proceeding of the European Academy of Wind Energy 3rd Conference: "The Science of making Torque from Wind" TORQUE 2010, Heraklion, Greece, 811-828, 2010
[28] Estarriaga J. Innovative load application procedure for loading wind turbine FE blades; PREGEN (pressure fields generator), CENER, INNWIND.EU report, 2014
[29] Capellaro M. Three methods for applying aerodynamic loads to a wind turbine finite element blade, University of Stuttgart, INNWIND.EU report, 2013
[30] VDI 2230, Part 1, Systematic Calculation of High Duty Bolted Joints with One Cylindrical Bolt, Verein Deutscher Ingenieure, Beuth Verlag GmbH, Berlin, 2003
[31] Pollicino F, Schleesselmann R. Berechnung der hochbelasteten Schraubenverbindung des Rotorblattes einer Windkraftanlage mittels FEM und VDI2230 unter Beruecksichtung der Montage, Germanischer Lloyd WindEnergie GmbH Report, 2005 (in German)
[32] Vionis P, Lekou DJ, Costales G, Mieres J, Kossivas T, Soria E, Gutierrez E, Galiotis C, Philippidis TP, Voutsinas S, Hofmann D, Development of a MW scale wind turbine for high wind complex terrain sites; the MEGAWIND project, Proc. of EWEC 2003, Madrid, Spain, June 2003
[33] Vionis P, Lekou DJ, Costales G, Mieres J, Kossivas T, Soria E, Gutierrez E, Galiotis C, Philippidis TP, Voutsinas S, Hofmann D, Development of a MW scale wind turbine for high wind complex terrain sites; the MEGAWIND project, Presented at EWEC 2006, 27 February – 2 March 2006, CT3.3, Athens, Greece
[34] Zhu Y, Kedward K. Methods of Analysis and Failure Predictions for Adhesively Bonded Joints of Uniform and Variable Bondline Thickness, DOT/FAA/AR-05/12, 2005
[35] Overgaard LCT, Lund E, Thomsen OT. Structural collapse of a wind turbine blade; Part A: Static test and equivalent single layered models. Composites: Part A, 41, 257-270, 2010
[36] Nuin I, Amézqueta C, Trias D, Estarriaga J, del Río M, Fariñas AB. Fracture Mechanics techniques for the design of structural components with adhesive joints for wind turbines, EWEA paper no. 461, 2009
[37] Soden PD, Kaddour AS, Hinton MJ. Recommendations for designers and researchers resulting from the world-wide failure exercise, Composites Science and Technology, 64, 589-604, 2004
[38] Zinoviev PA, Lebedeva OV, Tairova LP. Coupled analysis of experimental and theoretical results on the deformation and failure of laminated composites under a plane state of stress. Composites Science and Technology, 62, 1711–1723, 2002

[39] Bogetti TA, Hoppel CPR, Harik VM, Newill JF, Burns BP. Predicting the nonlinear response and failure of composite laminates: correlation with experimental results. Composites Science and Technology, 64, 477–485, 2004
[40] Kuraishi A, Tsai SW, Liu K. A progressive quadratic failure criterion, Part B. Composites Science and Technology, 62, 1683–1695, 2002
[41] Puck A. Schuermann A. Failure analysis of FRP laminates by means of physically based phenomenological models. Composites Science and Technology, 62, 1633-1662, 2002
[42] Cuntze RG. The predictive capability of failure mode concept based strength criteria for multidirectional laminates: part B. Composites Science and Technology, 64, 487-516, 2004
[43] Kaddour AS, Hinton MJ. Maturity of 3D failure criteria for fibre reinforced composites: Comparison between theories and experiments: Part B of WWFE-II, Journal of Composite Materials, 47(6–7), 925–966, 2013
[44] Kaddour AS, Hinton MJ, Smith PA, Li S. A comparison between the predictive capability of matrix cracking, damage and failure criteria for fibre reinforced composite laminates: Part A of the third world-wide failure exercise, Journal of Composite Materials, 47(20–21), 2749–2779, 2013
[45] Philippidis TP, Vassilopoulos AP. Complex stress state effect on fatigue life of GRP laminates; Part II, Theoretical formulation. International Journal of Fatigue, 24, 825–830, 2002
[46] Sun XS, Haris A, Tan VBC, Tay TE, Narasimalu S, Della CN. A multi-axial fatigue model for fiber reinforced composite laminates based on Puck's criterion. Journal of Composite Materials, 46(4), 449–469, 2012
[47] Eliopoulos EN, Philippidis TP. A progressive damage simulation algorithm for GFRP composites under cyclic loading. Part I: Material constitutive model, Composites Science and Technology, 71, 742–749, 2011
[48] Eliopoulos EN, Philippidis TP. A progressive damage simulation algorithm for GFRP composites under cyclic loading. Part II: FE implementation and model validation. Composites Science and Technology, 71, 750–757, 2011
[49] Heijdra JJ, Borst MS, Van Delft DRV. Wind turbine blade structural performance testing, in Advances in Wind Turbine Blade Design and materials, Edited by P. Broendsted, R. P. L. Nijssen, Woodhead Publishing Series in Energy No. 47, Woodhead Publishing Limited, pp. 432-445, 2013
[50] Chen X, Zhao W, Zhao XL, Xu JZ. Failure test and finite element simulation of a large wind turbine composite blade under static loading. Energies 7, 2274-2297, 2014
[51] Beattie AG. Acoustic Emission Monitoring of a Wind Turbine Blade During a Fatigue Test. A collection of the 1997 ASME Wind Energy Symposium Technical Papers. AIAA, Reno 6-9 January 1997; 239-248
[52] Lekou DJ, Vionis P, Joosse PA, van Delft DRV, Kouroussis D, Anastasopoulos A, Blanch MJ, Dutton AG, Proust A, Full-scale blade testing enhanced by acoustic emission monitoring, Proc. of EWEC 2003, Madrid, Spain, June 2003
[53] PROFAR ~Probability Distribution of Fatigue strength of rotor blades. EU JOULE III Project JOR3-CT98-0266, http://www.wmc.eu/profarblade.php
[54] Jørgensen ER, Fahmüller AB, PROFAR - Evaluation of blade property tests, Risoe Report, Risoe-I-1740(EN), 2001

[55] Van Leeuwen H, van Delft D, Heijdra J, Braam H, Jørgensen E, Lekou D, Vionis P, Comparing Fatigue strength from Full Scale Blade Laboratory Tests with Coupon-Based Predictions, Journal of Solar Energy Engineering, 124(4), 404-411, 2002
[56] Heijdra JJ, Braam H, Jørgensen ER, Lekou DJ, Vionis PS, van Leeuwen JL, van Delft DRV, Probability Distribution of Fatigue Strength of Rotor Blades; Profar, Proc. of EWEC 2001, pp 234-237, Eds. P. Helm, A. Zervos, Publ. WIP-Munich & ETA, Copenhagen, Denmark, 2001
[57] Bulder B, van Dam J, van Delft DRV, Jensen MW, Joergensen ER, Kolovos V, Larwood S, Musial W, Verheul A, Vionis P, Pedersen TF, European Wind Turbine Testing Procedure Developments SMT4-CT96-2116; Blade Testing Methods – Subtask 2, ECN report, ECN-C--00-055, 2000
[58] IEC 17025:2005, General requirements for the competence of testing and calibration laboratories
[59] ISO/IEC Guide 98-3:2008, Uncertainty of measurement -- Part 3: Guide to the expression of uncertainty in measurement
[60] Snowberg D. 2013 Interlaboratory Comparison (ILC) for Participants Conducting Structural Blade Tests to IEC 61400-23; Final Results Assessment, NREL report, August 2013
[61] IEC 61400-22:2010, Wind turbines – Part 22: Conformity testing and certification
[62] Antoniou A, Saathoff M, Krause S. Trailing edge monitoring with acoustic emission during a static full scale blade test. Proc. of EWEC 2014, Barcelona, Spain, March 2014
[63] Stammes E. Beam test report – Comparison and evaluation of beams tested within WP3. WMC-2011-14, February 2011
[64] Stammes E, Westphal T, Nijssen RPL. Guidelines for design, stress analysis and testing of a structural blade detail. Deliverable D 3.1.4 / WMC-2010-95, February 2011
[65] Branner K. Modelling Failure in Cross-Section of Wind Turbine Blade, in: Proc. of 2nd NAFEMS Nordic Seminar, 31 May - 1 June 2006, Copenhagen/Roskilde, Denmark.
[66] Branner K, Bitsche RD, Jensen FM. Effect of Strain Rate on Sandwich Web Failure in the Load Carrying Girder of a Wind Turbine Blade, in: Proc. of 9th International Conference on Sandwich Structures, 14-16 June 2010, California Institute of Technology, Pasadena, California, USA.
[67] Brazier LG. On the flexure of thin cylindrical shells & other thin sections. Proceedings of the Royal Society London, A 116, pp. 104-114, 1927.
[68] Jensen FM. Ultimate strength of a large wind turbine blade, Risø-PhD-34(EN), PhD thesis, Risø National Laboratory for Sustainable Energy, Technical University of Denmark, Denmark, 2008.
[69] Branner K, Jensen FM, Berring P, Puri A, Morris A, Dear JP. Effect of Sandwich Core Properties on Ultimate Strength of a Wind Turbine Blade, in: Proc. of 8th International Conference on Sandwich Structures, 6-8 May 2008, University of Porto, Portugal.
[70] Jensen FM, Puri AS, Dear JP, Branner K, Morris A. Investigating the Impact of Non-linear Geometrical Effects on Wind Turbine Blade - Part 1: Current Issues and Future Challenges in Design Optimisation, Wind Energy, Volume 14 Issue 2, March 2011, pp. 239-254, DOI: 10.1002/we.415.

[71] Sayer F, Post N, van Wingerde A, Busmann HG, Kleiner F, Fleischmann W, Gansow M. Testing of Adhesive Joints in the Wind Industry, Proc. of EWEA 2009, Marseille, France, 2009
[72] Kleiner F, Abas R. Analysis of the fatigue behaviour of the adhesive layer in wind turbine blades. In adhesion society 2013 Annual meeting proceedings, 2013

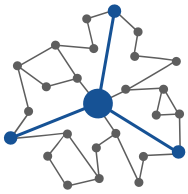

IRPWind

Integrated Research Programme on Wind Energy

Project acronym: **IRPWIND**
Grant agreement nº 609795
Collaborative project
Start date: 01st December 2013
Duration: 4 years

ANNEX 1: Comparison of blade test loads against design loads

Inaki Nuin, Carlos Amezqueta (CENER)

Lead Beneficiary: CENER
Delivery date: 10/2/2015
Dissemination level:

The research leading to these results has received funding from the European Union Seventh Framework Programme under the agreement 609795.

Author(s) information (alphabetical):		
Name	Organisation	Email
Iñaki Nuin	CENER	inuin@cener.com

Acknowledgements/Contributions:		
Name	Organisation	Email
Carlos Amezqueta	CENER	camezqueta@cener.com

Document Information

Version	Date	Description			
			Prepared by	**Reviewed by**	**Approved by**
		Name			

Definitions

Supported by:

Table of Contents

Supported by:

Executive Summary (Heading 1)

Introduction (Heading 1)

Detailed description of SMART deliverables WP 6.1 to WP 8.3
"The report will include the results of the review of the design methodology and the verification through testing of blades, combined with recommendation on the performance of testing in order to be used for the verification of the blade design."

1. Scope

The main objective of CENER's work is to compare the representativeness of the loads introduced into the blade during its certification tests in comparison with the loads supported by the blade during its operational life.

This report analyses the differences of these blade loading conditions for both extreme and fatigue loads by means of the minimum strength ratio and maximum damage reached at the critical areas of the blade according to most common failure theories and the SN approach suggested by most extended design guidelines.

2. Methodology

The methodology followed in the work performed is:

- ✓ Blade Baseline definition: Obtained from DTU report; *Description of the DTU 10MW Reference Wind Turbine* [1]. The blade model is defined both in BASSF[1] and also in PATRAN/NASTRAN using the FE information provided by DTU in ABAQUS format.
- ✓ Loads post-processing: Extreme and fatigue loads (provided by DTU and POLIMI respectively) are post-processed so that they are transformed to a common coordinate system that is fixed to the blade root (at 0º twist angle), but that rotates with the blade pitch. In the case of fatigue loads an extra hypothesis is assumed in order to obtain numerical values that fit better with the physical behaviour of the blade.
- ✓ Blade structural verification: DTU baseline is checked under extreme and fatigue loads using both the analytical approach and also FE calculations. These analyses are performed considering the loading conditions from operation and those ones from tests.
- ✓ Correlation and conclusions: The differences obtained in the blade structural behaviour (strength ratio and damage) from operational loads and test loads are analysed to take conclusions that could improve the representativeness of further certification tests.

[1] BASSF (Blade Analysis Strain Stress Failure) is the analytical tool of CENER for the structural pre-design of blades. It is an internally developed software based on analytical formulation available in the web-site for external users (http://www.cener.com/en/wind-energy/en_signup.asp)

3. Blade Description – DTU Baseline

Main objective of DTU design was to achieve a relatively light weight design. As it was decided to work with conventional glass fibre reinforced composites, the alternative option was to define airfoils with high relative thickness in order to increase the moment of inertia and thereby to increase the thickness.

According to this strategy, DTU selected FFA-W3-xxx airfoils [2] with relative thickness in-between 24.1% and 60%, using pure (up to 36%), scaled (48.0%) and interpolated airfoil geometries (60.0%).

3.1 Analytical model

3.1.1 Blade Simplification; From 101 sections to 41 sections

The Blade model of DTU is defined using 101 cross sections. In order to speed up the analyses and the post-processing tasks, it is decided to reduce the number of the intermediate sections to 41. Selected sections are in blue colour.

Table 1 Selection of representative sections. From 101 to 41

n°	Distance from Root [m]	Twist Aero [-]	Chord [-]	Relative Thickness [-]	n°	Distance from Root [m]	Twist Aero [-]	Chord [-]	Relative Thickness [-]
1	0.000	14.500	5.380	100.0	52	43.375	3.7577	5.052	27.2
2	0.521	14.500	5.380	100.0	53	44.193	3.5895	4.984	26.9
3	1.502	14.500	5.380	100.0	54	45.007	3.4211	4.916	26.7
4	1.990	14.500	5.380	100.0	55	45.818	3.2527	4.847	26.4
5	2.950	14.500	5.380	100.0	56	46.624	3.0839	4.779	26.2
6	3.882	14.500	5.380	100.0	57	48.222	2.7481	4.642	25.8
7	4.784	14.500	5.380	100.0	58	49.013	2.5822	4.573	25.6
8	5.717	14.500	5.382	99.5	59	49.798	2.4172	4.505	25.4
9	6.691	14.4967	5.397	98.4	60	50.576	2.2538	4.438	25.3
10	7.194	14.4846	5.412	97.5	61	51.349	2.0927	4.371	25.1
11	8.232	14.4285	5.454	95.2	62	52.114	1.9340	4.305	25.0
12	9.313	14.3030	5.514	92.0	63	52.871	1.7771	4.240	24.9
13	9.869	14.2003	5.549	90.2	64	53.622	1.6229	4.175	24.8
14	11.014	13.9123	5.630	86.0	65	55.098	1.3241	4.049	24.6
15	11.602	13.7110	5.674	83.7	66	55.824	1.1795	3.987	24.5
16	12.810	13.2070	5.769	78.6	67	56.541	1.0381	3.926	24.4
17	13.430	12.8903	5.818	75.9	68	57.248	0.9002	3.866	24.4
18	14.061	12.5412	5.867	73.2	69	58.636	0.6357	3.749	24.3
19	15.352	11.7435	5.963	67.5	70	59.316	0.5087	3.692	24.2
20	16.013	11.3037	6.007	64.7	71	59.986	0.3852	3.637	24.2
21	16.684	10.8677	6.049	61.9	72	60.646	0.2655	3.582	24.2
22	17.364	10.4132	6.086	59.1	73	61.936	0.0366	3.476	24.1
23	18.754	9.5538	6.146	54.0	74	62.566	-0.0727	3.425	24.1
24	19.463	9.2002	6.168	51.7	75	63.185	-0.1785	3.375	24.1
25	20.180	8.8745	6.185	49.5	76	64.391	-0.3799	3.279	24.1
26	20.907	8.5768	6.197	47.6	77	64.979	-0.4756	3.232	24.1
27	22.384	8.0597	6.206	44.2	78	66.122	-0.6579	3.142	24.1
28	23.135	7.8311	6.204	42.7	79	66.677	-0.7448	3.099	24.1
29	23.894	7.6180	6.196	41.4	80	67.756	-0.9097	3.016	24.1
30	24.659	7.4187	6.184	40.2	81	68.792	-1.0646	2.938	24.1

Supported by:

n°	Distance from Root [m]	Twist Aero [-]	Chord [-]	Relative Thickness [-]	n°	Distance from Root [m]	Twist Aero [-]	Chord [-]	Relative Thickness [-]
31	25.432	7.2326	6.168	39.1	82	69.294	-1.1389	2.900	24.1
32	26.211	7.0554	6.147	38.1	83	70.267	-1.2807	2.828	24.1
33	26.997	6.8831	6.122	37.2	84	71.198	-1.4146	2.760	24.1
34	27.788	6.7176	6.093	36.3	85	72.088	-1.5418	2.696	24.1
35	28.585	6.5575	6.060	35.5	86	72.938	-1.6623	2.635	24.1
36	30.193	6.2394	5.984	34.0	87	73.748	-1.7767	2.578	24.1
37	31.004	6.0797	5.941	33.4	88	74.520	-1.8858	2.524	24.1
38	31.819	5.9217	5.895	32.8	89	75.609	-2.0391	2.450	24.1
39	32.637	5.7672	5.846	32.2	90	76.617	-2.1816	2.380	24.1
40	33.458	5.6180	5.794	31.7	91	77.247	-2.2709	2.336	24.1
41	34.282	5.4728	5.741	31.2	92	78.130	-2.3961	2.272	24.1
42	35.107	5.3282	5.685	30.7	93	78.945	-2.5115	2.209	24.1
43	35.934	5.1810	5.627	30.3	94	79.930	-2.6502	2.125	24.1
44	36.763	5.0325	5.568	29.9	95	80.810	-2.7716	2.042	24.1
45	37.592	4.8831	5.507	29.5	96	81.593	-2.8772	1.961	24.1
46	38.421	4.7312	5.445	29.1	97	82.450	-2.9889	1.863	24.1
47	39.250	4.5754	5.382	28.7	98	83.322	-3.0966	1.744	24.1
48	40.078	4.4159	5.318	28.4	99	84.260	-3.2047	1.579	24.1
49	40.906	4.2538	5.253	28.1	100	85.069	-3.2934	1.385	24.1
50	41.731	4.0899	5.186	27.8	101	85.944	-3.3991	1.027	24.1
51	42.554	3.9248	5.119	27.5					

The selection of previous sections is defined so that the distance among two consecutive sections is 1.0-2.0m. From maximum chord till the blade tip this distance is increased to ~2.5m.

There are three more sections that are selected due to the following reasons:

- ✓ Section 24: Third web stars at this position
- ✓ Section 27: Maximum chord
- ✓ Section 55: Critical section according the structural results performed for InnWind.eu project – Structural Benchmarking

3.1.2 Blade mechanical properties

Although the definition of the blade is reduced to more than half (from 101 cross sections to 41), its representativeness is fully respected. As it is shown in Table 2, the differences in the overall mass properties and centre of gravity are negligible.

Table 2 Mass & center of gravity differences

Blade definition by 101 sections	
Overall mass of the blade (Kg)	41643Kg
Location of centre of gravity from hub centre (z axis)	z: 28.638
Blade definition by 41 sections	
Overall mass of the blade (Kg)	41600Kg
Location of centre of gravity from hub centre (z axis)	z: 28.636

Supported by:

The mechanical properties of DTU baseline blade for these new 41 sections, and according to the analyses performed with BASSF, are the following:

Table 3 Distribution of DTU blade mechanical properties

Section ID	Distance from Root [m]	Mass/unit length [Kg/m]	Flapwise Stiffness [Nm2]	Edgewise Stiffness [Nm2]	Torsional Rigidity [Nm2]	Centre of mass [%]	Elastic axis [-]
1	0.000	1203.33	6.276E+10	6.163E+10	2.731E+10	50.06	50.07
2	1.502	1203.53	6.277E+10	6.169E+10	2.731E+10	50.08	50.09
3	2.950	1208.21	6.332E+10	6.181E+10	2.729E+10	50.13	50.14
4	4.784	1205.56	6.259E+10	6.076E+10	2.625E+10	50.45	50.36
5	6.691	1152.64	5.721E+10	5.663E+10	2.321E+10	50.47	50.24
6	8.232	1093.24	5.106E+10	5.171E+10	2.011E+10	50.40	50.08
7	9.869	1026.22	4.267E+10	4.567E+10	1.568E+10	49.32	48.84
8	11.602	962.13	3.410E+10	4.059E+10	1.153E+10	48.28	47.60
9	13.430	907.40	2.661E+10	3.714E+10	8.246E+09	47.09	46.17
10	15.352	855.96	2.031E+10	3.360E+10	5.776E+09	45.60	44.50
11	16.684	809.74	1.684E+10	3.117E+10	4.378E+09	45.08	43.69
12	18.754	755.97	1.356E+10	2.874E+10	3.280E+09	44.20	42.54
13	19.463	734.31	1.259E+10	2.764E+10	3.066E+09	44.19	42.26
14	20.180	713.30	1.172E+10	2.655E+10	2.746E+09	43.93	41.92
15	22.384	664.79	9.547E+09	2.418E+10	2.105E+09	43.00	40.67
16	23.894	627.96	8.341E+09	2.198E+10	1.702E+09	42.21	39.68
17	26.211	586.25	6.923E+09	1.949E+10	1.294E+09	41.32	38.46
18	28.585	565.04	5.853E+09	1.767E+10	1.063E+09	40.65	37.65
19	31.004	541.63	4.931E+09	1.604E+10	8.934E+08	40.49	37.21
20	33.458	519.39	4.167E+09	1.412E+10	7.390E+08	39.98	36.58
21	35.934	492.46	3.506E+09	1.253E+10	6.192E+08	39.64	36.32
22	38.421	468.42	2.924E+09	1.084E+10	5.104E+08	39.37	36.02
23	40.906	443.04	2.424E+09	9.388E+09	4.206E+08	39.44	35.96
24	43.375	418.58	2.008E+09	8.079E+09	3.516E+08	39.54	35.84
25	45.818	388.56	1.653E+09	6.792E+09	2.853E+08	39.22	35.64
26	48.222	366.86	1.376E+09	5.775E+09	2.396E+08	39.14	35.51
27	50.576	339.68	1.138E+09	4.863E+09	1.956E+08	38.93	35.42
28	52.871	314.75	9.484E+08	4.086E+09	1.652E+08	38.82	35.39
29	55.098	291.85	7.972E+08	3.400E+09	1.385E+08	38.51	35.22
30	57.248	268.63	6.645E+08	2.858E+09	1.166E+08	38.52	35.38
31	59.316	251.43	5.612E+08	2.395E+09	1.001E+08	38.55	35.33
32	61.936	224.25	4.461E+08	1.893E+09	8.108E+07	38.56	35.39
33	64.391	199.14	3.540E+08	1.492E+09	6.654E+07	38.69	35.63
34	66.677	176.88	2.776E+08	1.184E+09	5.405E+07	38.97	35.83
35	69.294	152.43	2.084E+08	8.976E+08	4.292E+07	38.97	36.05
36	72.088	129.79	1.503E+08	6.605E+08	3.359E+07	39.69	36.52
37	74.520	107.38	1.076E+08	4.947E+08	2.595E+07	40.34	37.24
38	77.247	86.60	7.178E+07	3.462E+08	1.988E+07	40.95	38.08
39	79.930	66.85	4.293E+07	2.256E+08	1.379E+07	42.04	39.12
40	82.450	46.28	2.081E+07	1.320E+08	8.552E+06	44.20	41.27
41	85.944	16.48	1.165E+06	1.546E+07	8.537E+05	48.81	47.97

Supported by:

3.2 FE model by 2D shell elements

3.2.1 FE model description

The FE model of the blade defined by DTU is imported in MSC.PATRAN. As the information regarding the element properties is lost in the communication between ABAQUS and MSC.PATRAN, it is necessary to renumber the elements under a logical codification in order to assign every PCOMP entry with the matching groups of elements. Analogous to the FE model based on 1D beam elements the blade root is fixed using a RBE2 rigid link.

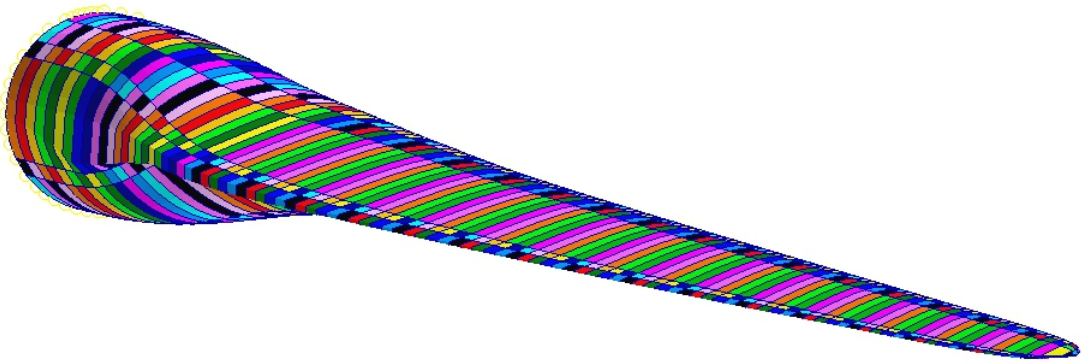

Figure 1 FE model defined by DTU in ABAQUS and imported to PATRAN/NASTRAN

3.2.2 Load introduction

The introduction of loads into the FE model is done by the definition of RBE3 equations (NASTRAN format). These multi-point-equations transfer the forces & moments at the master node (located at the blade pitch axis) into the slave nodes of the airfoil section by the use of equivalent forces.

For a better understanding of the blade loads physic supported by the blade, it is recommended to obtain the loads calculated by the aero-elastic code in a coordinate system fixed to the blade root but rotating with the pitch.

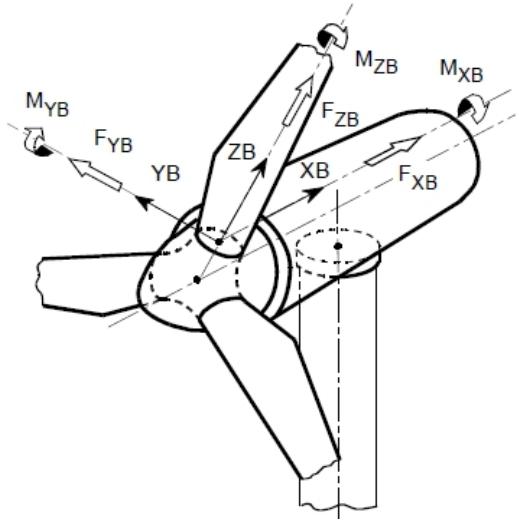

This coordinate system is analogous to the "Blade Coordinate System" defined by GL but rotating with the pitch.

Origin: At the intersection between the blade pitch axis and the root plane

ZB: From blade root to blade tip

YB: From blade leading edge to trailing edge at plane of twist angle = 0°

XB: So that XB, YB, ZB rotate clockwise

Supported by:

4. Extreme Loads

4.1 Design loads

The extreme loads provided by DTU are computed using the aero-elastic code HAWC2 at 27 cross sections along the blade. Forces and moments are defined at the elastic centre of these cross sections with reference to a coordinate system aligned with its elastic axis.

- ✓ The x-axis is aligned with the first elastic axis and points towards the leading edge of the blade.
- ✓ The y-axis is aligned with the second elastic axis and points towards the suction side of the blade.

At each cross section, both the extreme magnitudes for each load component (FX, FY, F_{res}, FZ, MX, MY, M_{res}, MZ) and also the simultaneous load components are defined.

This information is adequate when the blade design is checked according to analytical approaches where the cross sections are calculated independently. However, in the case of working with FE models, it is necessary to have the loading information of all the extreme load-cases at every section of the blade occurring simultaneously. In addition, the definition of the certification tests assume that these load envelopes are defined along the blade flapwise and blade edgewise directions that fit with the coordinate system described in section 3.2.2

According to these assumptions, the aero-elastic analyses for the DTU 10MW Reference Wind Turbine are repeated by CENER using the BLADED model defined by Garrad Hassan. Information post-processed is the following:

- ✓ Load components at a common coordinate system fixed to the blade root but rotating with the pitch.
- ✓ Information for the maximum loads at every section with the loads components occurring simultaneously at all the cross sections.

These extreme loads are defined at 25 cross sections. The total number of cases is 400 (25 x 16). However, many of them are redundant, so, after a deeper check these load cases are reduced to 84

In Annex A, the extreme loads for every cross section of the blade are shown in different tables. The simultaneous values for all the other sections are calculated but not printed. These loads are introduced directly when working with the analytical approach (BASSF). However, when the blade structural check is done using the FE model, these loads are uncoupled according to the following criterion:

- ✓ $Fx_{i-1} = Fx_i + fx_{i-1}$
- ✓ $Fy_{i-1} = Fy_i + fy_{i-1}$
- ✓ $Fz_{i-1} = Fz_i + fz_{i-1}$
- ✓ $Mx_{i-1} = Mx_i - Fy_i.(z_i - z_{i-1}) - fy_i.(z_i - z_{i-1})/2$
- ✓ $My_{i-1} = My_i + Fx_i.(z_i - z_{i-1}) + fx_i.(z_i - z_{i-1})/2$
- ✓ $Mz_{i-1} = Mz_i + mz_{i-1}$

Supported by:

This approach is valid when the FE loads are introduced at intermediate sections located in the middle point in-between those sections where the aero-elastic code calculates the accumulated loads.

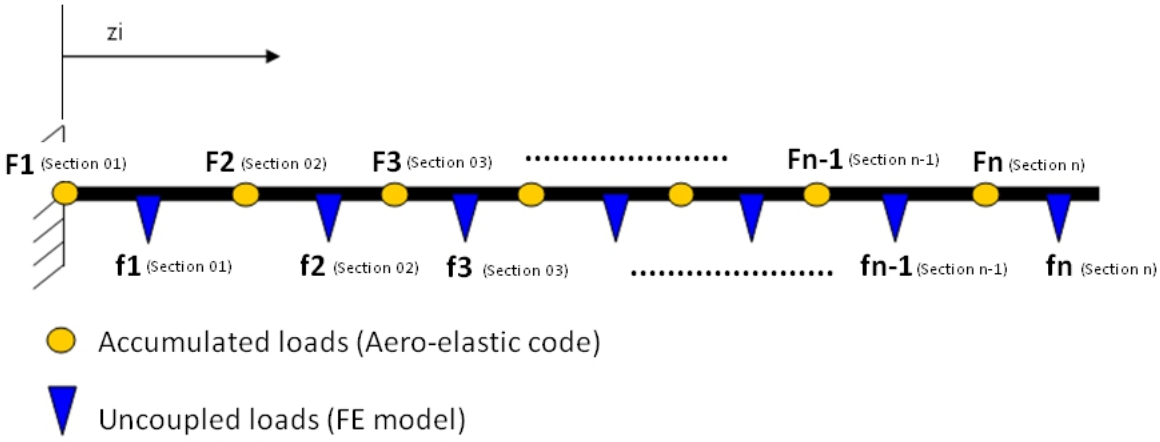

Figure 2 Criterion used for loads uncoupling

4.2 Test loads

4.2.1 Limitations of the Test-Rig & common procedure

The mechanical tests used for blade certification depend on the designer strategy and the agreements reached with the certification body.

These tests are directly influenced by the limitations of the blade testing facilities. In particular, for the static case, one of the main restrictions is the limitation of loading the blade only along one plane.

There are other limitations not considered as; maximum available load with the pullers, blade maximum deflections and also foundation capacity. Figure 3 shows the test-rig used in CENER for blade certification

Figure 3 Test-rig used for blade certification (static tests)

According to these main limitations, it is common to test the blade along four main directions:

- ✓ Flapwise – Positive: Pressure to Suction (PTS)
- ✓ Flapwise – Negative: Suction to Pressure (STP)
- ✓ Edgewise – Positive: Trailing to Leading (TTL)
- ✓ Edgewise – Negative: Leading to Trailing (LTT)

Supported by:

These tests are required by most of the standards. If the certification of the blade is performed under GL-2010 [4], it is satisfactory to perform only these static tests for the structural assessment. In case of certifying the blade according to DNV-2002 [5], it is necessary to perform also the fatigue tests.

Near future guideline versions will probably require the execution of both static & fatigue tests. For instance, a new update of IEC-61400-23 [3] has been delivered in April 2014, requiring:

- ✓ Static Tests
- ✓ Fatigue Tests
- ✓ Post-Fatigue static tests

4.2.2 Test Design

The design of the tests is done so that the location of the clamps is fixed for all of the tests. This assumption reduces the manpower necessary for the setting up of the tests along the four main directions described above.

Additionally, according to the blade length (86.3m) and the bending moment values reached at the blade root (~60.000kNm), it is decided to work with 7 clamps. This configuration implies reasonable shear forces, comparable with those ones supported by the blade under operation. For edgewise negative test, only 5 pullers are used.

4.2.2.1 Test Factor

According to the standard, the load level applied during the tests is scaled by the following factors:

$$F_{target-u} = F_{du} \cdot \gamma_{nu} \cdot \gamma_{su}$$

- ✓ γ_{nu}: Partial factor for consequence of failure. It is assumed to be 1.0, considering that a periodic maintenance is carried on during the blade operational life and that the consequences of an unexpected failure do not imply the destruction of the wind turbine or the endangering of people.

Table 4 Consequence of failure according to GL2010 [4]

Inspection and accessibility	Component failure results in destruction of wind turbine or endangers people	Component failure results in wind turbine failure or consequential damage	Component failure results in interruption of operation
Periodic monitoring and maintenance; good accessibility	1.15	1.00	1.00
Periodic monitoring and maintenance; poor accessibility	1.25	1.15	1.00

- ✓ γ_{su}: Test load factor for blade to blade variation. It is assumed to be 1.1 as it is recommended in the guideline

Last version of the standard includes an environmental factor, due to the benign conditions of the test facilities in comparison with the operational ones. The work performed does not consider this factor. Considering all these effects, the load level applied for full blade testing is scaled by a 10%.

Supported by:

4.2.2.2 *Flapwise – Positive (PTS)*

Table 5 show the loads applied at every puller. For all the configurations, the deviations between the target loads and the test ones are not of significance.

Table 5 Position of the pullers & load levels (PTS)

	Distance from root [m]	Applied Forces [kN]
PULLER 01	30.0	391,77
PULLER 02	44.0	152,71
PULLER 03	56.0	197,82
PULLER 04	64.0	114,02
PULLER 05	70.0	83,77
PULLER 06	76.0	114,16
PULLER 07	82.0	136,08

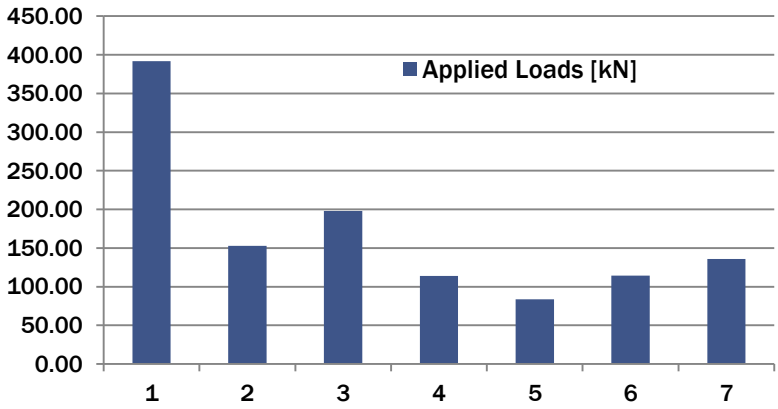

Table 6 Deviation between target loads and test loads (PTS)

	TARGET LOADS		TEST LOADS		
Distance from root [m]	FX [kN]	MY [kN]	FX [kN]	MY [kN]	MY – deviation [%]
0.000	1282,82	63167,5	1190,3	62545,8	-0,98%
2.015	1279,2	60578,1	1190,3	60147,3	-0,71%
5.470	1270,6	56164,9	1190,3	56034,8	-0,23%
8.348	1260,8	52518,4	1190,3	52609,0	0,17%
10.634	1250,9	49650,7	1190,3	49887,9	0,48%
12.377	1242,1	47482,6	1190,3	47813,2	0,70%
14.091	1232,7	45370,6	1190,3	45773,0	0,89%
15.833	1221,8	43253,1	1190,3	43699,5	1,03%
17.559	1209,6	41169,7	1190,3	41645,0	1,15%
21.016	1165,8	37148,1	1190,3	37530,0	1,03%
24.470	1106,7	33324,5	1190,3	33418,6	0,28%
27.926	1042,8	29687,9	1190,3	29304,9	-1,29%
31.381	999,9	26309,8	798,6	25733,4	-2,19%
33.109	977,4	24688,4	798,6	24353,4	-1,36%
34.836	954,5	23112,1	798,6	22974,3	-0,60%
38.292	891,7	20156,4	798,6	20214,5	0,29%
43.477	810,2	16089,7	798,6	16074,0	-0,10%
48.806	727,0	12353,0	645,8	12552,4	1,61%
55.721	611,2	8171,2	645,8	8086,4	-1,04%
62.554	452,7	4971,1	448,0	4969,8	-0,03%
69.564	329,7	2466,9	334,0	2463,5	-0,14%
74.699	227,4	1142,2	250,2	1142,0	-0,02%
81.647	77,2	147,6	136,1	48,0	-67,46%
83.382	43,0	49,2	0,0	0,0	-100,00%
85.165	10,7	4,6	0,0	0,0	-100,00%

Supported by:

4.2.2.3 *Flapwise – Negative (STP)*

Table 7 Position of the pullers & load levels (STP)

	Distance from root [m]	Applied Forces [kN]
PULLER 01	30,0	-185,06
PULLER 02	44,0	-175,65
PULLER 03	56,0	-138,35
PULLER 04	64,0	-109,06
PULLER 05	70,0	-67,14
PULLER 06	76,0	-78,89
PULLER 07	82,0	-82,92

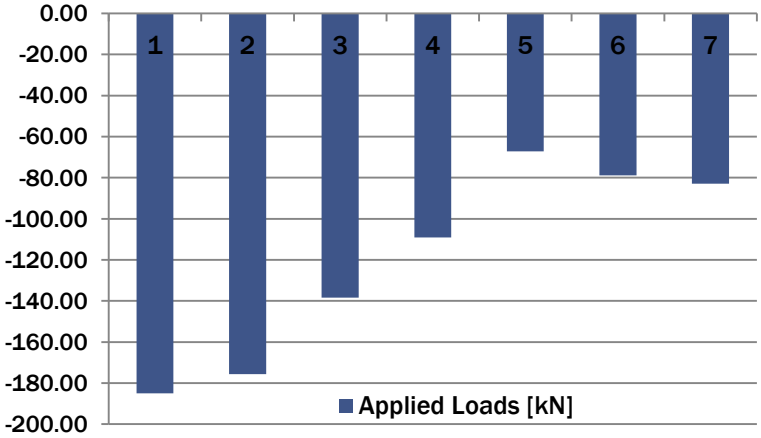

Table 8 Deviation between target loads and test loads (STP)

	TARGET LOADS		TEST LOADS		
Distance from root [m]	FX [kN]	MY [kN]	FX [kN]	MY [kN]	MY – deviation [%]
0.000	-885,5	-45654,4	-837,1	-45502,9	-0,33%
2.015	-880,3	-43897,7	-837,1	-43816,2	-0,19%
5.470	-873,4	-40925,5	-837,1	-40924,1	0,00%
8.348	-871,1	-38479,1	-837,1	-38515,0	0,09%
10.634	-872,9	-36544,2	-837,1	-36601,5	0,16%
12.377	-866,9	-35079,0	-837,1	-35142,4	0,18%
14.091	-872,1	-33642,4	-837,1	-33707,7	0,19%
15.833	-878,1	-32166,2	-837,1	-32249,5	0,26%
17.559	-882,0	-30713,1	-837,1	-30804,7	0,30%
21.016	-885,1	-27805,8	-837,1	-27911,0	0,38%
24.470	-860,5	-24974,4	-837,1	-25019,7	0,18%
27.926	-843,4	-22258,5	-837,1	-22126,8	-0,59%
31.381	-808,4	-19665,8	-652,0	-19490,3	-0,89%
33.109	-795,3	-18416,2	-652,0	-18363,6	-0,29%
34.836	-781,0	-17199,6	-652,0	-17237,6	0,22%
38.292	-739,5	-14894,0	-652,0	-14984,2	0,61%
43.477	-674,7	-11742,5	-652,0	-11603,5	-1,18%
48.806	-606,4	-8853,6	-476,4	-8973,1	1,35%
55.721	-497,5	-5735,2	-476,4	-5679,1	-0,98%
62.554	-382,8	-3331,8	-338,0	-3330,9	-0,03%
69.564	-256,9	-1571,6	-229,0	-1568,3	-0,21%
74.699	-167,2	-710,9	-161,8	-708,1	-0,40%
81.647	-52,9	-91,1	-82,9	-29,3	-67,86%
83.382	-29,2	-29,9	0,0	0,0	-100,00%
85.165	-6,9	-2,8	0,0	0,0	-100,00%

Supported by:

4.2.2.4 *Edgewise – Positive (TTL)*

Table 9 Position of the pullers & load levels (TTL)

	Distance from root [m]	Applied Forces [kN]
PULLER 01	30,0	-311,49
PULLER 02	44,0	-28,37
PULLER 03	56,0	-112,57
PULLER 04	64,0	-40,61
PULLER 05	70,0	-34,41
PULLER 06	76,0	-33,70
PULLER 07	82,0	-31,39

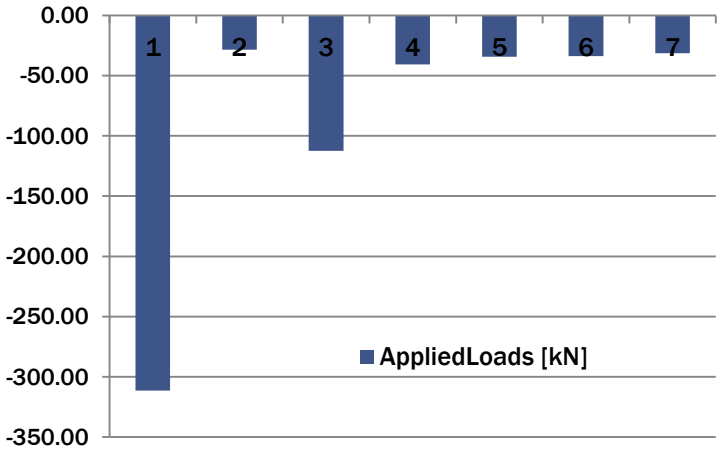

Table 10 Deviation between target loads and test loads (TTL)

	TARGET LOADS		TEST LOADS		
Distance from root [m]	FY [kN]	MX [kN]	FY [kN]	MX [kN]	MX – deviation [%]
0.000	-843,37	28241,4	-592,5	27040,0	-4,25%
2.015	-814,44	26571,6	-592,5	25846,0	-2,73%
5.470	-763,95	23851,3	-592,5	23798,8	-0,22%
8.348	-721,6	21721,7	-592,5	22093,4	1,71%
10.634	-616	20137,7	-592,5	20738,9	2,99%
12.377	-602,91	19078,4	-592,5	19706,1	3,29%
14.091	-590,04	18059,8	-592,5	18690,5	3,49%
15.833	-576,4	17047,8	-592,5	17658,3	3,58%
17.559	-562,87	16067,7	-592,5	16635,5	3,53%
21.016	-503,91	14272,5	-592,5	14587,1	2,20%
24.470	-477,4	12582,9	-592,5	12540,5	-0,34%
27.926	-439,12	11000	-592,5	10492,6	-4,61%
31.381	-407,77	9543,16	-281,1	8875,6	-7,00%
33.109	-391,6	8856,32	-281,1	8389,9	-5,27%
34.836	-374,99	8198,3	-281,1	7904,5	-3,58%
38.292	-342,1	6968,17	-281,1	6933,2	-0,50%
43.477	-293,92	5334,67	-281,1	5476,0	2,65%
48.806	-246,84	3910,5	-252,7	4114,6	5,22%
55.721	-184,58	2445,3	-252,7	2367,3	-3,19%
62.554	-133,32	1380,06	-140,1	1378,5	-0,11%
69.564	-86,46	622,93	-99,5	622,3	-0,11%
74.699	-50,93	271,04	-65,1	273,0	0,73%
81.647	-17,16	37,73	-31,4	11,1	-70,63%
83.382	-9,537	13,64	0,0	0,0	-100,00%
85.165	-2,915	1,881	0,0	0,0	-100,00%

Supported by:

4.2.2.5 *Edgewise – Negative (LTT)*

Table 11 Position of the pullers & load levels (LTT)

	Distance from root [m]	Applied Forces [kN]
PULLER 01	30,0	275,06
PULLER 02	44,0	0,00
PULLER 03	56,0	116,09
PULLER 04	64,0	0,00
PULLER 05	70,0	17,28
PULLER 06	76,0	36,72
PULLER 07	82,0	33,27

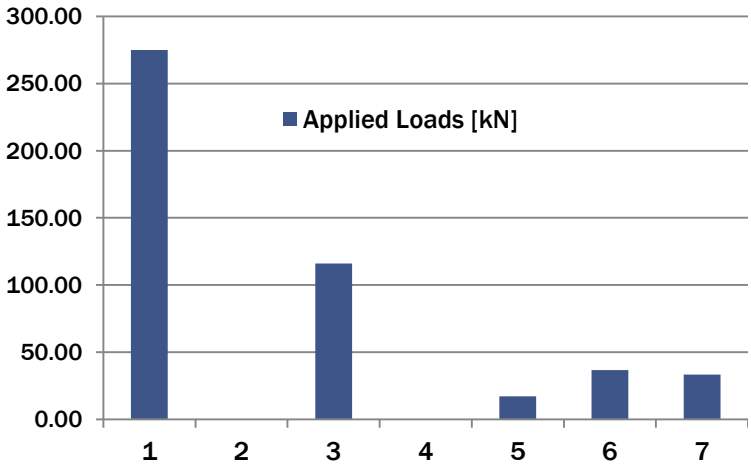

Table 12 Deviation between target loads and test loads (LTT)

	TARGET LOADS		TEST LOADS		
Distance from root [m]	FY [kN]	MX [kN]	FY [kN]	MX [kN]	MX – deviation [%]
0.000	739,3	-22679,8	478,4	-21481,0	-5,29%
2.015	706,3	-21224,5	478,4	-20517,0	-3,33%
5.470	648,9	-18891,4	478,4	-18864,1	-0,14%
8.348	604,7	-17098,4	478,4	-17487,2	2,27%
10.634	574,3	-15760,8	478,4	-16393,6	4,01%
12.377	477,5	-14907,2	478,4	-15559,7	4,38%
14.091	461,0	-14113,0	478,4	-14739,7	4,44%
15.833	445,9	-13334,2	478,4	-13906,3	4,29%
17.559	431,6	-12590,6	478,4	-13080,5	3,89%
21.016	403,8	-11182,6	478,4	-11426,7	2,18%
24.470	381,2	-9871,6	478,4	-9774,2	-0,99%
27.926	361,7	-8636,3	478,4	-8120,8	-5,97%
31.381	340,1	-7475,3	203,4	-6847,7	-8,39%
33.109	328,6	-6924,1	203,4	-6496,3	-6,18%
34.836	316,5	-6393,2	203,4	-6145,1	-3,88%
38.292	272,5	-5458,2	203,4	-5442,3	-0,29%
43.477	237,5	-4210,4	203,4	-4387,9	4,22%
48.806	201,5	-3111,5	203,4	-3304,3	6,20%
55.721	109,1	-1994,1	203,4	-1898,1	-4,82%
62.554	106,7	-1296,7	87,3	-1269,4	-2,11%
69.564	86,0	-647,8	87,3	-657,6	1,52%
74.699	59,4	-289,9	70,0	-290,7	0,29%
81.647	18,6	-34,5	33,3	-11,7	-66,00%
83.382	10,1	-12,0	0,0	0,0	-100,00%
85.165	3,3	-1,7	0,0	0,0	-100,00%

Supported by:

5. Structural behaviour of the Blade under extreme loads

The extreme load carrying capacity analysis of the blade (strength analysis) is calculated using both the analytical approach with BASSF and also the FE method. The objective is to compare the minimum strength ratios obtained when the blade is loaded under the design conditions (section 4.1) and when it is loaded under the test conditions (section 4.2)

Blade design is checked with the analytical tool (BASSF) and also using the FE model. Following failure criteria are used:

- ✓ Hill
- ✓ Hoffman
- ✓ Tsai-Wu
- ✓ Max-Strain

Puck criterion is also checked with the analytical approach for the UD plies. However, as this criterion is not implemented yet into the FE model, it is decided not to focus the work on these values to be able to extract general conclusions for both approaches.

Additionally, as the failure indexes obtained in the balsa are not representative for the blade design (also the application of these failure criteria for this material is questionable), its material properties have been doubled to mask their value.

The elastic properties and allowable used for the strength analysis are defined in [1] and summarized in Table 13 and Table 14. For the strength analysis, the admissible values of Table 14 are reduced by 2.205 according to GL guideline [4]

Table 13 Elastic properties of the blade materials

Material ID	Material Name	Ply Thickness [mm]	Density [Kgm3]	E1 [MPa]	E2 [MPa]	G12 [MPa]	μ12 [-]
1	CORE PVC	5.00	110.0	50.0	50.0	16.7	0.500
2	UD	0.10	1915.5	41630.0	14930.0	5047.0	0.241
3	BIAX	0.10	1845.0	13920.0	13920.0	11500.0	0.533
4	TRIAX	0.10	1845.0	21790.0	14670.0	9413.0	0.478

Table 14 Material limits. Characteristic values without applying the reduction factor.

Material ID	Material Name	ε_{11_COMP} [-]	ε_{22_COMP} [-]	γ_{12} [-]	ε_{11_TRACC} [-]	ε_{22_TRACC} [-]
1	CORE PVC	----	----	----	----	----
2	UD	1.50E-02	1.27E-02	1.12E-02	2.10E-02	4.94E-03
3	BIAX	1.50E-02	1.50E-02	1.22E-02	1.60E-02	1.60E-02
4	TRIAX	1.80E-02	1.04E-02	1.21E-02	2.20E-02	6.15E-03
Material ID	**Material Name**	σ_{11_COMP} [-]	σ_{22_COMP} [-]	ζ_{12} [-]	σ_{11_TRACC} [-]	σ_{22_TRACC} [-]
1	CORE PVC	----	----	----	----	----
2	UD	624.0	188.95	56.4	874.15	73.9
3	BIAX	208.77	208.77	140.0	222.68	222.68
4	TRIAX	392.5	152.4	113.8	479.32	90.2

Supported by:

5.1 Results from the analytical approach (BASSF)

5.1.1 Minimum strength ratio for design extreme loads

Table 15 Minimum strength ratio for the baseline blade under the design load cases

Section	Strength ratio – Design Load Cases						
nº	Distance from root [m]	Hill [-]	Hoffman [-]	Tsai-Wu [-]	Max-Strain [-]	Puck – FF [-]	Puck – IFF [-]
1	0.000	1,635	1,669	2,070	2,698	5,673	2,113
2	1.502	1,688	1,723	2,136	2,791	5,867	2,179
3	2.950	1,764	1,800	2,231	2,919	6,138	2,274
4	4.784	1,849	1,887	2,339	3,052	6,416	2,378
5	6.691	1,846	1,884	2,334	3,021	6,351	2,373
6	8.232	1,796	1,833	2,270	2,922	6,144	2,305
7	9.869	1,686	1,720	2,130	2,675	5,625	2,034
8	11.602	1,561	1,592	1,969	2,392	5,030	2,241
9	13.430	1,442	1,458	1,745	2,120	4,456	1,496
10	15.352	1,275	1,286	1,527	1,852	3,894	1,269
11	16.684	1,164	1,171	1,381	1,681	3,534	1,120
12	18.754	1,069	1,072	1,252	1,559	3,277	0,984
13	19.463	1,039	1,041	1,210	1,522	3,198	0,942
14	20.180	1,015	1,015	1,176	1,497	3,145	0,906
15	22.384	0,956	0,954	1,095	1,449	3,044	0,827
16	23.894	0,911	0,907	1,032	1,413	2,967	0,763
17	26.211	0,865	0,859	0,968	1,384	2,909	0,809
18	28.585	0,844	0,837	0,938	1,316	2,896	0,782
19	31.004	0,830	0,821	0,917	1,267	2,882	0,766
20	33.458	0,815	0,806	0,895	1,212	2,882	0,745
21	35.934	0,802	0,792	0,877	1,169	2,879	0,728
22	38.421	0,789	0,778	0,858	1,129	2,870	0,707
23	40.906	0,772	0,761	0,837	1,085	2,851	0,688
24	43.375	0,783	0,772	0,851	1,072	2,865	0,701
25	45.818	0,767	0,755	0,829	1,013	2,831	0,681
26	48.222	0,774	0,762	0,831	0,993	2,853	0,684
27	50.576	0,763	0,751	0,811	0,954	2,845	0,672
28	52.871	0,774	0,761	0,809	0,943	2,875	0,663
29	55.098	0,793	0,783	0,819	0,948	2,962	0,660
30	57.248	0,796	0,788	0,820	0,946	2,995	0,653
31	59.316	0,809	0,801	0,838	0,960	3,064	0,667
32	61.936	0,841	0,832	0,871	0,989	3,181	0,675
33	64.391	0,870	0,861	0,900	1,021	3,257	1,084
34	66.677	0,892	0,883	0,919	1,054	3,334	1,085
35	69.294	0,977	0,966	0,996	1,147	3,654	1,135
36	72.088	1,075	1,064	1,096	1,269	4,002	1,194
37	74.520	1,237	1,223	1,237	1,424	4,682	1,286
38	77.247	1,407	1,396	1,460	1,739	5,157	1,364
39	79.930	1,811	1,799	1,866	2,227	6,715	1,564
40	82.450	2,542	2,541	2,541	2,541	45,296	2,098
41	85.994	------	------	------	------	------	------

Supported by:

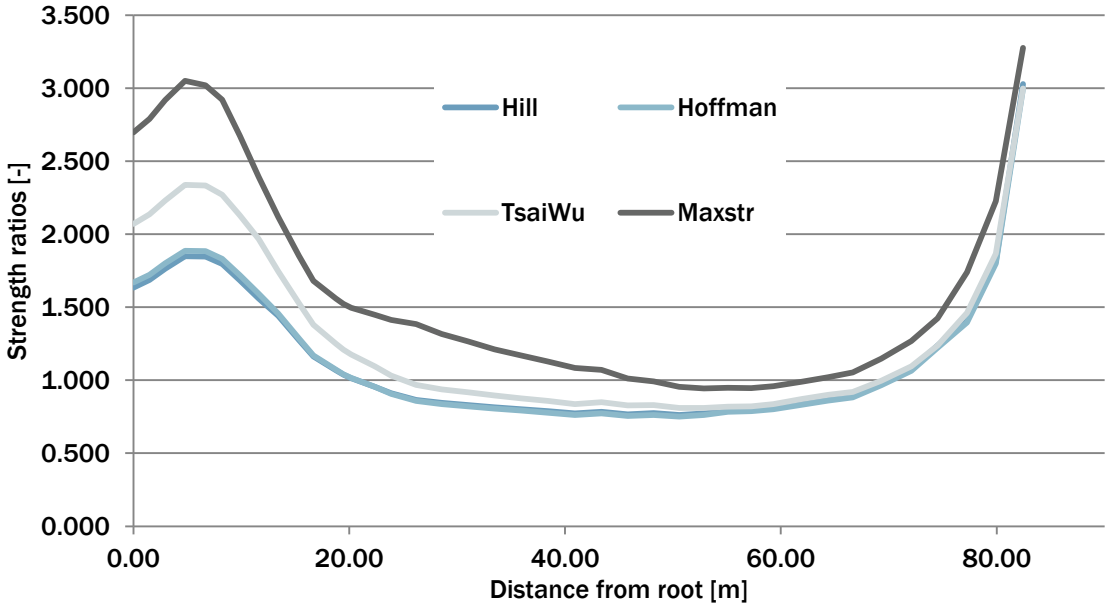

Figure 4 Evolution of minimum strength ratio along the blade span for design loads

S27 (50.576m from blade root) is the limiting blade section under the design extreme loads defined. Following results are obtained at this section:

- ✓ Hill and Hoffman are the most limiting criteria with minimum strength ratios of 0.763 and 0.751 respectively. Failure of TRIAX material, located at the leading panel of the airfoil pressure side, is predicted.
- ✓ Tsai-Wu criterion provides a minimum strength ratio of 0.811, approximately ~7% higher than previous values from Hill & Hoffman. The limiting material is also TRIAX
- ✓ Max-Strain criterion identifies BIAX material located at the leading edge web as the most limiting. Minimum strength ratio is 0.954

5.1.2 Minimum strength ratio for test extreme loads

Table 16 Minimum strength ratio for the baseline blade under the test load cases

Section	Strength ratio – Test Load Cases						
nº	Distance from root [m]	Hill [-]	Hoffman [-]	Tsai-Wu [-]	Max-Strain [-]	Puck – FF [-]	Puck – IFF [-]
1	0.000	1,663	1,701	2,125	2,542	5,345	2,303
2	1.502	1,711	1,750	2,186	2,615	5,499	2,369
3	2.950	1,784	1,825	2,280	2,729	5,737	2,471
4	4.784	1,863	1,905	2,380	2,853	5,998	2,580
5	6.691	1,854	1,896	2,369	2,844	5,979	2,566
6	8.232	1,812	1,854	2,315	2,787	5,861	2,488
7	9.869	1,683	1,721	2,150	2,641	5,553	2,308
8	11.602	1,538	1,573	1,963	2,436	5,123	2,241
9	13.430	1,396	1,427	1,780	2,217	4,661	1,855
10	15.352	1,249	1,275	1,580	1,959	4,119	1,613

Supported by:

Section	Strength ratio – Test Load Cases						
nº	Distance from root [m]	Hill [-]	Hoffman [-]	Tsai-Wu [-]	Max-Strain [-]	Puck – FF [-]	Puck – IFF [-]
11	16.684	1,147	1,170	1,440	1,776	3,734	1,461
12	18.754	1,064	1,084	1,318	1,631	3,429	1,313
13	19.463	1,039	1,058	1,278	1,588	3,337	1,272
14	20.180	1,019	1,038	1,245	1,556	3,270	1,237
15	22.384	0,973	0,990	1,174	1,486	3,122	1,147
16	23.894	0,945	0,960	1,131	1,442	3,032	1,086
17	26.211	0,919	0,932	1,087	1,406	2,955	1,202
18	28.585	0,907	0,927	1,093	1,403	2,949	1,227
19	31.004	0,895	0,915	1,141	1,392	2,927	1,228
20	33.458	0,876	0,895	1,116	1,367	2,875	1,202
21	35.934	0,857	0,876	1,092	1,341	2,819	1,175
22	38.421	0,841	0,859	1,070	1,315	2,765	1,152
23	40.906	0,828	0,846	1,050	1,293	2,720	1,132
24	43.375	0,824	0,842	1,029	1,285	2,702	1,122
25	45.818	0,807	0,824	1,016	1,255	2,638	1,099
26	48.222	0,804	0,821	1,023	1,248	2,624	1,096
27	50.576	0,801	0,819	1,009	1,242	2,611	1,090
28	52.871	0,813	0,831	0,988	1,259	2,647	1,091
29	55.098	0,845	0,863	0,981	1,306	2,745	1,106
30	57.248	0,853	0,871	0,985	1,315	2,766	1,109
31	59.316	0,868	0,887	1,013	1,336	2,810	1,130
32	61.936	0,902	0,922	1,067	1,385	2,913	1,172
33	64.391	0,926	0,946	1,096	1,418	2,982	1,191
34	66.677	0,949	0,970	1,102	1,452	3,052	1,198
35	69.294	1,041	1,064	1,170	1,591	3,344	1,262
36	72.088	1,142	1,166	1,241	1,685	3,662	1,323
37	74.520	1,333	1,349	1,349	1,750	4,277	1,420
38	77.247	1,510	1,501	1,501	1,919	4,944	1,492
39	79.930	1,789	1,773	1,773	2,007	7,569	1,648
40	82.450	------	------	------	------	------	------
41	85.994	------	------	------	------	------	------

Supported by:

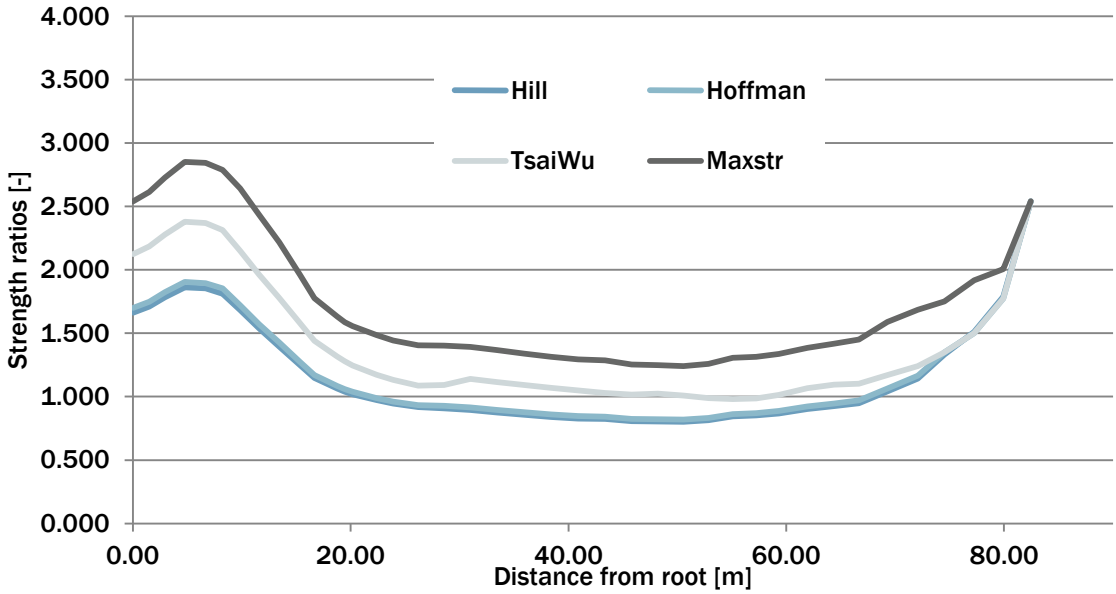

Figure 5 Evolution of minimum strength ratio along the blade span for test loads

S27 (50.576m from blade root) is also the limiting blade section under the test extreme loads. Following results are obtained at this section:

- ✓ Hill and Hoffman are the most limiting criteria with minimum strength ratios of 0.801 and 0.819 respectively for the PTS test. Failure of TRIAX material, located at the trailing panel of the airfoil pressure side, is predicted.
- ✓ Tsai-Wu criterion provides a minimum strength ratio of 1.009, approximately 26-23% higher than previous values from Hill & Hoffman also for PTS test. The limiting material is also TRIAX
- ✓ Max-Strain criterion identifies UD material located at the spar-cap of the suction side as the most limiting. Minimum strength ratio is 1.242 for the PTS test

Supported by:

5.1.3 Comparison; Design versus Test

To make the conclusions more evident, Table 17 shows the strength ratios for only Hill and Hoffman criteria. These failure theories are the most restrictive for this exercise.

Table 17 Comparison of minimum strength ratio (design loads versus tests)

	Distance from root [m]	Strength ratio (Hill) Design [-]	Test [-]	Deviation [%]	Strength ratio (Hoffman) Design [-]	Test [-]	Deviation [%]
S01	0	1,635	1,663	1,71%	1,669	1,701	1,92%
S02	1,5	1,688	1,711	1,36%	1,723	1,750	1,57%
S03	2,95	1,764	1,784	1,13%	1,800	1,825	1,39%
S04	4,78	1,849	1,863	0,76%	1,887	1,905	0,95%
S05	6,69	1,846	1,854	0,43%	1,884	1,896	0,64%
S06	8,23	1,796	1,812	0,89%	1,833	1,854	1,15%
S07	9,87	1,686	1,683	-0,18%	1,720	1,721	0,06%
S08	11,6	1,561	1,538	-1,47%	1,592	1,573	-1,19%
S09	13,43	1,442	1,396	-3,19%	1,458	1,427	-2,13%
S10	15,35	1,275	1,249	-2,04%	1,286	1,275	-0,86%
S11	16,68	1,164	1,147	-1,46%	1,171	1,170	-0,09%
S12	18,75	1,069	1,064	-0,47%	1,072	1,084	1,12%
S13	19,46	1,039	1,039	0,00%	1,041	1,058	1,63%
S14	20,18	1,015	1,019	0,39%	1,015	1,038	2,27%
S15	22,38	0,956	0,973	1,78%	0,954	0,990	3,77%
S16	23,89	0,911	0,945	3,73%	0,907	0,960	5,84%
S17	26,21	0,865	0,919	6,24%	0,859	0,932	8,50%
S18	28,58	0,844	0,907	7,46%	0,837	0,927	10,75%
S19	31,00	0,830	0,895	7,83%	0,821	0,915	11,45%
S20	33,46	0,815	0,876	7,48%	0,806	0,895	11,04%
S21	35,93	0,802	0,857	6,86%	0,792	0,876	10,61%
S22	38,42	0,789	0,841	6,59%	0,778	0,859	10,41%
S23	40,91	0,772	0,828	7,25%	0,761	0,846	11,17%
S24	43,38	0,783	0,824	5,24%	0,772	0,842	9,07%
S25	45,82	0,767	0,807	5,22%	0,755	0,824	9,14%
S26	48,22	0,774	0,804	3,88%	0,762	0,821	7,74%
S27	50,58	0,763	0,801	4,98%	0,751	0,819	9,05%
S28	52,87	0,774	0,813	5,04%	0,761	0,831	9,20%
S29	55,1	0,793	0,845	6,56%	0,783	0,863	10,22%
S30	57,25	0,796	0,853	7,16%	0,788	0,871	10,53%
S31	59,32	0,809	0,868	7,29%	0,801	0,887	10,74%
S32	61,94	0,841	0,902	7,25%	0,832	0,922	10,82%
S33	64,39	0,870	0,926	6,44%	0,861	0,946	9,87%
S34	66,68	0,892	0,949	6,39%	0,883	0,970	9,85%
S35	69,29	0,977	1,041	6,55%	0,966	1,064	10,14%
S36	72,09	1,075	1,142	6,23%	1,064	1,166	9,59%
S37	74,52	1,237	1,333	7,76%	1,223	1,349	10,30%
S38	77,25	1,407	1,510	7,32%	1,396	1,501	7,52%
S39	79,93	1,811	1,789	-1,21%	1,799	1,773	-1,45%
S40	82,45	3,029	------		2,998	------	

Supported by:

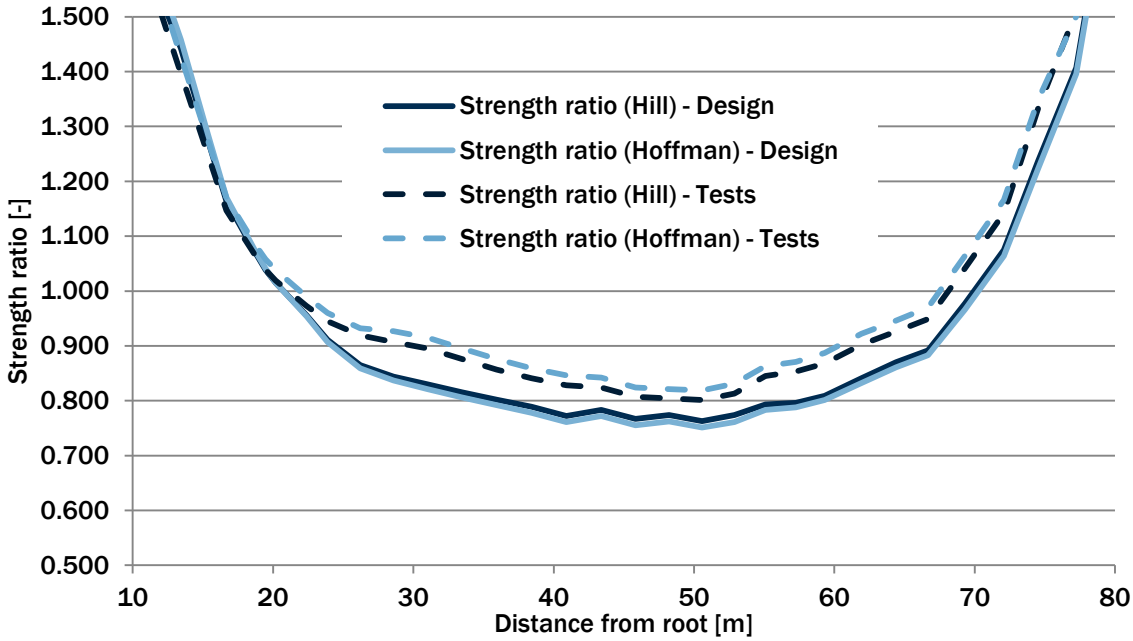

Figure 6 Comparison of minimum strength ratios; design versus tests

From the results shown in Table 17, following conclusions are obtained

- ✓ For the blade, certification tests are in general more benign than extreme operational loads considering that, at most of the sections, minimum strength ratio obtained for the tests are higher than that one from the design loads.
- ✓ For the critical sections (from S15 to S35), the maximum deviation between tests and design is located at S19 with deviation of 7.83% for Hill criterion and 11,45% for Hoffman
- ✓ At the most critical section (S27), the deviation is 4.98% for Hill and 9.05% for Hoffman
- ✓ In addition, the locations of the first ply failure change. For the design loads, Hill and Hoffman predict failure initiation of the TRIAX layers at the leading panel of the airfoil pressure side. However, under test loads, this critical area is moved to the trailing panel.

5.2 Results from the FE model

The strength analyses are also performed using the FE model defined by DTU (see section 3.2). The structural behaviour of the blade is checked for both the design loads and also for the test loads, working in an analogous way as it is done with the analytical approach (BASSF).

5.2.1 Minimum strength ratio for design extreme loads

The structural analyses are performed for the 84 load cases described in section 4.1. Table 18 shows those critical load cases (37) with minimum strength ratios lower than 1.0.

Supported by:

According to the results obtained, the baseline blade could fail under these 37 extreme loading conditions

Table 18 Maximum Failure Indexes & Minimum strength ratios for the design loads

Load Case ID	Load Case Name	Maximum Failure Index		Minimum Strength ratio		Critical area
		Hill [-]	Hoffman [-]	Hill [-]	Hoffman [-]	
26	dlc62j_h_1_1	2.653	2.340	0.614	0.654	Leading Panel - Suction
31	dlc62a_h_1_1	2.644	2.323	0.615	0.656	Leading Panel - Suction
24	dlc13bb1	2.523	2.184	0.630	0.677	Leading Panel - Suction
27	dlc13bb1	2.523	2.180	0.630	0.677	Leading Panel - Suction
9	dlc13bb1	2.520	2.181	0.630	0.677	Leading Panel - Suction
30	dlc13bb1	2.505	2.158	0.632	0.681	Leading Panel - Suction
38	dlc13bb1	2.472	2.131	0.636	0.685	Leading Panel - Suction
42	dlc13bb1	2.443	2.116	0.640	0.687	Leading Panel - Suction
50	dlc13bb1	2.434	2.112	0.641	0.688	Leading Panel - Suction
57	dlc11e1	2.382	2.047	0.648	0.699	Leading Panel - Suction
49	dlc21ba	2.381	2.080	0.648	0.693	Leading Panel - Suction
29	dlc21aa	2.325	2.004	0.656	0.706	Leading Panel - Suction
41	dlc21aa	2.325	2.004	0.656	0.706	Leading Panel - Suction
84	dlc11f1	2.313	2.050	0.658	0.698	Leading Panel - Suction
7	dlc21aa	2.295	1.998	0.660	0.707	Leading Panel - Suction
81	dlc21aa	2.165	1.841	0.680	0.737	Leading Panel - Suction
1	dlc13ab1	2.030	1.693	0.702	0.769	Leading Panel - Suction
76	dlc13cb1	1.856	1.582	0.734	0.795	Leading Panel - Suction
60	dlc13bb1	1.803	1.478	0.745	0.823	Leading Panel - Suction
72	dlc21ba	1.693	0.862	0.769	1.077	Leading Panel - Suction
64	dlc23ba_3	1.631	1.354	0.783	0.859	Leading Panel - Suction
78	dlc13cb1	1.618	1.364	0.786	0.856	Leading Panel - Suction
39	dlc14cb	1.536	0.871	0.807	1.071	Leading Panel - Pressure
43	dlc14cb	1.533	0.864	0.808	1.076	Leading Panel - Pressure
55	dlc14cb	1.523	0.857	0.810	1.080	Leading Panel - Pressure
32	dlc14cb	1.518	0.868	0.812	1.073	Leading Panel - Pressure
63	dlc14cb	1.503	0.840	0.816	1.091	Leading Panel - Pressure
28	dlc14cb	1.486	0.857	0.820	1.080	Leading Panel - Pressure
68	dlc14cb	1.472	0.818	0.824	1.106	Leading Panel - Pressure
20	dlc14cb	1.448	0.845	0.831	1.088	Leading Panel - Pressure
10	dlc14cb	1.397	0.828	0.846	1.099	Leading Panel - Pressure
33	dlc14cb	1.333	0.804	0.866	1.115	Leading Panel - Pressure
2	dlc14cb	1.270	0.779	0.888	1.133	Leading Panel - Pressure
61	dlc23ba_2	1.206	0.893	0.911	1.058	Leading Panel - Suction
13	dlc14cb	1.201	0.748	0.912	1.156	Leading Panel - Pressure
74	dlc14bb	1.138	0.897	0.937	1.056	Leading Panel - Suction
69	dlc14bb	1.064	0.820	0.969	1.104	Leading Panel - Suction

Most critical area of the blade is located at the leading edge panel at 23.5m from blade root. However, the area of the leading panels working under strength ratios lower than 1.0 goes over a total span from ~13m to ~71m

Supported by:

Following pictures show the minimum strength ratios obtained at every point of the blade considering the 84 design load cases. As it can be observed, the leading panel of airfoil suction side is the most critical. In any case, trailing panel neither satisfies the structural requirements. In addition, small areas of the airfoil pressure side also works under strength ratios slightly lower than 1.0

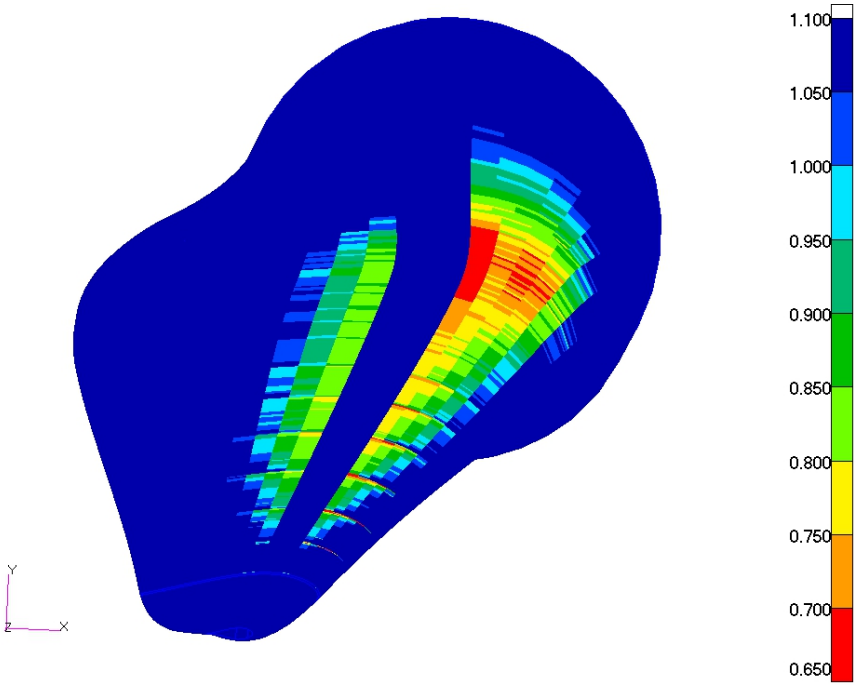

Figure 7 Minimum strength ratio (HILL theory) for the design cases – Suction side

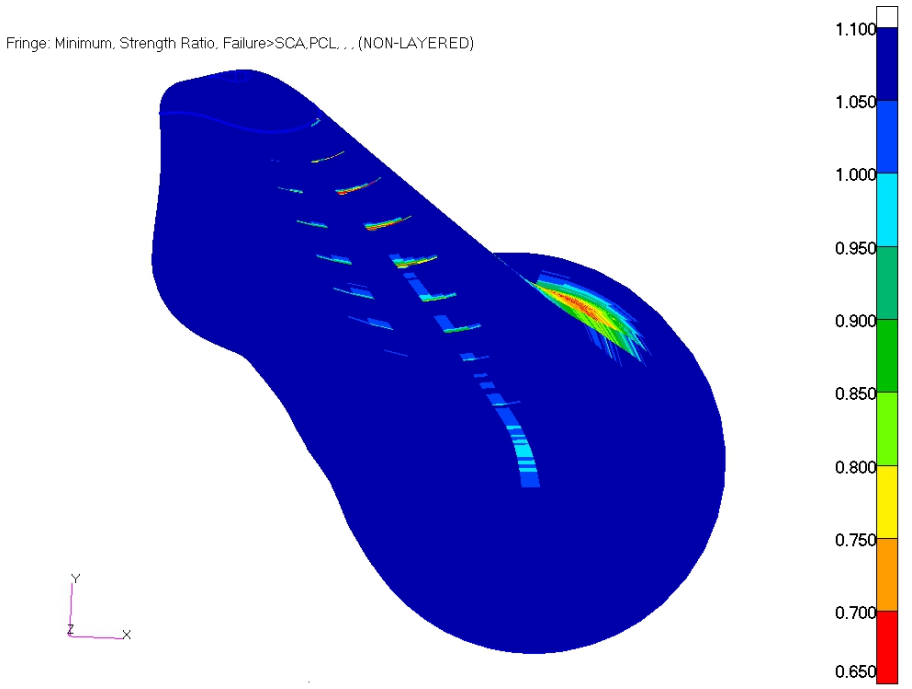

Figure 8 Minimum strength ratio (HILL theory) for the design cases – Pressure side

Supported by:

5.2.2 Minimum strength ratio for test extreme loads

The structural analyses are performed for the load tests defined in section 4.2.2. Following results are obtained:

Table 19 Maximum Failure Index & Minimum strength ratio for the tests

Test	Maximum Failure Index		Minimum Strength ratio		Critical area
	Hill [-]	Hoffman [-]	Hill [-]	Hoffman [-]	
PTS	2,251	1,721	0,667	0,762	Leading Panel - Suction
STP	1,270	1,092	0,887	0,957	Leading Panel - Pressure
TTL	0,471	0,402	1,457	1,577	Leading Edge
LTT	0,409	0,301	1,564	1,823	Trailing Edge

Depending on the test, the location of the critical area changes significantly. For Flapwise tests, there are significant areas of the blade with a strength ratio lower than 1.0, while for the Edgewise Tests there are not any blade areas arising a strength ratio around 1.0, but greater than 1.45.

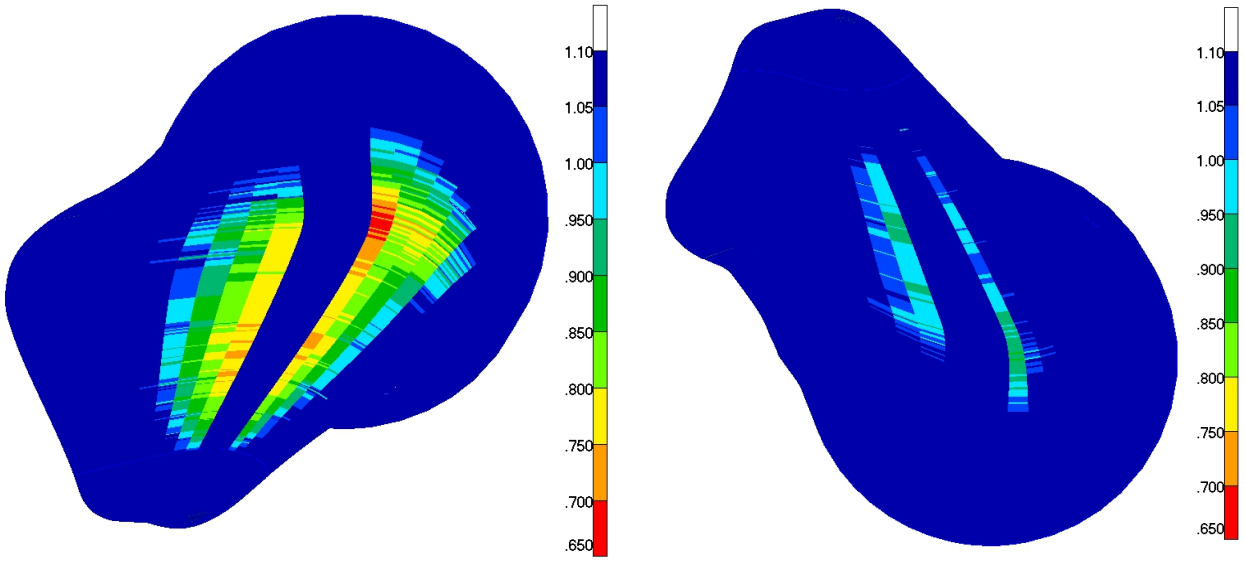

Figure 9 Minimum strength ratios (HILL theory) for the PTS & STP tests

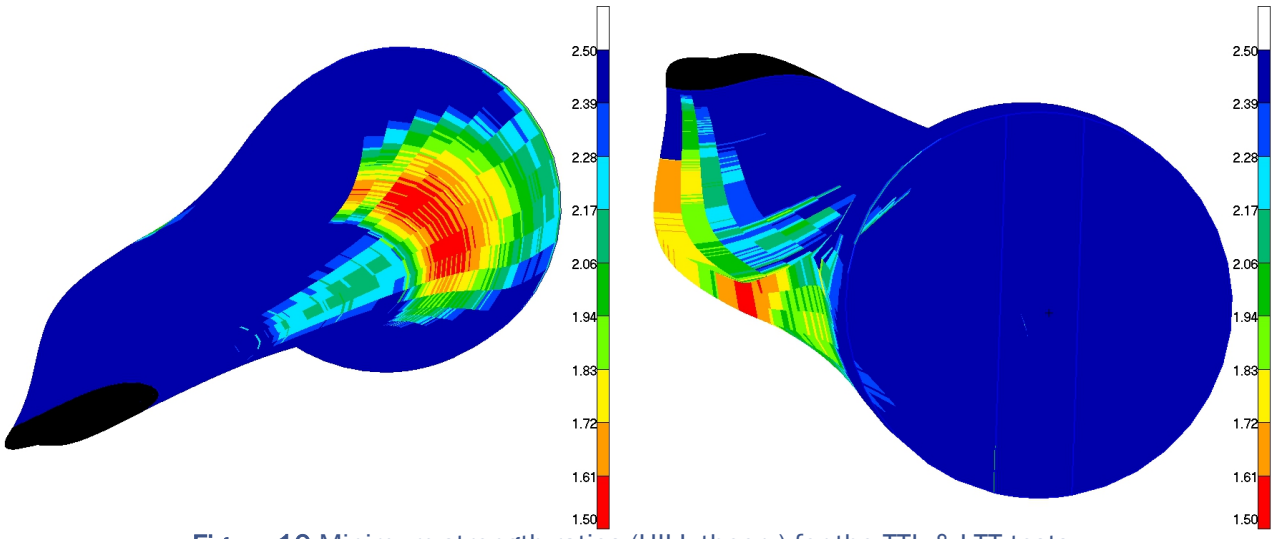

Figure 10 Minimum strength ratios (HILL theory) for the TTL & LTT tests

Supported by:

5.2.3 Comparison; Design versus Test

The limitation of the tests, with puller forces acting in one unique plane makes the blade work in a "general" more benign environment in comparison with the operational loading, although there are some hints to consider.

Table 20 Comparison of minimum strength ratios (design loads versus tests)

Critical Area	Minimum Strength Ratio Design Loads		Minimum Strength Ratio Test Loads	
	Load Case Name	Hill [-]	Test Name	Hill [-]
Leading Panel - Suction	dlc62j_h_1_1	0.614	PTS	0.667
Leading Panel - Pressure	dlc14cb	0.807	STP	0.887

As it is shown in Table 20, and for the case studied, the comparison between the design loads and the test provides always same tendencies:

- ✓ For the leading panel at suction side of the blade, the tests are ~8% more benign than the design loads
- ✓ For the leading panel at pressure side of the blade, the tests are also ~9.5% more benign than the design loads

Supported by:

6. Fatigue Loads

6.1 Design loads

Fatigue loads are provided by POLIMI using the reference wind turbine defined by DTU with the same control parameters but without pre-bending. The time series are given for ten sections along the blade.

6.1.1 Coordinate system assumption

A simplified statistical post-processing is performed considering that these time series are given with reference to coordinate systems rotating with the rotor, with the pitch angle, and that also fit with the local chord coordinate systems of the blade airfoils (as it is stated in [6]). Based on this assumption, the times series are transformed firstly to a common coordinate system with twist angle = 0 (see section 3.2.2). Afterwards, RMS (root mean square), maximum and minimum values for each load components (FX, FY, FZ, MX, MY, MZ) are obtained. Table 21 and Figure 11 show the values obtained for RMS according to the load case dlc11_3a.

Table 21 RMS values for each load component – Load Case dlc11_3a

RMS Values for each load component – Load Case dlc11_3a						
Distance from root [m]	FX [kN]	FY [kN]	FZ [kN]	MX [kNm]	MY [kNm]	MZ [kNm]
0,00	102,83	289,77	548,91	7571,83	4458,75	50,73
8,64	156,04	177,76	491,63	4594,19	4502,79	51,09
17,27	88,57	163,34	426,73	3663,29	2946,40	49,83
25,91	72,61	123,47	360,22	2442,07	2238,82	44,26
34,55	61,99	90,02	290,79	1545,51	1661,19	36,45
43,18	52,30	62,15	219,23	895,43	1171,54	28,02
51,82	42,88	39,32	151,63	463,68	763,17	19,58
60,46	33,23	22,39	92,78	201,71	437,48	12,50
69,09	22,97	10,42	46,18	64,73	196,29	6,69
77,73	11,77	3,11	14,61	10,01	47,25	2,37

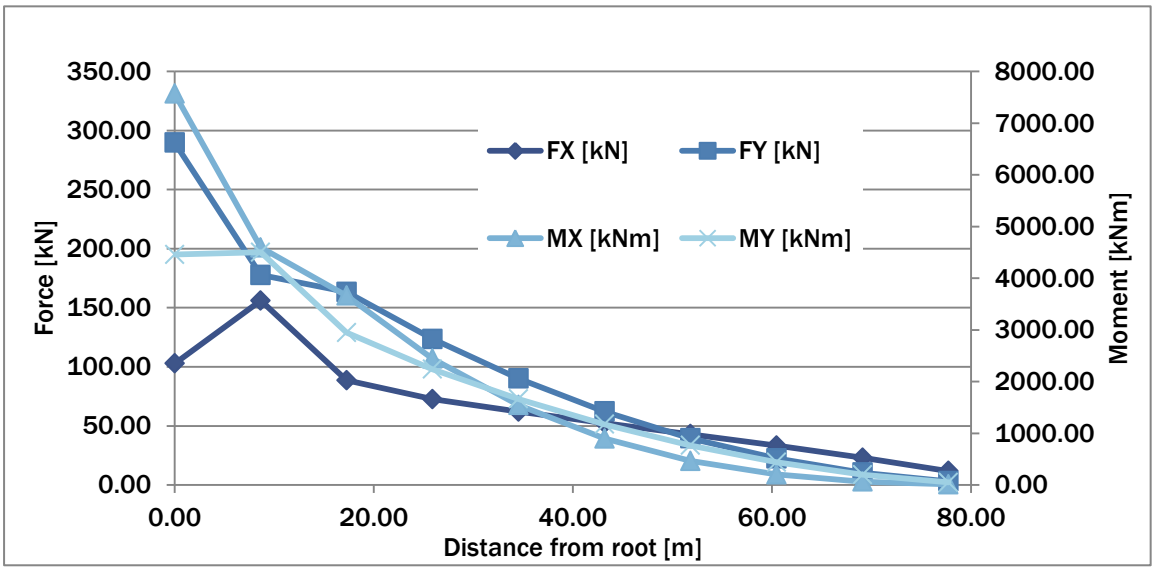

Figure 11 Shear forces and bending moments for dlc11_3a – RMS values

Supported by:

From the experience with other aero-elastic analyses, it is not easy to understand the results obtained at the two first sections located close to the root. This non-logical behavior is repeated for the rest of the load cases and also for maximum and minimum values.

From a deeper analysis is assumed that POLIMI time series are given with reference to coordinate systems rotating with the rotor, with the pitch angle, and that also fit with the principal axis of the structural coordinate systems defined by DTU (no with the local ones of the chord). Considering this assumption, the loads obtained converge into an expected physical behaviour of the blade.

Table 22 RMS values for each load component – Updated values – Load Case dlc11_3a

RMS Values for each load component – Load Case dlc11_3a						
Distance from root [m]	FX [kN]	FY [kN]	FZ [kN]	MX [kNm]	MY [kNm]	MZ [kNm]
0,00	102,83	289,77	548,91	7571,83	4458,75	50,73
8,64	93,68	217,19	491,63	5247,11	3721,50	51,09
17,27	81,26	167,10	426,73	3724,49	2868,65	49,83
25,91	71,25	124,26	360,22	2454,50	2225,18	44,26
34,55	61,54	90,33	290,79	1549,04	1657,90	36,45
43,18	52,20	62,23	219,23	895,96	1171,14	28,02
51,82	42,87	39,33	151,63	463,45	763,31	19,58
60,46	33,24	22,37	92,78	201,46	437,60	12,50
69,09	22,98	10,40	46,18	64,60	196,34	6,69
77,73	11,77	3,09	14,61	9,99	47,26	2,37

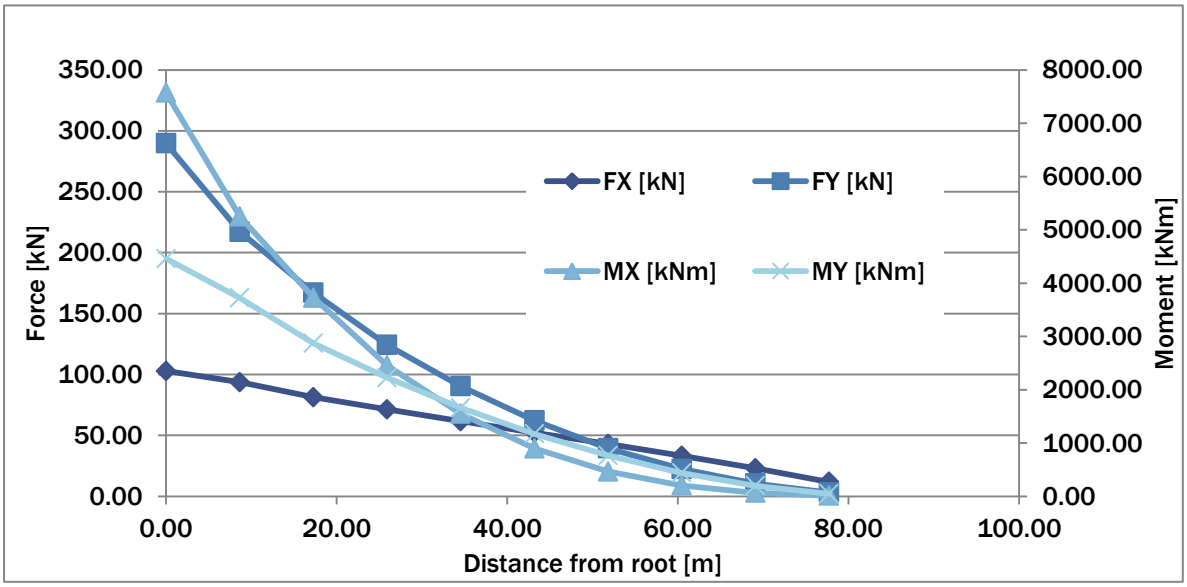

Figure 12 Updated shear forces and bending moments for dlc11_3a – RMS values

According to the results obtained, all the work presented below, and related with fatigue issues, is done considering this last assumption for POLIMI's coordinate system.

Supported by:

6.1.2 Loads update for fatigue analysis

POLIMI fatigue loads are modified to adequate the information for the input requirements of the analysis methods:

- ✓ Analytical approach: Fatigue loads are interpolated to those 41sections where the blade is defined (see section 3.1)
- ✓ FE model: The introduction of loads is defined at 10 points using RBE3 equations, but at intermediate sections located in the middle point in-between those sections where the aero-elastic code provides these time series. The uncoupling of these loads is done according to the criterion of section 4.1 but for all of the time steps.

6.2 Test loads

6.2.1 Equivalent loads

Test loads reproduce the equivalent damage as that one induced from the time series when they are applied for 2.0e6 cycles. The methodology used to obtain these loads is based on the following steps:

1.) Peak and valley extraction
2.) Rain-flow counting according to ASTM E1049-85
3.) Markov matrix definition (64x64 bins)
4.) Equivalent load definition based on SN-approach, Miner's rule and m slope = 10

Table 23 shows the equivalent loads (amplitude) that should be introduced in the blade during 2.0e6cycles to generate equal damage as that one from the time series

Table 23 Equivalent loads for 2.0e6 cycles

Equivalent LOADS for 2.0e6 cycles						
Distance from root [m]	FX [kN]	FY [kN]	FZ [kN]	MX [kNm]	MY [kNm]	MZ [kNm]
0.00	372.52	618.63	725.12	16591.00	17889.00	280.51
8.64	363.73	466.58	602.90	11582.00	15371.00	257.01
17.27	339.93	365.01	492.62	8385.90	12000.00	240.85
25.91	315.55	274.37	397.04	5641.10	9361.00	197.62
34.55	278.89	202.45	307.49	3652.70	6939.80	143.58
43.18	233.67	142.84	225.42	2193.40	4852.10	97.94
51.82	186.27	93.94	151.01	1196.60	3143.00	62.10
60.46	140.32	56.94	90.08	561.97	1809.50	39.67
69.09	96.20	29.35	43.94	202.77	799.08	23.53
77.73	47.38	10.58	13.61	38.45	187.10	10.01

6.2.2 Fatigue tests description

According to GL-Guideline [4], fatigue tests are only mandatory in the following situations:

- ✓ When blade design is different from the state of the art
- ✓ When damages are revealed during operation
- ✓ When exceptional deformation behaviour is observed under operational loads (e.g. strong deformation of the blade cross section)

Supported by:

As it is stated in section 4.2.1, since April 2014, a new update of IEC-61400-23 [3] was delivered. This standard requires fatigue test execution.

Considering CENER experience, it is common to perform fatigue tests according to the following sequence:

- ✓ 1st fatigue test: Flapwise direction during 2.0e6 - 3.0e6 cycles
- ✓ 2nd fatigue test: Edgewise direction during 2.0e6 – 5.0e6 cycles

Recently, it is observed a trend to perform coupled fatigue tests that combine Flapwise and Edgewise moments. These tests are significantly more complex than the traditional ones due to the nature of the loading devices' controllers and also due to the added complexity associated to tests definition and results interpretation.

The analyses performed in this report are focused only on the conventional tests where the fatigue loads are applied according to an uncoupled way. Table 24 and Table 25 detail the amplitude of the loads introduced during Flapwise and Edgewise tests.

Table 24 Loads of Flapwise test for 2.0e6 cycles

Distance from root [m]	FX [kN]	MY [kNm]
0.00	372.52	17889.00
8.64	363.73	15371.00
17.27	339.93	12000.00
25.91	315.55	9361.00
34.55	278.89	6939.80
43.18	233.67	4852.10
51.82	186.27	3143.00
60.46	140.32	1809.50
69.09	96.20	799.08
77.73	47.38	187.10

Table 25 Loads of Edgewise test for 2.0e6 cycles

Distance from root [m]	FY [kN]	MX [kNm]
0.00	618.63	16591.00
8.64	466.58	11582.00
17.27	365.01	8385.90
25.91	274.37	5641.10
34.55	202.45	3652.70
43.18	142.84	2193.40
51.82	93.94	1196.60
60.46	56.94	561.97
69.09	29.35	202.77
77.73	10.58	38.45

Target bending moment envelopes are achieved with the introduction of sinusoidal forces into the blade and with the addition of dead-weights at different span-wise sections. For load introduction, either oscillating-mass actuators or actuators fixed to the ground can be used.

Supported by:

In order to reduce the energy for the tests, these sinusoidal loads are applied at a frequency coincident with the first natural frequency of the test set-up. This value depends on the blade to be tested and also on the dead masses added.

Both the location and magnitude of these dead-weights and also the values of the oscillating forces are defined by the test laboratory according to their capabilities.

Figure 13 shows the installations of CENER fatigue test rig. Besides the MTS oscillating masses of the picture, an additional actuator fixed to the ground has been recently acquired with a maximum load range of 200kN (±100kN).

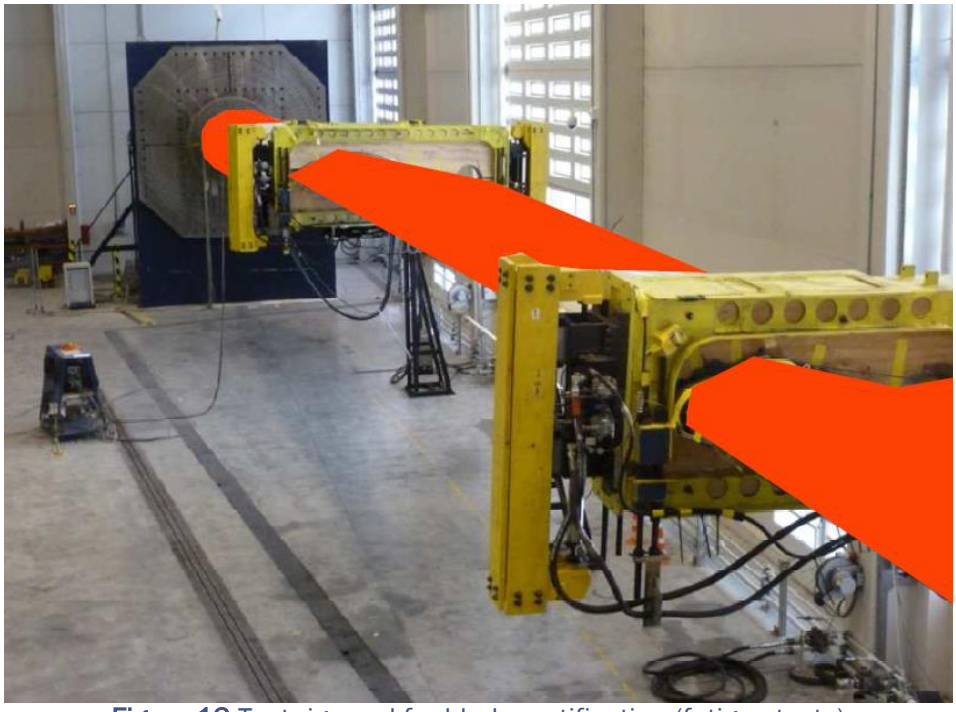

Figure 13 Test-rig used for blade certification (fatigue tests)

6.2.3 Test Factor

According to the standard, the equivalent loads applied during the tests should be scaled by the following factors:

$$F_{target-f} = F_{df} \cdot \gamma_{nf} \cdot \gamma_{sf} \cdot \gamma_{ef}$$

- ✓ γ_{nf}: Partial factor for consequence of failure. It is assumed to be 1.0 (see section 4.2.2.1)
- ✓ γ_{sf}: Test load factor for blade to blade variation. It is assumed to be 1.1
- ✓ γ_{ef}: Test load factor for errors in fatigue formulation. This number depends on the number of cycles of the fatigue tests. It is assumed to be 1.05 for reference.

As it happens for the static tests, last version of the standard includes an environmental factor, due to the benign conditions of the test facilities in comparison with the operational ones. The work performed does not consider this factor.

Considering this recommendation of IEC-61400-23 [3] equivalent fatigue loads from Table 24 and Table 25 are multiplied by 1.155

Supported by:

7. Structural behaviour of the Blade under fatigue loads

As it is done in section 5, blade fatigue analysis is performed using both the analytical approach with BASSF and also the FE method. The objective of this task is to compare maximum damage values obtained when the blade is loaded under the design conditions (section 5.1) and when it is loaded under the test conditions (section 5.2) using the results from both methods. However, as it is explained in section 7.2, the results obtained from the FE model are not reliable enough to extract robust conclusions, so, only the results from BASSF are used for this purpose.

The mathematical approach used for damage estimation is based on the SN method defined in GL-Guideline [4]. This method is focused on proportional stress states where the absolute maximum principal values are aligned with the blade pitch axis direction (0°). **Following formula represents** the cyclic behaviour of every ply of the blade lay-up:

$$N = \left[\frac{R_{k,t} + |R_{k,c}| - |2.\gamma_{Ma}.S_{k,M} - R_{k,t} + |R_{k,c}||}{2.(\gamma_{Mb}/-).S_{k,A}}\right]^{m} \quad where;$$

$S_{k,M}$ = Mean value of the characteristic actions
$S_{k,A}$ = Amplitude of the characteristic actions
$R_{k,t}$ = Characteristic short-term structural member resistance for tension
$R_{k,c}$ = Characteristic short-term structural member resistance for tension
m = Slope parameter m of the S/N curve
N = Permissible load cycle number
γ_{Ma} = Partial safety factor for the material – short term strength
γ_{Mb} = Partial safety factor for the material – fatigue strength

$S_{k,M}, S_{k,A}, R_{k,t}\ and\ R_{k,c}$ could be expressed in terms of stresses or strains although it is not trivial and it should be treated with caution. In addition, the equivalent stress component used for damage should be discussed in detail for further life predictions.

In this report, following assumptions are considered:

- ✓ Analytical approach (BASSF): Based on stresses. Equivalent stress value = $\boldsymbol{\sigma}_{axial}$
- ✓ FE model: Based on strains. Equivalent strain value = $\boldsymbol{\varepsilon}_{axial}$

The fatigue behaviour of UD, BIAX and TRIAX plies are checked. Balsa is not considered in these analyses.

Table 26 Characteristic stress values for fatigue analysis – analytical approach

Material ID	Material Name	R_{KT} [MPa]	R_{KC} [MPa]	γ_{Mb} [-]	m_{slope} [-]
1	CORE PVC	----	----	----	----
2	UD	874.15	624.0	1.485	10
3	BIAX	222.68	208.77	1.6335	10
4	TRIAX	479.32	392.5	1.6335	10

Supported by:

Table 27 Characteristic strain values for fatigue analysis – analytical approach

Material ID	Material Name	R_{KT} [με]	R_{KC} [με]	γ_{Mb} [-]	m_{slope} [-]
1	CORE PVC	----	----	----	----
2	UD	20998	14999	1.485	10
3	BIAX	15997	14998	1.6335	10
4	TRIAX	21997	17997	1.6335	10

7.1 Results from the analytical approach (BASSF)

7.1.1 Maximum damage for design fatigue loads

Table 28 Maximum damage for the blade under the design load cases

Section	Maximum Damage – Design Load Cases			
n°	Distance from root [m]	UD mat [-]	BIAX mat [-]	TRIAX mat [-]
1	0.000	< 1.0e-5	0.0065	< 1.0e-5
2	1.502	< 1.0e-5	0.0046	< 1.0e-5
3	2.950	< 1.0e-5	0.0030	< 1.0e-5
4	4.784	< 1.0e-5	0.0018	< 1.0e-5
5	6.691	< 1.0e-5	0.0020	< 1.0e-5
6	8.232	< 1.0e-5	0.0031	< 1.0e-5
7	9.869	< 1.0e-5	0.0073	< 1.0e-5
8	11.602	< 1.0e-5	0.0220	< 1.0e-5
9	13.430	< 1.0e-5	0.0692	< 1.0e-5
10	15.352	0.0001	0.2737	0.0001
11	16.684	0.0001	0.7973	0.0003
12	18.754	0.0002	2.0958	0.0006
13	19.463	0.0003	3.0109	0.0007
14	20.180	0.0004	4.1681	0.0009
15	22.384	0.0006	7.6464	0.0013
16	23.894	0.0009	10.9294	0.0018
17	26.211	0.0016	13.5745	0.0025
18	28.585	0.0023	11.2322	0.0033
19	31.004	0.0032	8.8577	0.0043
20	33.458	0.0038	6.6589	0.0048
21	35.934	0.0044	6.0075	0.0054
22	38.421	0.0051	6.1750	0.0063
23	40.906	0.0057	5.4771	0.0072
24	43.375	0.0059	4.6724	0.0075
25	45.818	0.0069	5.2275	0.0090
26	48.222	0.0068	3.9534	0.0090
27	50.576	0.0069	3.2933	0.0091
28	52.871	0.0067	2.6474	0.0090
29	55.098	0.0068	2.1107	0.0086
30	57.248	0.0067	1.6836	0.0084
31	59.316	0.0053	0.9687	0.0064
32	61.936	0.0044	0.6065	0.0053

Supported by:

Section	Maximum Damage – Design Load Cases			
n°	Distance from root [m]	UD mat [-]	BIAX mat [-]	TRIAX mat [-]
33	64.391	0.0039	0.4421	0.0046
34	66.677	0.0024	0.2766	0.0034
35	69.294	0.0013	0.0783	0.0014
36	72.088	0.0009	0.0524	0.0010
37	74.520	0.0004	0.0217	0.0005
38	77.247	< 1.0e-5	0.0008	< 1.0e-5
39	79.930	< 1.0e-5	0.0005	< 1.0e-5
40	82.450	< 1.0e-5	0.0014	< 1.0e-5
41	85.994	< 1.0e-5	0.0002	< 1.0e-5

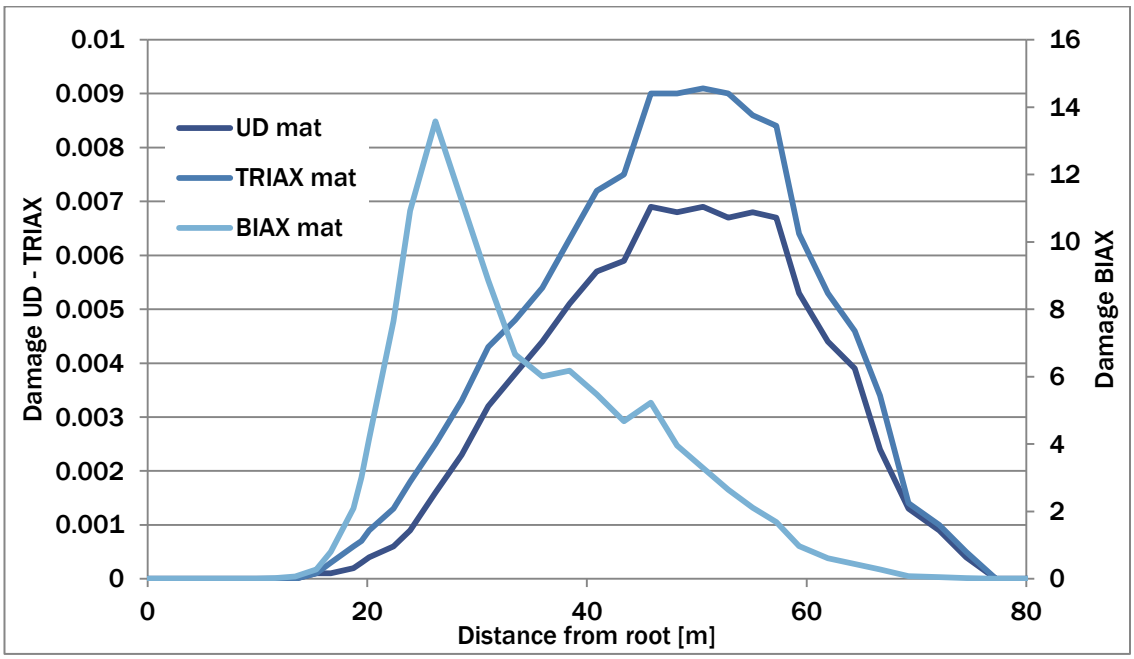

Figure 14 Evolution of damage at UD, TRIAX and BIAX plies – design loads

According to the results detailed in Table 28 and Figure 14, following remarks are defined:

- ✓ Accumulated damage at UD and TRIAX plies increases progressively from root to section 27 (50.576m) and then it decreases till the blade tip. Its maximum value goes up to 0.0069 for UD plies to 0.0091 for TRIAX plies.
- ✓ Accumulated damage at BIAX plies is maximum at section 17 (26.211m) with a value of 13.57. The critical point is located at the shear-web of the leading edge with a BIAX lay-up total thickness of ≈8mm.

Supported by:

7.1.2 Maximum damage for test fatigue loads

In order to verify the structural behaviour of the blade, both Flapwise and Edgewise tests should be performed to introduce the equivalent damage as that one due to design loads (see section 6.2.2). As it is stated in section 6.2.3, a test load factor of 1.155 is applied to the equivalent loads defined in section 6.2.1

The analyses executed confirm that Edgewise test does not introduce any significant damage (<1.0e-5).

Maximum damage values of Table 29 are caused under Flapwise test.

Table 29 Maximum damage for the blade under fatigue test (FLAPWISE)

Section	Maximum Damage – TEST Load Case (FLAPWISE)			
n°	Distance from root [m]	UD mat [-]	BIAX mat [-]	TRIAX mat [-]
1	0.000	< 1.0e-5	0.0008	< 1.0e-5
2	1.502	< 1.0e-5	0.0006	< 1.0e-5
3	2.950	< 1.0e-5	0.0005	< 1.0e-5
4	4.784	< 1.0e-5	0.0003	< 1.0e-5
5	6.691	< 1.0e-5	0.0003	< 1.0e-5
6	8.232	< 1.0e-5	0.0004	< 1.0e-5
7	9.869	< 1.0e-5	0.0008	0.0001
8	11.602	< 1.0e-5	0.0016	0.0001
9	13.430	< 1.0e-5	0.0038	0.0003
10	15.352	0.0002	0.0111	0.0007
11	16.684	0.0009	0.0261	0.0016
12	18.754	0.0018	0.0582	0.0032
13	19.463	0.0023	0.0769	0.0039
14	20.180	0.0026	0.0991	0.0047
15	22.384	0.0055	0.1641	0.0070
16	23.894	0.0080	0.2156	0.0093
17	26.211	0.0121	0.2674	0.0127
18	28.585	0.0168	0.2522	0.0160
19	31.004	0.0218	0.2342	0.0196
20	33.458	0.0254	0.2068	0.0211
21	35.934	0.0282	0.2124	0.0230
22	38.421	0.0333	0.2372	0.0265
23	40.906	0.0357	0.2416	0.0290
24	43.375	0.0368	0.2548	0.0291
25	45.818	0.0419	0.2912	0.0349
26	48.222	0.0435	0.3339	0.0349
27	50.576	0.0429	0.3346	0.0341
28	52.871	0.0385	0.3138	0.0321
29	55.098	0.0372	0.2905	0.0308
30	57.248	0.0358	0.2731	0.0301
31	59.316	0.0271	0.1961	0.0229
32	61.936	0.0216	0.1465	0.0183
33	64.391	0.0188	0.1177	0.0158
34	66.677	0.0137	0.0850	0.0117
35	69.294	0.0051	0.0315	0.0045

Supported by:

Section	Maximum Damage – TEST Load Case (FLAPWISE)			
nº	Distance from root [m]	UD mat [-]	BIAX mat [-]	TRIAX mat [-]
36	72.088	0.0036	0.0225	0.0033
37	74.520	0.0017	0.0110	0.0016
38	77.247	0.0001	0.0006	0.0001
39	79.930	< 1.0e-5	0.0004	< 1.0e-5
40	82.450	< 1.0e-5	0.0003	< 1.0e-5
41	85.994	< 1.0e-5	0.0001	< 1.0e-5

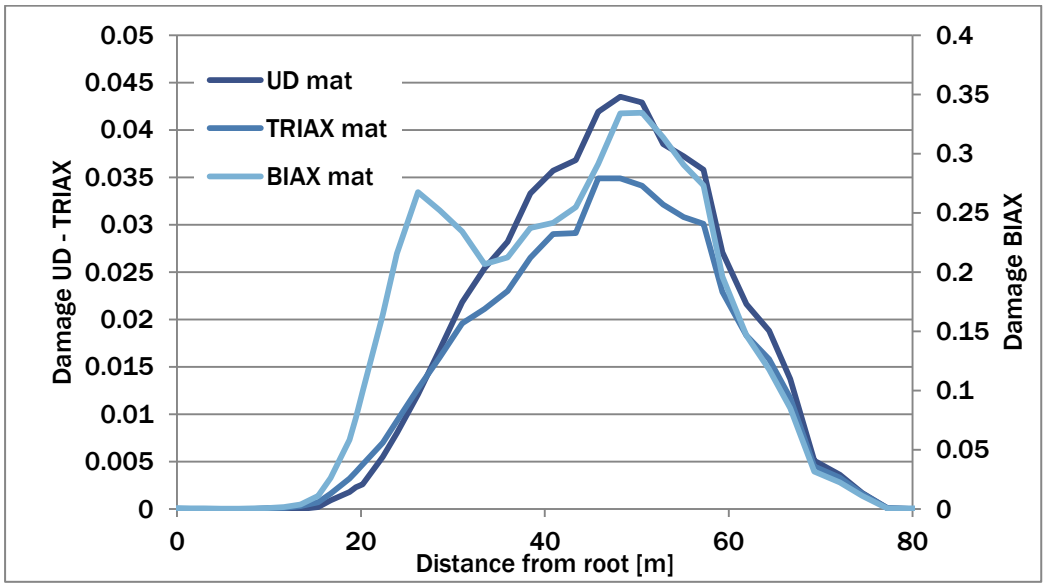

Figure 15 Evolution of damage at UD, TRIAX and BIAX plies – FLAPWISE test loads

According to the results detailed in Table 29 and Figure 15 following remarks are defined:

- ✓ Accumulated damage at UD and TRIAX plies increases progressively from root to section 26-27 (48.222m - 50.576m) and then it decreases till the blade tip. In this case, its maximum value does goes up to 0.0435 for UD plies or 0.0349 for TRIAX plies.
- ✓ Accumulated damage at BIAX plies is maximum at section 27 (50.576m) with a value of 0.346 located at the shear-web of the trailing edge with a BIAX lay-up total thickness of ≈9mm. At section 17 (26.211m) and located at the shear-web of the leading edge the accumulated damage goes up to 0.2674

Supported by:

7.1.3 Comparison; Design versus Test

Before comparing the results from sections 7.1.1 and 7.1.2, it is important to remark two main restrictions of the tests that influence directly on the accumulated damage introduced to the blade.

- ✓ Uncoupled loading: In operational conditions, the rotor blade is working under a multi-axial spectrum of loads since, in the tests, this loading condition is uniaxial.
- ✓ Mean effect: Due to the restrictions of the testing facilities, it is not possible to consider properly the mean values of the loading time series. When using mass-oscillating masses, mean loads are conditioned by gravitational effects. The hydraulic actuator can minimize this effect but, in any of the cases, it is not possible to match with those values from operation.

These limitations affect directly to the estimation of damage. Material curves proposed by GL are extremely influenced by the mean values of the stresses. In addition, the logarithmic approach of the material behaviour deals into significant differences in damage when the input stresses are slightly modified.

From the results shown in Table 28 and Table 29, following statements are concluded:

- ✓ UD & TRIAX plies: Flapwise test loads introduce higher damage than that one from design loads, considering its value and progression along the span-wise locations of the blade. The reason of this result is affected by the test factor considered (1.155). In both cases, obtained damage values are lower than 1.0. As a consequence, it is expected that the blade life could go over 25 years.
- ✓ BIAX plies: Damage differences obtained from design and Flapwise tests are quite significant. Main reason of this mismatch is caused by the no consideration of the mean effects from axial loading and Flapwise moments. During operation, the existence of cycles with high mean values makes the material working near to the limits, causing a significant damage that leads to damage values higher than 1.0 when they are computed for the total number of occurrences.

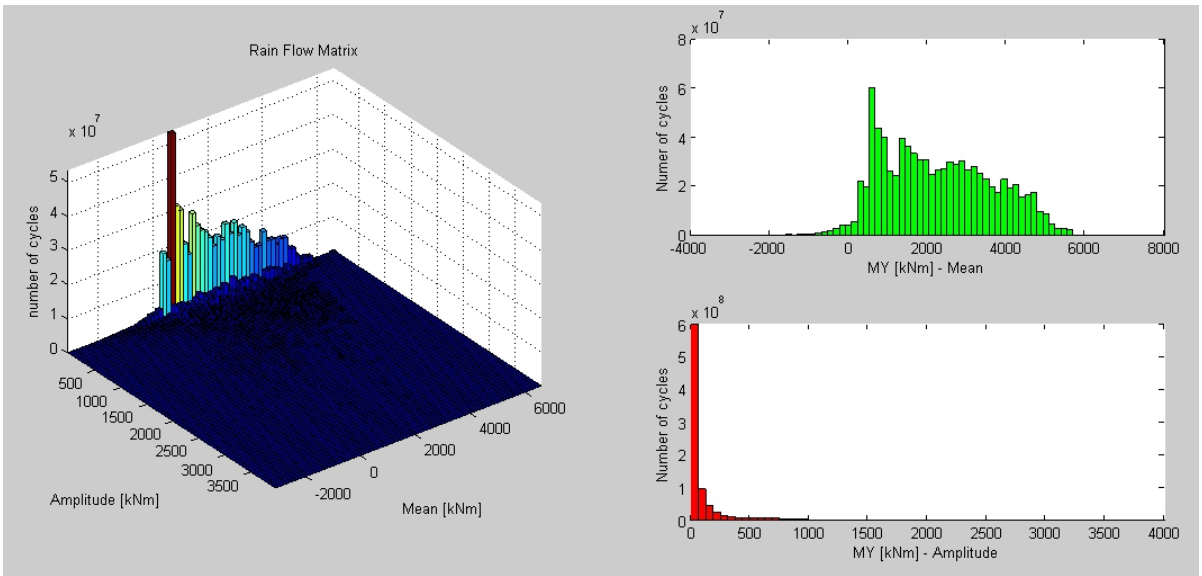

Figure 16 Rain-flow matrix for MY [kNm] at 54.62m from root.

Supported by:

7.2 Results from the FE model

The fatigue analysis of the baseline blade provided by DTU is done using MSC.NASTRAN and MSC.FATIGUE software. Damage estimation is based on SN approach, Miner's rule and the material formulation defined in GL-Guideline [4].

This FE model is loaded at 10 points using RBE3 equations, but at intermediate sections located in the middle point in-between those sections where the aero-elastic code provides these time series. The uncoupling of these loads is done according to the criterion of section 4.1 but for all of the time steps.

Once the loads are updated and prepared for the required format, the method followed for damage estimation is the following:

- ✓ Execution of linear static analyses for unitary loads. Considering 10 load introduction points and 6 load components (FX, FY, FZ, MX, MY, MZ), 60 FE analyses are done
- ✓ Linear combination of the strain results for every load case considering the values of the time series previously uncoupled
- ✓ Peak-valley extraction for the axial strain time-series at the outer surface of every element
- ✓ Rain-flow counting
- ✓ Damage estimation for every element and every load case. Material formulation is defined using strain values.
- ✓ Linear superposition of damage taking into account all the events (20) and occurrences defined by POLIMI

The results obtained are significantly affected by the RBE3 equations used for load introduction. Although the progression of damage is similar to that one observed with BASSF, expected damage is at least of one order higher than that one from the analytical code.

Further research and a deeper validation of this FE method is needed for a reliable fatigue assessment of the blade. Assuming this situation, it is decided not to extract conclusions from these FE results. The expected damage for the design load cases using this method is shown for reference.

Table 30 shows maximum damage obtained in UD, BIAX and TRIAX plies at those sections where POLIMI time series are defined

Table 30 Damage progression obtained from the FEM model

Section	Maximum Damage – Design Load Cases			
nº	Distance from root [m]	UD mat [-]	BIAX mat [-]	TRIAX mat [-]
1	2.800	0.00	1.17	0.00
2	11.437	0.00	113.20	0.00
3	20.073	0.06	362.10	0.01
4	28.710	0.24	341.40	0.06
5	37.346	0.38	85.77	0.09
6	45.983	0.26	85.30	0.06

Supported by:

Section	Maximum Damage – Design Load Cases			
n°	Distance from root [m]	UD mat [-]	BIAX mat [-]	TRIAX mat [-]
7	54.620	0.22	9.31	0.05
8	63.256	0.08	0.02	0.02
9	71.893	0.01	0.00	0.01
10	80.529	0.00	0.00	0.00

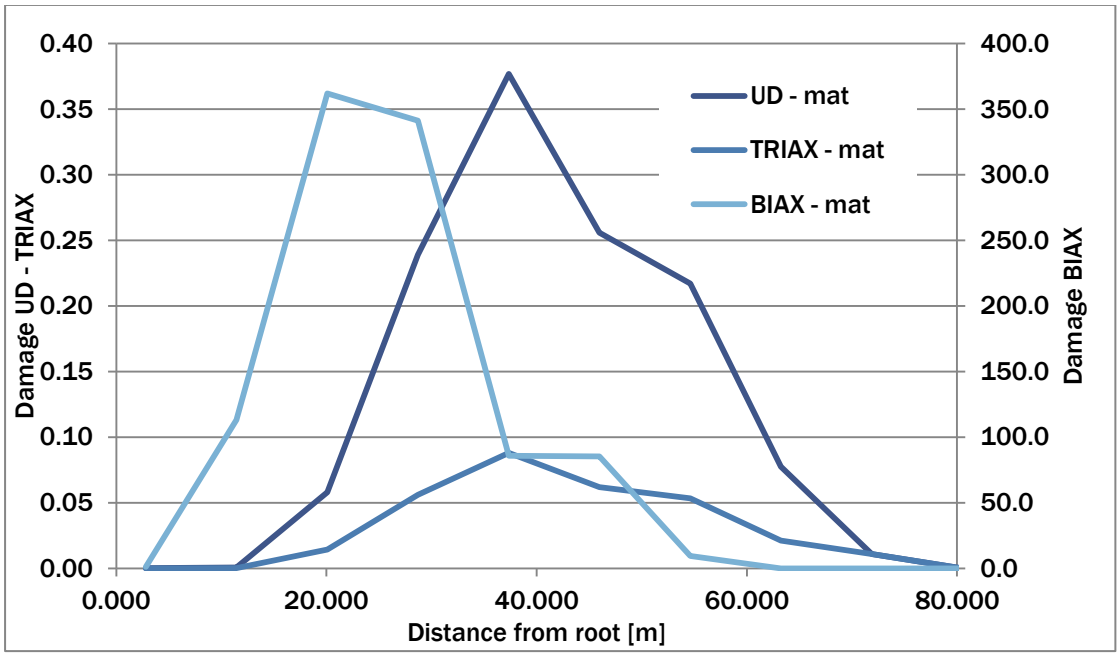

Figure 17 Evolution of damage at UD, TRIAX and BIAX plies – design loads

Supported by:

8. Conclusions

8.1 Conclusions for extreme load cases; design versus tests

According to the work done and for the case studied, the certification tests proposed by IEC standard are in general more benign than the extreme design loads. It is checked that, at most of the blade sections, the minimum strength ratios obtained for the tests are higher than those ones obtained when loading the blade with the design cases.

From these considerations, it can be remarked that the representativeness of the tests is directly influenced by the particularities of the blade design and its operational loads.

As a consequence, it is suggested to evaluate the option of defining the tests not only from maximum load envelopes but with the support of more detailed structural analyses.

8.2 Conclusions for fatigue load cases; design versus tests

Fatigue tests are conditioned by the influence of the mechanical systems used for load application and the common loading-methodology assumed by main blade manufacturers.

As a consequence, it is not easy to reproduce with the tests that damage expected from wind turbine operation. Main reasons are:

- ✓ Uncoupled loading: In operational conditions, the rotor blade is working under a multi-axial spectrum of loads since, in the tests, this loading condition is uniaxial.
- ✓ Uniform amplitude loading: In operational conditions, the rotor blade is loaded with a high dispersion of cycles (amplitude and mean) which deals into spread histograms. Although from the theoretical point of view, it is possible to reproduce the same damage of operation using equivalent loads, there are factors not considered as non-linear behaviour and local buckling
- ✓ Mean effect: Due to the restrictions of the testing facilities, it is not possible to consider properly the mean values of the loading time series. When using mass-oscillating masses, mean loads are conditioned by gravitational effects. The hydraulic actuator can minimize this effect but, in any of the cases, it is not possible to match with those values from operation.

These limitations affect directly to the estimation of damage. In addition, the material formulation (highly influenced by the stresses mean values) and the logarithmic approach of the material behaviour deals into significant differences in damage between tests and operation.

Under the case studied, Flapwise test is more critical for UD and BIAX layers than the operational loading conditions while for the shear webs (BIAX), the effect is the opposite.

8.3 Conclusions – further work

It is recommended to research on the improvement of tests, both static and also fatigue, in order to reproduce with higher accuracy the real conditions of the blade when the wind turbine is operating.

This work shall be done in collaboration with the testing facilities which can define the limits of the loading devices and their main restrictions.

Supported by:

Focused only on the loading strategy, assumptions such us; static test principal directions, uniaxial & uniform amplitude loading and no-mean effect consideration are general accepted procedures that give the challenge to improve or, at least to work on the improvement of these blade testing methods.

Supported by:

9. References

1. Description of the DTU 10 MW Reference Wind Turbine. DTU Wind Energy Report-I-0092, July 2013
2. Anders Bjørk. Coordinates and calculations for the ffa-w1-xxx, ffa-w2-xxx and ffaw3-xxx series of airfoils for horizontal axis wind turbines. Technical Report FFA TN1990-15, FFA, Stockholm, Sweden, 1990.
3. IEC-61400-23. Wind turbines – Part 23: Full-scale structural testing of rotor blades. Edition 1.0. 2014-4
4. Guideline for the Certification of Wind Turbines. Edition 2010. Germanischer Lloyd Industrial Services GmbH
5. Guidelines for design of wind turbines. Det Norske Veritas, Copenhagen (Wind.Turbine.Certification@dnv.com) and Wind Energy Department, Risø National Laboratory (Certification@risoe.dk) 2002
6. Information on the Benchmark of blade structural FATIGUE models. D. J. Lekou from CRES and A. Crocce from POLIMI, July 2014

Supported by:

10. Appendix A – Extreme loads

Following tables show the extreme load values for each section of the blade. The simultaneous values for all the other cross sections are not shown but calculated.

Table A.1 Extreme loads at 0.00m from blade root

Distance from root [m]			0.00	FX	FY	FZ	Fres	MX	MY	MZ	Mres
Load Case			γ_F [-]	[kN]	[kN]	[kN]	[kN]	[kNm]	[kNm]	[kNm]	[kNm]
FX	max	dlc13ab1	1.35	**1205**	-370	2305.6	1260.5	12064	56205	74.3	57485
	min	dlc14cb	1.35	**-809.3**	126.2	2468.2	819.1	2970.2	-41266	-55	41373
FY	max	dlc11k1	1.35	230	**711.7**	1854.7	747.9	-20108	8280	-251.3	21746
	min	dlc11i1	1.35	341.1	**-766.7**	1551.8	839.1	25674	1820	158.1	25738
FZ	max	dlc14bb	1.35	146.9	-12.5	**3150.3**	147.4	1442.9	6543.8	-500.4	6701
	min	dlc61ab_h_2_1	1.35	-1.06	70.7	**-575**	70.7	-1110	1486.4	-126.1	1855.2
F_{res}	max	dlc21aa	1.35	1186.5	-571.7	2439.6	**1317**	17343	56287	-70.8	58898
MX	max	dlc11i1	1.35	341.1	-766.7	1551.8	839.1	**25674**	1820	158.1	25738
	min	dlc11k1	1.35	77	672.1	1672.6	676.5	**-20618**	3712.6	-357	20949
MY	max	dlc13bb1	1.35	1166.2	-583.3	1321.6	1304	18963	**57425**	-54.7	60475
	min	dlc14cb	1.35	-805	156.6	2377.9	820.1	2441.5	**-41504**	9.81	41576
MZ	max	dlc23ba_3	1.10	-175.2	-619.6	1238.1	643.9	21903	-18403	**487.3**	28608
	min	dlc61ab_h_1_1	1.35	-52.4	244	-59.4	249.5	-5806.7	-12290	**-542.2**	13593
M_{res}	max	dlc62j_h_1_1	1.10	1166.2	-583.3	1321.6	1304	18963	57425	-54.7	**60475**

Table A.2 Extreme loads at 2.015m from blade root

Distance from root [m]			2.015	FX	FY	FZ	Fres	MX	MY	MZ	Mres
Load Case			γ_F [-]	[kN]	[kN]	[kN]	[kN]	[kNm]	[kNm]	[kNm]	[kNm]
FX	max	dlc13ab1	1.35	**1199.3**	-356.7	2262.4	1251.3	11333	53770	69.9	54952
	min	dlc14cb	1.35	**-805.9**	97.5	2470.4	811.8	3249.7	-39318	-84.2	39452
FY	max	dlc11k1	1.35	232.2	**679.5**	1829.7	718.1	-18708	7800.7	-248	20269
	min	dlc11i1	1.35	319.8	**-740.4**	1533.2	806.5	24156	1142.3	150.9	24183
FZ	max	dlc14bb	1.35	139.9	-17.7	**3099**	141	1411.6	6232.7	-499.7	6390.6
	min	dlc61ab_h_2_1	1.35	-1.01	58.9	**-541.9**	58.9	-979.4	1492.6	-121.4	1785.3
F_{res}	max	dlc21aa	1.35	1180.1	-546.5	2406.4	**1300.5**	16218	53889	-76.2	56276
MX	max	dlc11i1	1.35	319.8	-740.4	1533.2	806.5	**24156**	1142.3	150.9	24183
	min	dlc11k1	1.35	86	642.1	1660.9	647.8	**-19295**	3536.8	-353.9	19617
MY	max	dlc13bb1	1.35	1162.9	-561	1330.1	1291.2	17811	**55071**	-60	57880
	min	dlc14cb	1.35	-800.3	131.9	2341.4	811.1	2731.8	**-39907**	11.8	40001
MZ	max	dlc23ba_3	1.10	-189.1	-596.4	1228.5	625.7	20679	-18046	**482.5**	27446
	min	dlc11k1	1.35	-178.4	300	1829.9	349	-10536	-11361	**-531.2**	15494
M_{res}	max	dlc62g_h_1_1	1.10	1162.9	-561	1330.1	1291.2	17811	55071	-60	**57880**

Supported by:

Table A.3 Extreme loads at 5.470m from blade root

Distance from root [m]			5.470	FX	FY	FZ	Fres	MX	MY	MZ	Mres
Load Case			γ_F [-]	[kN]	[kN]	[kN]	[kN]	[kNm]	[kNm]	[kNm]	[kNm]
FX	max	dlc13ab1	1.35	**1188**	-334	2171.5	1234	10143	49634	62	50660
	min	dlc14cb	1.35	**-803**	60.4	2380.7	805.3	3521.6	-36593	-80.6	36762
FY	max	dlc11k1	1.35	235.1	**621.3**	1771.5	664.3	-16467	6967.7	-241.4	17880
	min	dlc11i1	1.35	279.9	**-694.5**	1487.9	748.8	21683	82.3	135.9	21683
FZ	max	dlc14bb	1.35	175.3	-48.3	**2986.4**	181.9	1904.7	7891.7	-501.9	8118.3
	min	dlc61ab_h_2_1	1.35	-1.23	40.2	**-485.1**	40.2	-808.1	1503.9	-114	1707.2
F_{res}	max	dlc21aa	1.35	1166.8	-504.1	2329.4	**1271**	14410	49821	-85.7	51863
MX	max	dlc11i1	1.35	279.9	-694.5	1487.9	748.8	**21683**	82.3	135.9	21683
	min	dlc11k1	1.35	101.7	589.9	1625	598.6	**-17174**	3189.3	-348.6	17467
MY	max	dlc13bb1	1.35	1155.1	-522.9	1329.1	1267.9	15944	**51059**	-69.3	53490
	min	dlc14cb	1.35	-794	90.7	2259.7	799.2	3115.2	**-37205**	15.8	37336
MZ	max	dlc23ba_3	1.10	-214	-555.8	1200.5	595.5	18693	-17373	**472.7**	25520
	min	dlc11k1	1.35	-177.7	268.8	1750.7	322.2	-9557.8	-10778	**-529.8**	14405
M_{res}	max	dlc62a_h_2_1	1.10	1155.1	-522.9	1329.1	1267.9	15944	51059	-69.3	**53490**

Table A.4 Extreme loads at 8.348m from blade root

Distance from root [m]			8.348	FX	FY	FZ	Fres	MX	MY	MZ	Mres
Load Case			γ_F [-]	[kN]	[kN]	[kN]	[kN]	[kNm]	[kNm]	[kNm]	[kNm]
FX	max	dlc13ab1	1.35	**1176.4**	-315.6	2085.3	1218	9212.6	46225	55.2	47134
	min	dlc14cb	1.35	**-803.7**	32.9	2292.9	804.3	3654.8	-34342	-80.5	34536
FY	max	dlc11k1	1.35	234.9	**574.5**	1712.2	620.7	-14756	6265.7	-235.2	16031
	min	dlc11i1	1.35	244.2	**-656**	1440.6	700	19747	-695.8	120.4	19759
FZ	max	dlc14bb	1.35	160.9	-50.3	**2876.5**	168.6	1761.5	7367.3	-503.2	7575
	min	dlc61ab_h_2_1	1.35	-2.8	27.2	**-440.7**	27.3	-711	1516.1	-113.5	1674.6
F_{res}	max	dlc13bb1	1.35	1146.2	-492.8	1314.1	**1247.6**	14488	47744	-77.3	49893
MX	max	dlc11i1	1.35	244.2	-656	1440.6	700	**19747**	-695.8	120.4	19759
	min	dlc11k1	1.35	113	549.7	1582.7	561.2	**-15544**	2855.8	-343.3	15804
MY	max	dlc13bb1	1.35	1146.2	-492.8	1314.1	1247.6	14488	**47744**	-77.3	49893
	min	dlc14cb	1.35	-791.9	60	2178.8	794.2	3330.7	**-34981**	18.2	35140
MZ	max	dlc23ba_3	1.10	-234.6	-523.2	1168.3	573.4	17148	-16753	**463**	23973
	min	dlc11k1	1.35	-179.9	246.1	1677.3	304.8	-8823.9	-10297	**-529.5**	13561
M_{res}	max	dlc51ab1	1.35	1146.2	-492.8	1314.1	1247.6	14488	47744	-77.3	**49893**

Supported by:

Table A.5 Extreme loads at 10.634m from blade root

Distance from root [m]			10.63	FX	FY	FZ	Fres	MX	MY	MZ	Mres
Load Case			γ_F [-]	[kN]	[kN]	[kN]	[kN]	[kNm]	[kNm]	[kNm]	[kNm]
FX	max	dlc13ab1	1.35	**1165.4**	-301.2	2014.4	1203.7	8514.1	43554	50.3	44379
	min	dlc14cb	1.35	**-807.3**	14.4	2219.3	807.5	3709.6	-32555	-88.7	32766
FY	max	dlc11k1	1.35	286	**541.1**	1508	612	-13600	8792.4	-156.4	16194
	min	dlc11i1	1.35	215.5	**-626.1**	1399.6	662.2	18291	-1239.7	106.9	18333
FZ	max	dlc14bb	1.35	199.4	-69.7	**2784.5**	211.3	2070.7	9000.1	-490.7	9235.2
	min	dlc61ab_h_2_1	1.35	-7.17	19.7	**-408.8**	20.9	-657.8	1531.2	-122.6	1666.5
F_{res}	max	dlc13bb1	1.35	1137.2	-470.3	1294.9	**1230.6**	13394	45137	-82.8	47082
MX	max	dlc14bb	1.35	-185.2	-560	633.2	589.8	**18307**	-11786	378.4	21773
	min	dlc11k1	1.35	119.4	522.1	1544	535.5	**-14328**	2571.4	-340.9	14557
MY	max	dlc13bb1	1.35	1137.2	-470.3	1294.9	1230.6	13394	**45137**	-82.8	47082
	min	dlc14cb	1.35	-793.5	39.4	2110.6	794.4	3444.6	**-33222**	12.4	33400
MZ	max	dlc23ba_3	1.10	-250.6	-499	1139	558.4	15987	-16221	**454.9**	22775
	min	dlc11k1	1.35	-183.7	231.6	1617.6	295.6	-8283.9	-9908	**-531**	12915
M_{res}	max	dlc62g_h_1_1	1.10	1137.2	-470.3	1294.9	1230.6	13394	45137	-82.8	**47082**

Table A.6 Extreme loads at 10.377m from blade root

Distance from root [m]			12.38	FX	FY	FZ	Fres	MX	MY	MZ	Mres
Load Case			γ_F [-]	[kN]	[kN]	[kN]	[kN]	[kNm]	[kNm]	[kNm]	[kNm]
FX	max	dlc13ab1	1.35	**1155.8**	-290.4	1959.1	1191.7	8004	41540	46	42304
	min	dlc14cb	1.35	**-812.1**	2.12	2161.3	812.1	3724.2	-31190	-99.5	31412
FY	max	dlc11k1	1.35	284.3	**519.1**	1471.9	591.8	-12684	8283.6	-154.9	15149
	min	dlc11i1	1.35	193.9	**-603.9**	1366.6	634.2	17227	-1611.2	97	17302
FZ	max	dlc14bb	1.35	185.4	-67.2	**2711.9**	197.2	1952.1	8644.4	-492.5	8862.1
	min	dlc61ab_h_2_1	1.35	-13.5	15.8	**-386.2**	20.8	-626.6	1551.7	-137.2	1673.4
F_{res}	max	dlc13bb1	1.35	1129.2	-453.9	1276.6	**1217**	12594	43166	-87.2	44966
MX	max	dlc14bb	1.35	-200.3	-548.1	610.9	583.6	**17344**	-11458	372	20787
	min	dlc11k1	1.35	326.6	434.1	1350.6	543.3	**-13552**	9491.4	-136.9	16545
MY	max	dlc13bb1	1.35	1129.2	-453.9	1276.6	1217	12594	**43166**	-87.2	44966
	min	dlc14cb	1.35	-788.1	33.3	2021	788.8	3405.6	**-31890**	36.9	32071
MZ	max	dlc23ba_3	1.10	-263	-481.4	1114.8	548.5	15140	-15792	**448.2**	21877
	min	dlc11k1	1.35	-187.8	222.4	1571.5	291.1	-7893.9	-9606.1	**-532.2**	12434
M_{res}	max	dlc62d_l_1_1	1.10	1129.2	-453.9	1276.6	1217	12594	43166	-87.2	**44966**

Supported by:

Table A.7 Extreme loads at 14.091m from blade root

Distance from root [m]			14.09	FX	FY	FZ	Fres	MX	MY	MZ	Mres
Load Case			γ_F [-]	[kN]	[kN]	[kN]	[kN]	[kNm]	[kNm]	[kNm]	[kNm]
FX	max	dlc13ab1	1.35	**1145.3**	-279.8	1903.9	1179	7520.8	39581	41.4	40289
	min	dlc14cb	1.35	**-818.9**	-8.44	2102.8	818.9	3717.8	-29845	-115.6	30075
FY	max	dlc11k1	1.35	280.7	**499.1**	1435.2	572.7	-11821	7787.5	-153.5	14155
	min	dlc11i1	1.35	173.7	**-582.3**	1332.9	607.6	16219	-1941.7	87.7	16335
FZ	max	dlc14bb	1.35	168.1	-63.6	**2638.7**	179.8	1839.3	8321.2	-493.7	8522
	min	dlc61ab_h_2_1	1.35	-23.3	14	**-365.2**	27.2	-600.4	1585.2	-160.2	1695.1
F_{res}	max	dlc13bb1	1.35	1120.6	-438.2	1256	**1203.2**	11837	41246	-91.8	42911
MX	max	dlc14bb	1.35	-214.6	-536.4	589.3	577.7	**16418**	-11111	364.9	19825
	min	dlc11k1	1.35	322.5	419.1	1321.2	528.9	**-12830**	8924.4	-136.7	15629
MY	max	dlc13bb1	1.35	1120.6	-438.2	1256	1203.2	11837	**41246**	-91.8	42911
	min	dlc14cb	1.35	-792.8	20.9	1967.8	793.1	3450.6	**-30584**	23.2	30778
MZ	max	dlc23ba_3	1.10	-275.4	-464.6	1089.7	540.1	14336	-15352	**439.3**	21005
	min	dlc61ab_h_1_1	1.35	-258.4	98.9	-37.9	276.7	-3523.4	-10088	**-543.6**	10686
M_{res}	max	dlc62g_l_1_1	1.10	1120.6	-438.2	1256	1203.2	11837	41246	-91.8	**42911**

Table A.8 Extreme loads at 15.833m from blade root

Distance from root [m]			15.83	FX	FY	FZ	Fres	MX	MY	MZ	Mres
Load Case			γ_F [-]	[kN]	[kN]	[kN]	[kN]	[kNm]	[kNm]	[kNm]	[kNm]
FX	max	dlc13ab1	1.35	**1133.6**	-269.2	1845.9	1165.2	7048.6	37626	38.3	38280
	min	dlc14cb	1.35	**-826.4**	-18.2	2040.9	826.6	3692.2	-28457	-132.6	28696
FY	max	dlc11k1	1.35	276.2	**479**	1396.1	552.9	-10980	7298.8	-154.7	13185
	min	dlc11i1	1.35	153.7	**-560.3**	1296.8	581	15233	-2235.6	81.7	15396
FZ	max	dlc14bb	1.35	149.2	-59.4	**2561.4**	160.6	1730.5	8041.4	-493.4	8225.5
	min	dlc61ab_h_2_1	1.35	-34.1	13.1	**-344.6**	36.6	-575.4	1635.7	-183.5	1734
F_{res}	max	dlc13bb1	1.35	1110.7	-422.4	1232.1	**1188.3**	11095	39321	-93.9	40856
MX	max	dlc14bb	1.35	-228.5	-524	567.2	571.7	**15498**	-10731	360.7	18851
	min	dlc11k1	1.35	316.8	405.4	1289	514.5	**-12122**	8364.5	-138.8	14728
MY	max	dlc13bb1	1.35	1110.7	-422.4	1232.1	1188.3	11095	**39321**	-93.9	40856
	min	dlc14cb	1.35	-798.3	9.28	1911.3	798.4	3474.3	**-29242**	8.37	29448
MZ	max	dlc14bb	1.35	-222.7	-484.7	562.1	533.4	15344	-10380	**433.9**	18525
	min	dlc61ab_h_1_1	1.35	-281.5	90.3	-35.8	295.6	-3358.5	-9616.7	**-560.8**	10186
M_{res}	max	dlc62d_l_1_1	1.10	1110.7	-422.4	1232.1	1188.3	11095	39321	-93.9	**40856**

Supported by:

Table A.9 Extreme loads at 17.559m from blade root

Distance from root [m]			17.56	FX	FY	FZ	Fres	MX	MY	MZ	Mres
Load Case			γ_F [-]	[kN]	[kN]	[kN]	[kN]	[kNm]	[kNm]	[kNm]	[kNm]
FX	max	dlc13ab1	1.35	**1121.3**	-259.1	1787.9	1150.8	6598.1	35704	34.7	36309
	min	dlc14cb	1.35	**-831.2**	-27.2	1978.6	831.6	3648.4	-27089	-139.2	27334
FY	max	dlc11k1	1.35	271.3	**459.2**	1356.5	533.3	-10184	6814.4	-151.6	12254
	min	dlc11i1	1.35	132.6	**-538.5**	1260.1	554.6	14293	-2500.1	72.7	14510
FZ	max	dlc14bb	1.35	134.1	-56	**2483.5**	145.3	1627.4	7780.2	-492.6	7948.6
	min	dlc61ab_h_2_1	1.35	-40.2	12.4	**-325.4**	42.1	-551.5	1702.8	-189.4	1789.9
F_{res}	max	dlc13bb1	1.35	1099.6	-407	1206.4	**1172.4**	10387	37427	-97.4	38842
MX	max	dlc14bb	1.35	-240.4	-511.7	545.7	565.4	**14607**	-10336	355.3	17894
	min	dlc11k1	1.35	310.2	392.4	1255.9	500.2	**-11446**	7812.8	-137	13859
MY	max	dlc13bb1	1.35	1099.6	-407	1206.4	1172.4	10387	**37427**	-97.4	38842
	min	dlc14cb	1.35	-801.8	-1.35	1854.3	801.8	3476.4	**-27921**	2.52	28137
MZ	max	dlc14bb	1.35	-234.3	-473	541.5	527.9	14520	-9994.7	**429.3**	17627
	min	dlc61ab_h_1_1	1.35	-296.7	83	-33.8	308.1	-3208.9	-9115.7	**-557.8**	9664
M_{res}	max	dlc62g_h_2_1	1.10	1099.6	-407	1206.4	1172.4	10387	37427	-97.4	**38842**

Table A.10 Extreme loads at 21.016m from blade root

Distance from root [m]			21.02	FX	FY	FZ	Fres	MX	MY	MZ	Mres
Load Case			γ_F [-]	[kN]	[kN]	[kN]	[kN]	[kNm]	[kNm]	[kNm]	[kNm]
FX	max	dlc13ab1	1.35	**1093.6**	-240.2	1673.1	1119.6	5743.6	31956	29.8	32468
	min	dlc14cb	1.35	**-835.1**	-43	1854.2	836.2	3508.3	-24349	-135.3	24600
FY	max	dlc11k1	1.35	258.9	**421.3**	1276.7	494.5	-8698	5881.6	-146.7	10500
	min	dlc11i1	1.35	92.8	**-497.3**	1186	505.9	12521	-2916.3	58.8	12856
FZ	max	dlc14bb	1.35	166.1	-64.9	**2328.1**	178.4	1681.8	8861.3	-468.2	9019.4
	min	dlc61ab_h_2_1	1.35	-42.4	11	**-290.4**	43.8	-505.3	1852.4	-176.1	1920
F_{res}	max	dlc13bb1	1.35	1074.3	-377.5	1150.5	**1138.7**	9048.4	33722	-100.7	34915
MX	max	dlc14bb	1.35	-256.9	-458.1	503.7	525.2	**12975**	-9341.3	409.8	15988
	min	dlc11k1	1.35	297.5	367.1	1187.4	472.6	**-10166**	6751.1	-135.9	12204
MY	max	dlc13bb1	1.35	1059.8	-373.2	1158.1	1123.6	8971.5	**33771**	-99.9	34943
	min	dlc14cb	1.35	-804.6	-20.1	1740	804.8	3420.8	**-25278**	5.48	25509
MZ	max	dlc14bb	1.35	-252.6	-450.7	501.7	516.6	12928	-9170.8	**425.2**	15851
	min	dlc14bb	1.35	-329.3	57.4	2265.9	334.2	-624.8	-5100.9	**-548.4**	5139.1
M_{res}	max	dlc62j_h_1_1	1.10	990	-388.7	1104.4	1063.6	10689	33298	-201.5	**34971**

Supported by:

Table A.11 Extreme loads at 24.470m from blade root

Distance from root [m]			24.47	FX	FY	FZ	Fres	MX	MY	MZ	Mres
Load Case			γ_F [-]	[kN]	[kN]	[kN]	[kN]	[kNm]	[kNm]	[kNm]	[kNm]
FX	max	dlc13ab1	1.35	**1052.3**	-219.7	1558.9	1075	4958.6	28370	21.9	28800
	min	dlc14cb	1.35	**-819.2**	-53.9	1729.4	820.9	3317.8	-21646	-121.5	21899
FY	max	dlc11k1	1.35	233.3	**388.5**	1195.8	453.1	-7341.2	5022.4	-152	8894.8
	min	dlc14bb	1.35	-266.2	**-459.6**	464.5	531.1	11253	-8597	340.6	14162
FZ	max	dlc14bb	1.35	157.1	-58.7	**2172.4**	167.7	1452	8325.4	-451	8451
	min	dlc61ab_h_2_1	1.35	-19.7	11.3	**-259.1**	22.7	-461.3	1965	-152.3	2018.4
F_{res}	max	dlc13bb1	1.35	1039.2	-348.5	1089.6	**1096.1**	7813.3	30154	-102.5	31150
MX	max	dlc14bb	1.35	-263.3	-434	464.5	507.6	**11439**	-8457.5	401.9	14226
	min	dlc11k1	1.35	271.6	346.5	1116.3	440.3	**-8974.2**	5759.3	-149.1	10663
MY	max	dlc13bb1	1.35	1006.1	-317.9	1103	1055.1	7757.7	**30295**	-115.8	31273
	min	dlc14cb	1.35	-782.3	-28.3	1596.8	782.8	3307.2	**-22704**	53.4	22944
MZ	max	dlc14bb	1.35	-258.5	-425.5	463.3	497.9	11419	-8302.8	**422.3**	14119
	min	dlc14bb	1.35	-317.4	47.5	2113.7	321	-480.6	-4052.5	**-531.7**	4080.9
M_{res}	max	dlc62j_h_1_1	1.10	965.3	-362.6	1044.9	1031.2	9412.4	29999	-204.3	**31441**

Table A.12 Extreme loads at 27.926m from blade root

Distance from root [m]			27.93	FX	FY	FZ	Fres	MX	MY	MZ	Mres
Load Case			γ_F [-]	[kN]	[kN]	[kN]	[kN]	[kNm]	[kNm]	[kNm]	[kNm]
FX	max	dlc21aa	1.35	**1005.6**	-258.4	1632.4	1038.3	5539.7	26508	-95.4	27080
	min	dlc14cb	1.35	**-795.9**	-61.9	1603.1	798.3	3092.5	-19074	-107.1	19323
FY	max	dlc11k1	1.35	95.8	**360.1**	1163.6	372.6	-6962	306.5	-312.7	6968.7
	min	dlc14bb	1.35	-265.8	**-429.9**	425.8	505.5	9721.9	-7706	322.6	12406
FZ	max	dlc14bb	1.35	156.8	-53.6	**2014.9**	165.8	1238.1	7784.2	-428	7882.1
	min	dlc61ab_h_2_1	1.35	8.03	12.3	**-230.6**	14.6	-414	1989.1	-124.6	2031.8
F_{res}	max	dlc13bb1	1.35	993.2	-319.2	1024	**1043.2**	6679.9	26740	-99.5	27561
MX	max	dlc14bb	1.35	-257.8	-399.2	425.7	475.2	**10000**	-7439.3	409.3	12464
	min	dlc11k1	1.35	239.8	328.8	1042.5	407	**-7851.2**	4862.1	-152.7	9234.7
MY	max	dlc13bb1	1.35	948	-280.5	1043.3	988.7	6743.5	**26989**	-110.5	27818
	min	dlc14cb	1.35	-766.7	-42	1482.6	767.9	3160.6	**-20235**	59.8	20481
MZ	max	dlc14bb	1.35	-257.8	-399.2	425.7	475.2	10000	-7439.3	**409.3**	12464
	min	dlc14bb	1.35	-296	38.8	1959.9	298.6	-372.6	-3106.3	**-510.5**	3128.6
M_{res}	max	dlc62a_h_1_1	1.10	927.8	-336.4	988.5	986.9	8246.2	26822	-188.8	**28061**

Supported by:

Table A.13 Extreme loads at 31.381m from blade root

Distance from root [m]			31.38	FX	FY	FZ	Fres	MX	MY	MZ	Mres
Load Case			γ_F [-]	[kN]	[kN]	[kN]	[kN]	[kNm]	[kNm]	[kNm]	[kNm]
FX	max	dlc21aa	1.35	**964.3**	-234.5	1502.9	992.4	4711.2	23325	-93.2	23796
	min	dlc14cb	1.35	**-766.9**	-68.2	1451.4	770	2851.9	-17022	-63.6	17259
FY	max	dlc11k1	1.35	74.9	**330.7**	1075.6	339	-5822.3	-21.5	-299.3	5822.3
	min	dlc14bb	1.35	-258.8	**-394.7**	386.8	472	8301.1	-6826.9	313.2	10748
FZ	max	dlc14bb	1.35	161	-48.6	**1851.5**	168.2	1038.8	7269.1	-397.7	7343
	min	dlc61ab_h_2_1	1.35	36.2	13	**-203.8**	38.4	-363.7	1914	-97.7	1948.3
F_{res}	max	dlc21aa	1.35	964.3	-234.5	1502.9	**992.4**	4711.2	23325	-93.2	23796
MX	max	dlc14bb	1.35	-252.2	-370.7	387.7	448.3	**8675.6**	-6585.1	396.4	10892
	min	dlc11k1	1.35	213.4	309.2	964.3	375.7	**-6795.7**	4079.5	-161.8	7926.1
MY	max	dlc13bb1	1.35	909	-255.8	970.4	944.3	5838	**23918**	-113.8	24620
	min	dlc14cb	1.35	-734.9	-49.3	1340.2	736.6	2996.3	**-17878**	97.7	18128
MZ	max	dlc14bb	1.35	-252.2	-370.7	387.7	448.3	8675.6	-6585.1	**396.4**	10892
	min	dlc14bb	1.35	-268.5	31.7	1800.4	270.4	-297	-2234.1	**-482.6**	2253.7
M_{res}	max	dlc62j_h_2_1	1.10	896.9	-313.4	918.2	950	7147.6	23799	-183.4	**24849**

Table A.14 Extreme loads at 33.109m from blade root

Distance from root [m]			33.11	FX	FY	FZ	Fres	MX	MY	MZ	Mres
Load Case			γ_F [-]	[kN]	[kN]	[kN]	[kN]	[kNm]	[kNm]	[kNm]	[kNm]
FX	max	dlc21aa	1.35	**941.7**	-222.9	1436.9	967.7	4328.8	21801	-89.6	22227
	min	dlc14cb	1.35	**-750.9**	-71	1386	754.2	2718	-15842	-57.8	16073
FY	max	dlc11k1	1.35	63.8	**315.4**	1030.2	321.8	-5291.4	-159.5	-289.1	5293.8
	min	dlc14bb	1.35	-253.6	**-375.9**	367.5	453.4	7638.5	-6400.2	306.7	9965.3
FZ	max	dlc14bb	1.35	164.8	-46.2	**1768.5**	171.2	946.4	7007.9	-381.3	7071.5
	min	dlc61ab_h_2_1	1.35	47.1	13	**-190.9**	48.9	-338.1	1842.8	-84.7	1873.6
F_{res}	max	dlc21aa	1.35	941.7	-222.9	1436.9	**967.7**	4328.8	21801	-89.6	22227
MX	max	dlc14bb	1.35	-247.5	-356	368.8	433.6	**8051.2**	-6169.2	386.6	10143
	min	dlc11k1	1.35	200.7	298.7	924	359.8	**-6294.6**	3721.7	-165.3	7312.6
MY	max	dlc13bb1	1.35	888.5	-244.3	932.2	921.5	5417.2	**22444**	-114.2	23088
	min	dlc14cb	1.35	-723	-54.8	1280.8	725.1	2893.2	**-16742**	100.9	16991
MZ	max	dlc14bb	1.35	-247.5	-356	368.8	433.6	8051.2	-6169.2	**386.6**	10143
	min	dlc14bb	1.35	-252.9	28.7	1719.3	254.5	-267	-1839.6	**-467.1**	1858.9
M_{res}	max	dlc61ab_h_2_1	1.35	880.2	-302	881.5	930.6	6628.9	22337	-179.2	**23300**

Supported by:

Table A.15 Extreme loads at 34.836m from blade root

Distance from root [m]			34.84	FX	FY	FZ	Fres	MX	MY	MZ	Mres
Load Case			γ_F [-]	[kN]	[kN]	[kN]	[kN]	[kNm]	[kNm]	[kNm]	[kNm]
FX	max	dlc21aa	1.35	**918**	-211.6	1370.4	942	3967.4	20326	-85.2	20710
	min	dlc14cb	1.35	**-733.6**	-73.2	1320.2	737.2	2580.5	-14698	-52.4	14922
FY	max	dlc11k1	1.35	53.3	**299.7**	984.2	304.4	-4787.1	-279.6	-277	4795.3
	min	dlc14bb	1.35	-247.2	**-356.7**	348.3	434	7009.2	-5984.6	299	9216.5
FZ	max	dlc14bb	1.35	169.4	-43.8	**1685**	175	859.3	6741.9	-364.3	6796.5
	min	dlc61ab_h_2_1	1.35	54.8	12.8	**-178.6**	56.3	-313	1755.6	-71.8	1783.3
F_{res}	max	dlc21aa	1.35	918	-211.6	1370.4	**942**	3967.4	20326	-85.2	20710
MX	max	dlc14bb	1.35	-241.8	-340.9	350	417.9	**7453**	-5763.3	375.3	9421.4
	min	dlc11k1	1.35	188.4	287.7	883.1	343.9	**-5812**	3385.7	-167	6726.3
MY	max	dlc13bb1	1.35	867.7	-233.3	893.2	898.5	5016.6	**21011**	-113.9	21601
	min	dlc14cb	1.35	-710	-59.6	1221	712.5	2782.1	**-15636**	103.7	15881
MZ	max	dlc14bb	1.35	-241.8	-340.9	350	417.9	7453	-5763.3	**375.3**	9421.4
	min	dlc14bb	1.35	-236.5	26	1637.9	237.9	-241	-1474.6	**-451.4**	1494.2
M_{res}	max	dlc23ba_2	1.10	862.7	-290.7	844.1	910.4	6130.5	20911	-174.3	**21791**

Table A.16 Extreme loads at 38.292m from blade root

Distance from root [m]			38.29	FX	FY	FZ	Fres	MX	MY	MZ	Mres
Load Case			γ_F [-]	[kN]	[kN]	[kN]	[kN]	[kNm]	[kNm]	[kNm]	[kNm]
FX	max	dlc21aa	1.35	**868.5**	-189.8	1236	889	3303.5	17521	-75.6	17830
	min	dlc14cb	1.35	**-696.9**	-75.5	1170.5	701	2346.6	-12850	-14.8	13063
FY	max	dlc11k1	1.35	150.1	**270.8**	807.4	309.6	-4618.3	2605.2	-140.8	5302.4
	min	dlc14bb	1.35	-223.8	**-322**	323.3	392.2	6089.3	-4732.4	249.2	7712
FZ	max	dlc14bb	1.35	223.3	-46	**1517**	227.9	780.7	6891.9	-313.2	6936
	min	dlc61ab_h_2_1	1.35	60.6	12.3	**-155.1**	61.8	-264.5	1556	-45.1	1578.4
F_{res}	max	dlc21aa	1.35	868.5	-189.8	1236	**889**	3303.5	17521	-75.6	17830
MX	max	dlc14bb	1.35	-229.2	-311	312.6	386.3	**6334.7**	-4985.5	349.1	8061.2
	min	dlc11k1	1.35	164.1	247.7	803.9	297.1	**-4962**	2760.9	-174	5678.4
MY	max	dlc13bb1	1.35	810.6	-214.3	821	838.5	4160.6	**18324**	-96.8	18790
	min	dlc14cb	1.35	-672.3	-65.6	1082.2	675.5	2545.3	**-13540**	131.6	13777
MZ	max	dlc14bb	1.35	-229.2	-311	312.6	386.3	6334.7	-4985.5	**349.1**	8061.2
	min	dlc11k1	1.35	-230.7	232.2	1060.9	327.3	-3801.9	-5360.1	**-421**	6571.5
M_{res}	max	dlc62a_h_2_1	1.10	824.5	-268.3	767.1	867	5192.7	18165	-163.9	**18893**

Supported by:

Table A.17 Extreme loads at 43.477m from blade root

Distance from root [m]			43.38	FX	FY	FZ	Fres	MX	MY	MZ	Mres
Load Case			γ_F [-]	[kN]	[kN]	[kN]	[kN]	[kNm]	[kNm]	[kNm]	[kNm]
FX	max	dlc21aa	1.35	**786.9**	-159.2	1033.9	802.8	2444.5	13655	-62.8	13873
	min	dlc14cb	1.35	**-633.6**	-75	948.1	638	2026.6	-10356	53.1	10552
FY	max	dlc11k1	1.35	124.4	**229.9**	680.3	261.4	-3386.8	1878.7	-126.8	3873
	min	dlc14bb	1.35	-200.7	**-276.5**	268.2	341.7	4545.9	-3697.7	202.1	5859.9
FZ	max	dlc14bb	1.35	231.4	-36.9	**1265.8**	234.3	549.5	5802.3	-260.7	5828.3
	min	dlc61ab_h_2_1	1.35	62.1	11	**-122.9**	63	-197.5	1246.2	-31.9	1261.8
F_{res}	max	dlc21aa	1.35	786.4	-165.1	1029.7	**803.5**	2603.4	13641	-70.8	13887
MX	max	dlc14bb	1.35	-206.7	-267.2	257.8	337.8	**4849.7**	-3920.3	294.7	6236
	min	dlc11k1	1.35	139.9	215.9	675.2	257.3	**-3827.6**	1959.8	-163.2	4300.2
MY	max	dlc13bb1	1.35	736.5	-188.9	701.9	760.3	3047.6	**14627**	-72.9	14941
	min	dlc14cb	1.35	-613.4	-73.3	889.6	617.8	2175.9	**-10675**	141.5	10894
MZ	max	dlc23ba_3	1.10	-331.1	-237	551.8	407.2	4291	-6513.2	**301.6**	7799.6
	min	dlc11k1	1.35	-199	137.5	715.1	241.9	-2762.4	-3300.8	**-378.6**	4304.2
M_{res}	max	dlc62a_h_2_1	1.10	736.5	-188.9	701.9	760.3	3047.6	14627	-72.9	**14941**

Table A.18 Extreme loads at 48.806m from blade root

Distance from root [m]			48.81	FX	FY	FZ	Fres	MX	MY	MZ	Mres
Load Case			γ_F [-]	[kN]	[kN]	[kN]	[kN]	[kNm]	[kNm]	[kNm]	[kNm]
FX	max	dlc21aa	1.35	**694.4**	-129.4	832.5	706.4	1723.7	10201	-48.5	10346
	min	dlc14cb	1.35	**-560.8**	-75.8	749.8	565.9	1657	-7833.2	79.3	8006.5
FY	max	dlc11i1	1.35	55.2	**188.1**	570.5	196	-2411.7	1097.1	-170.7	2649.5
	min	dlc14bb	1.35	-175.6	**-227.6**	211.7	287.5	3369.4	-2783.9	209.8	4370.7
FZ	max	dlc14bb	1.35	262	-32.3	**1016.8**	264	396.3	5073.8	-197.1	5089.3
	min	dlc61ab_h_1_1	1.35	-182.2	-58	**-94**	191.2	1004.2	-2590.5	0.34	2778.3
F_{res}	max	dlc21ba	1.35	691	-156.8	749.4	**708.5**	2188.8	10794	-99.4	11013
MX	max	dlc14bb	1.35	-180.6	-224.4	204.7	288	**3555**	-2951.6	240.9	4620.6
	min	dlc11k1	1.35	120.3	183.2	545.8	219.2	**-2828.6**	1263.7	-157.7	3098
MY	max	dlc13bb1	1.35	660.9	-161	575	680.3	2077.7	**11230**	-32	11420
	min	dlc14cb	1.35	-551.3	-76	715.8	556.6	1755.2	**-8048.7**	134.3	8237.9
MZ	max	dlc23ba_3	1.10	-307.8	-200.5	446	367.3	3157.4	-5028.8	**255**	5937.9
	min	dlc11k1	1.35	-174.5	125.2	573	214.7	-2122.6	-2473.5	**-326.3**	3259.4
M_{res}	max	dlc23ba_2	1.10	667.7	-153.6	570.6	685.2	2176.4	11221	-53.7	**11431**

Supported by:

Table A.19 Extreme loads at 55.721m from blade root

Distance from root [m]			55.72	FX	FY	FZ	Fres	MX	MY	MZ	Mres
Load Case			γ_F [-]	[kN]	[kN]	[kN]	[kN]	[kNm]	[kNm]	[kNm]	[kNm]
FX	max	dlc21ba	1.35	**572.5**	-116	534.3	584.1	1299.9	6953.8	-67.9	7074.2
	min	dlc14cb	1.35	**-456.7**	-72	521.9	462.4	1171.2	-5085.1	81.8	5218.2
FY	max	dlc11j1	1.35	-11.6	**144.6**	432.3	145	-1667.6	-198.9	-177.4	1679.4
	min	dlc11i1	1.35	-140	**-171.5**	381.5	221.4	2104.7	-1983.7	22.4	2892.2
FZ	max	dlc14bb	1.35	241.8	-20.3	**719.3**	242.6	208.4	3544.2	-136.6	3550.3
	min	dlc61ab_h_1_1	1.35	-117.2	-45.9	**-62.8**	125.9	650.9	-1542.8	12.7	1674.5
F_{res}	max	dlc21ba	1.35	572.5	-116	534.3	**584.1**	1299.9	6953.8	-67.9	7074.2
MX	max	dlc14bb	1.35	-140	-167.8	146.3	218.5	**2223**	-1825.2	149.3	2876.2
	min	dlc23ca_1	1.10	147.7	99.2	366.8	177.9	**-1812.8**	2022.7	-27.5	2716.2
MY	max	dlc13bb1	1.35	555.6	-111.9	412.4	566.8	1179.5	**7428.4**	-9.92	7521.4
	min	dlc14cb	1.35	-452.3	-74	498.8	458.3	1233.2	**-5213.8**	123.8	5357.7
MZ	max	dlc23ba_2	1.10	-260.8	-145.8	279.7	298.7	1899.7	-3378.7	**183.1**	3876.1
	min	dlc11k1	1.35	-134.9	107.5	404.4	172.5	-1384.2	-1638.7	**-247.8**	2145
M_{res}	max	dlc62g_h_2_1	1.10	555.6	-111.9	412.4	566.8	1179.5	7428.4	-9.92	**7521.4**

Table A.20 Extreme loads at 62.554m from blade root

Distance from root [m]			62.55	FX	FY	FZ	Fres	MX	MY	MZ	Mres
Load Case			γ_F [-]	[kN]	[kN]	[kN]	[kN]	[kNm]	[kNm]	[kNm]	[kNm]
FX	max	dlc11e1	1.35	**433.3**	-67	266.7	438.5	590.9	4161.9	-4.45	4203.6
	min	dlc14cb	1.35	**-348.6**	-61.7	327.7	354	751.7	-3016.2	73.7	3108.5
FY	max	dlc11k1	1.35	36.5	**105.1**	252.3	111.2	-980.7	130.1	-86.5	989.3
	min	dlc14bb	1.35	-109.5	**-122.1**	91	164	1222.3	-1117.4	99.2	1656.1
FZ	max	dlc14bb	1.35	220.8	-12.2	**465.1**	221.2	104	2333.4	-82.7	2335.7
	min	dlc61ab_l_2_1	1.35	7.7	-5.94	**-38.9**	9.73	65.2	235.3	-14.1	244.2
F_{res}	max	dlc13bb1	1.35	432.8	-74.8	268.2	**439.3**	703.9	4359.9	-17.8	4416.4
MX	max	dlc14bb	1.35	-104.1	-121.2	94	159.8	**1254.6**	-1070.5	94.3	1649.2
	min	dlc23ca_1	1.10	113	97	237.7	148.9	**-1178.8**	1195.2	-14.7	1678.7
MY	max	dlc13bb1	1.35	411.5	-52	240.2	414.8	603.2	**4519.2**	-11.5	4559.2
	min	dlc14cb	1.35	-348	-62.5	322.8	353.6	756.3	**-3028.9**	82.8	3121.9
MZ	max	dlc23ba_2	1.10	319.8	40	217.4	322.3	-571.5	3165.8	**129.9**	3217
	min	dlc11k1	1.35	-107.2	84	261.1	136.2	-781.5	-1017.4	**-164.7**	1282.8
M_{res}	max	dlc62g_l_2_1	1.10	411.5	-52	240.2	414.8	603.2	4519.2	-11.5	**4559.2**

Supported by:

Table A.21 Extreme loads at 69.564m from blade root

Distance from root [m]			69.56	FX	FY	FZ	Fres	MX	MY	MZ	Mres
Load Case			γ_F [-]	[kN]	[kN]	[kN]	[kN]	[kNm]	[kNm]	[kNm]	[kNm]
FX	max	dlc13bb1	1.35	**300.9**	-38.1	150.3	303.3	242.1	2120	8.82	2133.8
	min	dlc14cb	1.35	**-234.5**	-45.1	179.7	238.8	370.1	-1418.5	32.6	1466
FY	max	dlc23ca_1	1.10	77.7	**78.2**	131	110.3	-588.9	571.2	-7.43	820.4
	min	dlc14bb	1.35	-71.4	**-78.6**	51.3	106.2	566.3	-517	42.4	766.8
FZ	max	dlc14bb	1.35	172.1	-6.09	**255.4**	172.2	47	1209.7	-44.7	1210.6
	min	dlc61ab_l_2_1	1.35	15.3	-4.34	**-20.9**	15.9	30.8	166.7	-3.04	169.5
F_{res}	max	dlc13bb1	1.35	300.9	-38.1	150.3	**303.3**	242.1	2120	8.82	2133.8
MX	max	dlc14bb	1.35	-71.4	-78.6	51.3	106.2	**566.3**	-517	42.4	766.8
	min	dlc23ca_1	1.10	77.7	78.2	131	110.3	**-588.9**	571.2	-7.43	820.4
MY	max	dlc13bb1	1.35	299.7	-37	134.8	302	297.8	**2242.6**	-5.79	2262.3
	min	dlc14cb	1.35	-233.5	-47.3	175	238.2	388.2	**-1428.7**	43.7	1480.5
MZ	max	dlc23ba_3	1.10	247.3	20.8	163.8	248.2	-212.1	1699.8	**79.9**	1712.9
	min	dlc11k1	1.35	-108.2	29.8	191.2	112.3	-199.6	-609.4	**-89.3**	641.3
M_{res}	max	dlc62j_h_1_1	1.10	299.7	-37	134.8	302	297.8	2242.6	-5.79	**2262.3**

Table A.22 Extreme loads at 74.699m from blade root

Distance from root [m]			74.70	FX	FY	FZ	Fres	MX	MY	MZ	Mres
Load Case			γ_F [-]	[kN]	[kN]	[kN]	[kN]	[kNm]	[kNm]	[kNm]	[kNm]
FX	max	dlc13bb1	1.35	**206.7**	-25.2	74.2	208.2	137.8	1038.4	-2.28	1047.5
	min	dlc14cb	1.35	**-152.9**	-31	95.9	156	173.1	-642.5	11.1	665.4
FY	max	dlc23ca_1	1.10	51.9	**54**	71.2	74.9	-263.5	259.1	-5.58	369.6
	min	dlc14bb	1.35	-48.3	**-49.1**	27.7	68.9	244.9	-239	15.7	342.2
FZ	max	dlc14bb	1.35	117.4	-2.22	**138.4**	117.4	20	559	-26.5	559.3
	min	dlc61ab_h_1_1	1.35	-13.9	3.92	**-11.3**	14.5	-21.1	-66	-2.34	69.3
F_{res}	max	dlc13bb1	1.35	206.7	-25.2	74.2	**208.2**	137.8	1038.4	-2.28	1047.5
MX	max	dlc11k1	1.35	-67.5	-46.3	88.6	81.9	**246.4**	-331.9	-5.82	413.3
	min	dlc23ca_1	1.10	51.9	54	71.2	74.9	**-263.5**	259.1	-5.58	369.6
MY	max	dlc13bb1	1.35	206.7	-25.2	74.2	208.2	137.8	**1038.4**	-2.28	1047.5
	min	dlc14cb	1.35	-152	-34.9	93.5	156	196.5	**-646.3**	20.6	675.5
MZ	max	dlc23ba_3	1.10	164.7	19.3	89.3	165.9	-104.2	777.9	**40.8**	784.9
	min	dlc11k1	1.35	-68	20.6	103.3	71	-89.5	-251	**-50.9**	266.4
M_{res}	max	dlc62a_l_1_1	1.10	206.7	-25.2	74.2	208.2	137.8	1038.4	-2.28	**1047.5**

Supported by:

Table A.23 Extreme loads at 81.647m from blade root

Distance from root [m]			81.65	FX	FY	FZ	Fres	MX	MY	MZ	Mres
Load Case			γ_F [-]	[kN]	[kN]	[kN]	[kN]	[kNm]	[kNm]	[kNm]	[kNm]
FX	max	dlc13bb1	1.35	**70.2**	-8.15	18.1	70.6	18.4	134.2	0.29	135.4
	min	dlc14cb	1.35	**-49.8**	-12.6	22.3	51.3	27.7	-81.5	-1.71	86.1
FY	max	dlc23ca_1	1.10	17.2	**16.9**	17.1	24.1	-31.4	33	-2.7	45.6
	min	dlc11k1	1.35	-28.3	**-15.6**	21.1	32.3	34.3	-50.5	-5.79	61
FZ	max	dlc14bb	1.35	43.6	-0.74	**33.1**	43.6	6.12	78.5	-6.72	78.8
	min	dlc61ab_l_1_1	1.35	-13.1	0.014	**-2.88**	13.1	-0.48	-28.2	-0.96	28.2
F_{res}	max	dlc13bb1	1.35	70.2	-8.15	18.1	**70.6**	18.4	134.2	0.29	135.4
MX	max	dlc11k1	1.35	-28.3	-15.6	21.1	32.3	**34.3**	-50.5	-5.79	61
	min	dlc23ca_1	1.10	17.2	16.9	17.1	24.1	**-31.4**	33	-2.7	45.6
MY	max	dlc13bb1	1.35	70.2	-8.15	18.1	70.6	18.4	**134.2**	0.29	135.4
	min	dlc11k1	1.35	-48.1	-7.65	23.5	48.7	19.2	**-82.8**	-4.45	85
MZ	max	dlc23ba_3	1.10	54.7	7.03	21.5	55.1	-12.7	99.9	**5.6**	100.7
	min	dlc11k1	1.35	-14.8	2.21	21.4	14.9	-1.75	-24.3	**-13.1**	24.3
M_{res}	max	dlc62d_h_2_1	1.10	70.2	-8.15	18.1	70.6	18.4	134.2	0.29	**135.4**

Table A.24 Extreme loads at 83.382m from blade root

Distance from root [m]			83.38	FX	FY	FZ	Fres	MX	MY	MZ	Mres
Load Case			γ_F [-]	[kN]	[kN]	[kN]	[kN]	[kNm]	[kNm]	[kNm]	[kNm]
FX	max	dlc21ba	1.35	**39.1**	-0.68	13.8	39.1	2.66	44.7	-0.62	44.7
	min	dlc14cb	1.35	**-27**	-6.93	11.5	27.9	9.55	-26.4	-2.16	28.1
FY	max	dlc23ca_1	1.10	9.31	**9.2**	8.79	13.1	-10.9	10.8	-1.43	15.3
	min	dlc11k1	1.35	-16.3	**-8.67**	10.8	18.4	12.4	-17	-3.55	21
FZ	max	dlc14bb	1.35	23.5	-0.31	**17**	23.5	2.82	25.7	-3.48	25.8
	min	dlc61ab_l_1_1	1.35	-7.47	-0.02	**-1.51**	7.48	-0.25	-10.1	-0.43	10.1
F_{res}	max	dlc21ba	1.35	39.1	-0.68	13.8	**39.1**	2.66	44.7	-0.62	44.7
MX	max	dlc11k1	1.35	-16.3	-8.67	10.8	18.4	**12.4**	-17	-3.55	21
	min	dlc23ca_1	1.10	9.31	9.2	8.79	13.1	**-10.9**	10.8	-1.43	15.3
MY	max	dlc21ba	1.35	39.1	-0.68	13.8	39.1	2.66	**44.7**	-0.62	44.7
	min	dlc11k1	1.35	-26.5	-4.38	12	26.8	6.82	**-27.2**	-2.94	28.1
MZ	max	dlc23ba_3	1.10	29.6	4	11.1	29.9	-4.55	32.6	**2.06**	32.9
	min	dlc11k1	1.35	-8.52	1.2	11	8.6	-0.45	-7.61	**-6.5**	7.63
M_{res}	max	dlc11a1	1.35	38.2	-4.28	9.38	38.4	6.32	44.3	0.33	**44.8**

Supported by:

Table A.25 Extreme loads at 85.165m from blade root

Distance from root [m]			85.17	FX	FY	FZ	Fres	MX	MY	MZ	Mres
Load Case			γ_F [-]	[kN]	[kN]	[kN]	[kN]	[kNm]	[kNm]	[kNm]	[kNm]
FX	max	dlc21ba	1.35	**10.2**	-0.041	4.35	10.2	0.3	4.18	-0.087	4.19
	min	dlc14cb	1.35	**-6.75**	-1.68	3.6	6.95	1.02	-2.15	-0.83	2.38
FY	max	dlc23ca_1	1.10	2.33	**3.01**	2.78	3.81	-1.53	1	-0.33	1.83
	min	dlc11k1	1.35	-4.15	**-2.65**	3.4	4.93	1.71	-1.37	-0.94	2.19
FZ	max	dlc14bb	1.35	6.03	-0.18	**5.34**	6.03	0.6	2.31	-0.8	2.38
	min	dlc61ab_h_2_1	1.35	-0.17	0.061	**-0.49**	0.18	-0.072	-0.4	0.11	0.4
F_{res}	max	dlc21ba	1.35	10.2	-0.041	4.35	**10.2**	0.3	4.18	-0.087	4.19
MX	max	dlc11k1	1.35	-4.15	-2.65	3.4	4.93	**1.71**	-1.37	-0.94	2.19
	min	dlc23ca_1	1.10	2.33	3.01	2.78	3.81	**-1.53**	1	-0.33	1.83
MY	max	dlc13cb1	1.35	9.74	-0.97	3.03	9.79	0.67	**4.19**	0.12	4.24
	min	dlc11k1	1.35	-6.29	-1.21	3.44	6.4	0.86	**-2.51**	-0.94	2.65
MZ	max	dlc13cb1	1.35	7.29	-1.16	2.74	7.39	0.73	2.86	**0.41**	2.95
	min	dlc11k1	1.35	-2.99	-0.47	4.54	3.02	0.54	-0.47	**-1.54**	0.72
M_{res}	max	dlc23ba_2	1.10	9.74	-0.97	3.03	9.79	0.67	4.19	0.12	**4.24**

Supported by: